SYNTHESIS AND ELECTROCHEMISTRY OF OCTAPENTYLTHIO PHTHALOCYANINE COMPLEXES OF MANGANESE, TITANIUM AND VANADIUM

A thesis submitted in fulfillment of the requirement for the degree of

MASTERS IN SCIENCE

of

RHODES UNIVERSITY

By

GCINEKA MBAMBISA

January 2009

Acknowledgements

Firstly I would like to thank God Almighty, because without him, I wouldn't have gotten this far.

My gratitude goes to my supervisor, Prof Nyokong. Thank you Prof, for taking me under your wing when I was still a 'young one'. Your guidance and support are appreciated. Thank you Prof for the opportunity you gave me to do research in Japan and to attend a workshop at Gent university in Belgium.

I would also like to thank, my family, for their unwavering support. Throughout, you all constantly reminded me of your love. *Ndiyabulela baThembu nani booGatyeni*. My friends thank you for your understanding and support in all things.

Special thanks to:

- the S22 group; for their assistance and for providing a fun loving environment which I appreciate especially in hard times.
- Also the chemistry department and Rhodes University.
- NRF and Andrew Mellon foundation for funding.

Abstract

Synthesis of new thio derivatised Pcs with manganese, titanium and vanadium as a central metal is reported. The complexes synthesised were characterised using spectroscopic and electrochemical means. The complexes displayed interesting spectroscopic properties with absorption of the Q band being observed in the near infrared region. These complexes have unusual colours for MPc complexes, with purple or red colour being observed in solution.

Interesting electrochemical properties were observed, with rare observation of the Mn^{IV}/Mn^{III} redox couple. There was observation of oxidation peaks for the pentylthio derivatised Pc with titanium as the central metal; this is unusual since for reported thio derivatives based on TiPc, no oxidation was observed. The vanadium based Pc showed an interesting spectrum for the first ring based reduction. The absorption spectrum obtained for the 1^{st} reduction of the vanadium complex using spectroelectrochemistry would normally indicate a metal based process but comparing with literature it was concluded that it is a ring based reduction process.

Generally all the MPc complexes formed a well ordered stable monolayer on the gold electrode. Electrocatalytic studies using L-cysteine revealed that the SAM based on manganese (III) octapentylthio phthalocyanine (AcOMnOPTPc) was the most effective since it catalyses L-cysteine at much lower oxidation potentials and it is also much more stable.

List of Publications

A list of the publications that resulted from this work is provided below and they are not referenced in this thesis:

a) Synthesis and electrochemical properties of purple manganese (III) and red titanium (IV) phthalocyanine complexes octa-substituted at non-peripheral positions with pentylthio groups. ***Gcineka Mbambisa****, Prudence Tau, Edith Antunes, Tebello Nyokong,Polyhedron,* ***26*** *(18) (2007), 5355*

b) Synthesis and electrochemical characterisation of a near infrared absorbing oxo vanadium (IV) octapentylthio-phthalocyanine. ***Gcineka Mbambisa****, Tebello Nyokong, Polyhedron,* ***27*** *(13) (2008) 2799*

c) Effect of central metal on the formation of self-assembled monolayers of octapentylthiophthalocyanine complexes of titanium, vanadium and manganese. ***Gcineka Mbambisa****, Tebello Nyokong* (**submitted**)

Table of Contents

List of Abbreviations

A	=	Electrode surface area (cm^{-2})
Ag/AgCl	=	Silver/silver chloride reference electrode
CoOBTPc	=	Cobalt (II) octabutylthio Pc
CoTCAClPc	=	Cobalt (II) tetracarboxylic acid chloride Pc
CoTEThPc	=	Cobalt tetraethoxy thiophene Pc
CT	=	Charge transfer band
CV	=	Cyclic voltammetry
DMF	=	Dimethylformamide
DMSO	=	Dimethylsulfoxide
E_p	=	Peak potential
E_{pa}	=	Anodic peak potential
E_{pc}	=	Cathodic peak potential
GCE	=	Glassy carbon electrode
HOMO	=	Highest occupied molecular orbital
^{1}H NMR	=	Proton nuclear magnetic resonance
I_{pa}	=	Anodic peak current
I_{pc}	=	Cathodic peak current
IR	=	Infrared
LMCT	=	Ligand-to-metal charge transfer
LUMO	=	Lowest unoccupied orbital
MLCT	=	Metal-to-ligand charge transfer
MnTBMPc	=	Manganese (III)acetate tetrakis (benzyl-mercapto) Pc
MnTDMPc	=	Manganese(III)acetate tetrakis (dodecyl-mercapto) Pc
MPc	=	Metallophthalocyanine

MPc-SAM	=	Metallophthalocyanine-self assembled monolayer
NIR	=	Near infra red
(OAc)MnOPTPc	=	Manganese(III) acetate octapentylthio Pc
OTEs	=	Optically transparent electrodes
OTTLE	=	Optically transparent thin layer electrode
OTiOPTPc	=	Titanium (IV) oxide octapentylthio Pc
OVOPTPc	=	Vanadium(IV) oxde octapentylthio Pc
Pc	=	Phthalocyanine
SAM	=	Self-assembled monolayer
SCE	=	Standard calomel electrode
SWV	=	Square wave voltammetry
T	=	Temperature in Kelvin (K)
$TBABF_4$	=	Tetrabutylammonium tetrafluoroborate
THF	=	Tetrahydrofuran
UV-Vis	=	Ultraviolet-visible

List of Symbols

α	=	Non-peripheral position/ rate of electron transfer
β	=	Peripheral position
ε	=	Extinction coefficient
Γ	=	Surface coverage or concentration
Γ_{ibf}	=	Ion barrier factor
π	=	Pi bonding
λ	=	Wavelength
b	=	Tafel slope
C	=	Concentration of analyte
D	=	Diffusion coefficient
E	=	Potential
$E_{1/2}$	=	Half-wave potential
ΔE	=	Anodic-to-cathodic peak potential separation
F	=	Faraday's constant
i_{pa}	=	Anodic peak current
i_{pc}	=	Cathodic peak current
K	=	Kelvin
n	=	number of electrons
Q	=	Electrical charge (C)
Q_{Bare}	=	Integrated electrical charge due to bare gold electrode
Q_{SAM}	=	Integrated electrical charge due to MPc-SAM-modified gold electrode
R	=	Universal gas constant
ν	=	Scan rate
V	=	Volume of OTTLE cell (L)

List of Figures

Figure 3.10: UV-Vis spectral changes for **OTiOPTPc** observed during controlled potential electrolysis at +1.0 V (Process **I**), Electrolyte = DCM containing 0.1 M $TBABF_4$.

Figure 3.11: Cyclic voltammograms of (i) bare Au electrode (ii) **AcMnOPTPc**-SAM (iii) **OTiOPTPc**-SAM, (iv) **OVOPTPc**-SAM in 0.01 M KOH.

Figure 3.12: Cyclic voltammograms in (a) 1 mol cm^{-3} $Fe(NH_4)(SO_4)_2$ in 0.5 M $HClO_4$ and (b) 1mM $K_3Fe(CN)_6$ in 0.1 M KCl solution of (i) bare Au electrode (ii) **AcMnOPTPc**-SAM (iii) **OTiOPTPc**-SAM and (iv) **OVOPTPc**-SAM.

Figure 3.13: Cyclic voltammograms of (a) **AcMnOPTPc**-SAM (b) **OTiOPTPc**-SAM (c) **OVOPTPc**-SAM, all with their current vs scan rate graphs, in pH 4 buffer.

Figure 3.14: Cyclic voltammograms of 1 mM L-Cysteine (in ph 4 buffer) on (i) **AcMnOPTPc**-SAM (ii) **OVOPTPc**-SAM (iii) **OTiOPTPc**-SAM (iv) bare Au electrode.

Figure 3.15 : Plot of (a) Ep vs log *v*, (b) sweep-rate normalised current density ($I_p v^{-1/2}$) versus the sweep rate (inset = expansion of (ii) and (iii)), (c) peak current and square root of the scan rate and (d) current vs cyclic voltammogram scan number for analysis of L-cysteine by (i) **AcMnOPTPc**-SAM (ii) **OTiOPTPc**-SAM and (iii) **OVOPTPc**-SAM.

Figure 3.16: Dependence of cysteine concentration on currents for (i) **AcMnOPTPc**-SAM, (ii) **OVOPTPc**-SAM and **OTiOPTPc**-SAM

List of Schemes

List of Tables

CHAPTER 1

INTRODUCTION

1.1 Background on Metallophthallocyanines

The first metallophthalcyanine (MPc) was accidentally discovered in 1907 by Braun and Tchermiac; it was produced in the process of heating o-cyanamide at high temperatures to produce ortho-cyanobenzamide [1], but it remained uncharacterised. MPc was later accidentally observed in the 1930s in the industrial preparation of phthalic derivative and R.P Linstead characterised the complex in the same period, laying the foundation for the interest in industrial dyes [2] based on MPcs. MPcs have since been found useful not only as colorants but they have found a niche in photodynamic therapy (PDT) [3-5], chemical sensors [6-8], electrochromic display devices [9], as potential optical limiting devices [10,11], photovoltaic devices [12] and light absorbers in CD/RW [13,14]. This is due to the tunable structure and the characteristics displayed by the MPc. Metallophthalocyanines are symmetrical molecules which have an 18π conjugated system. The structure of the MPc is closely related to that of the porphyrin, with the difference being the presence of benzo groups and the nitrogen atoms at the *meso* positions on the MPc structure, Fig. 1.1. These molecules are chemically and thermally stable allowing for a variety of metals to be substituted at the core. The MPc displays a variety of oxidation states; this is used to tailor the MPc according to the area of interest. A variety of substituents can be accommodated at the peripheral ((2, 3) or β) and non- peripheral ((1, 4) or α) positions of the MPc, Fig. 1.1. This is mainly done to improve the solubility of the MPc with substitution at the non-peripheral position being reported to increase the solubility of MPcs [15] more than peripheral substitution. It has been found that substitution at the ring also changes the physical properties of the MPcs.

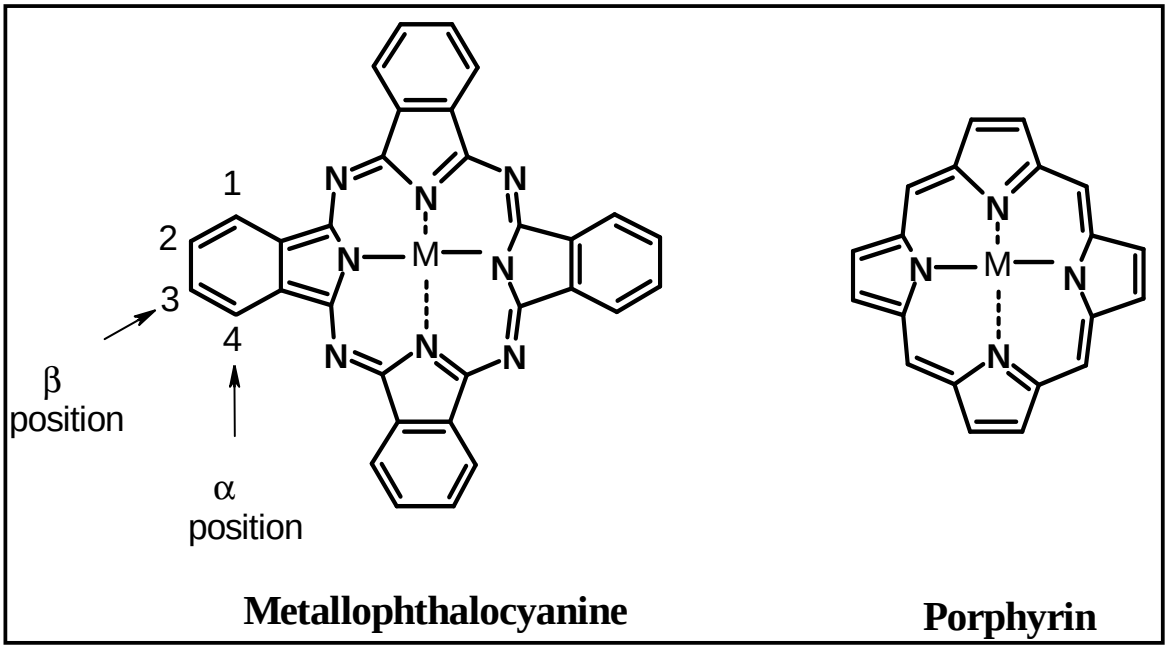

Figure 1.1: General structure of a metallophthalocyanine and porphyrin

1.2 Synthesis of Metallophthalocyanines

1.2.1 General synthesis of metallophthalocyanines

MPcs may be synthesised using various precursors such as phthalonitrile **(1)**, phthalic anhydrides **(2)**, phthalic acid **(3)** and phthalimide **(4)**. Formation of MPcs using phthalic anhydride, phthalic acid and phthalimide are facilitated by urea, which acts as a nitrogen source and with ammonium molybdate acting as a catalyst. Formation of the MPc in the presence of a phthalonitrile occurs upon condensation in a high boiling solvent such as 1-pentanol using 1, 8-diazabicyclo[5.4.0]undec-7-ene (DBU) as a catalyst , Scheme 1.1.

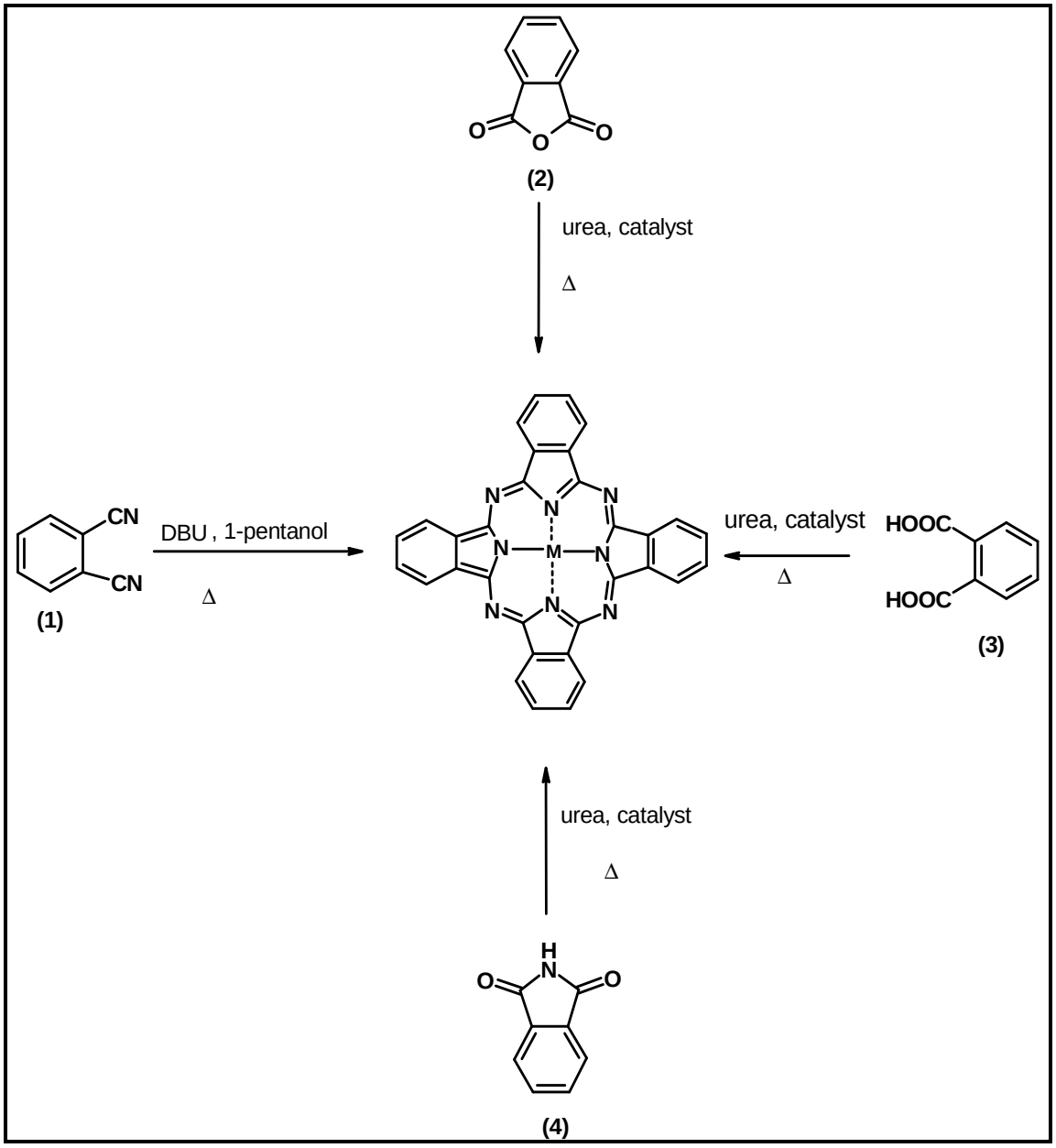

Scheme 1.1: General synthesis of metallophthalocyanine

In this work synthesis of alkylthio derivatised phthalocyanines is reported. Alkylthio derivatised phthalocyanines form metallophathalocyanines which are quite red shifted. The latter makes them very useful as NIR absorbers.

1.2.2 Tetrasubstituted MPcs

The synthesis of a tetra substituted MPc has been done using a 3 or 4- substituted nitrophthalonitriles [16, 17]. Nucleophilic aromatic substitution using compound **5** or **8** occurs in the presence of K_2CO_3 which acts as a base to form complex **6** or **9**, as shown in Scheme 1.2. The position of the nitro group is dependent on whether the interest is on α or β substituted MPc, for α substituted MPc a phthalonitrile substituted at the 3– position (**8**) is used, while for the β one that is substituted at the 4– position (**5**) is used. Tetrasubstition leads to formation of constitutional isomers [18]. Tetrasubstituted MPcs are soluble in a greater variety of solvents compared to octasubstituted MPcs because of the isomers formed.

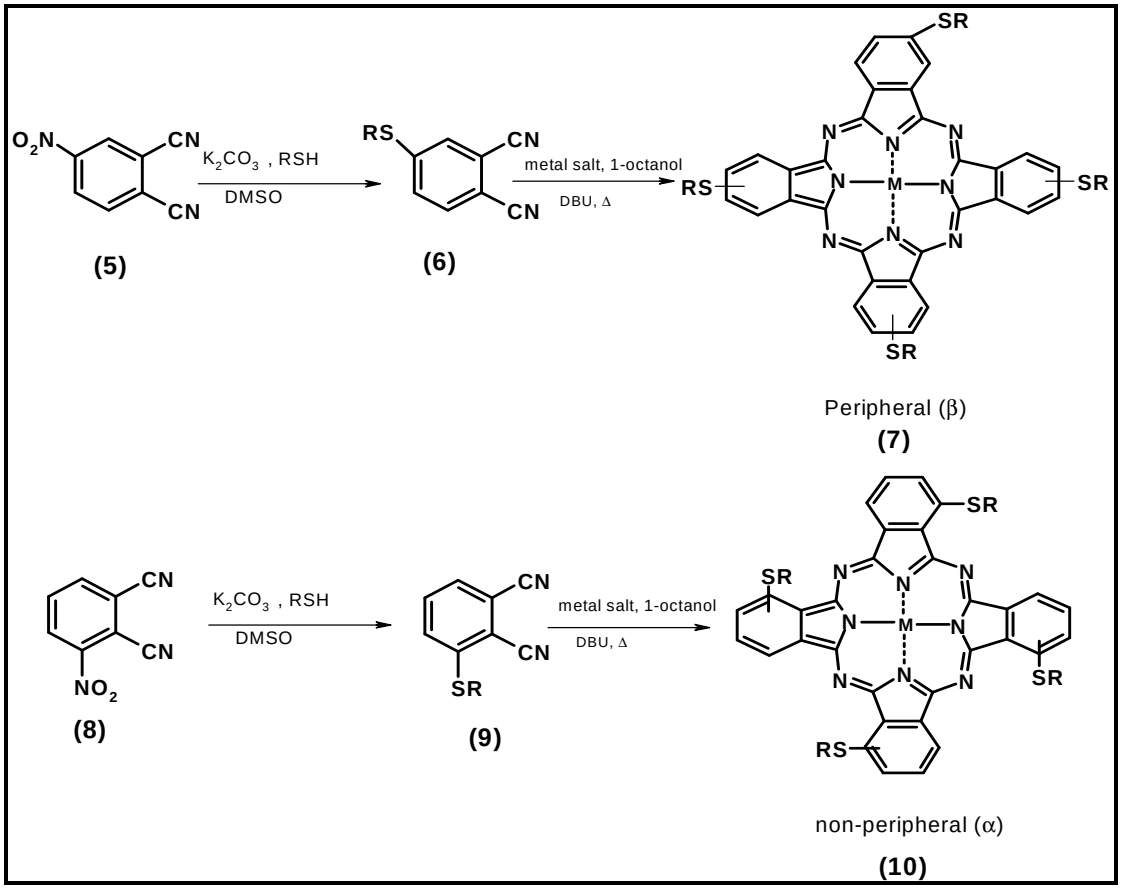

Scheme 1.2: Synthesis of tetrasubstituted alkylthio derivatised phthalocyanine

1.2.3 Octasubstituted MPcs

Octasubstituted MPcs are easier to purify compared to tetrasubstituted MPcs due to the formation of isomerically pure compounds. It has also been observed that octasubstituted alkylthio MPcs lead to complexes that absorb more in the infra red region [19] in comparism to tetrasubtituted alkythio MPcs.

Alkylthio derivatised phthalocyanines (**13**) that are substituted at the peripheral position have been synthesised by using a dichlorophthalonitrile (**11**), Scheme 1.3. Alkylthio phthalonitrile (**12**) derivative is formed in the presence of a base, potassium carbonate, a polar aprotic solvent, such as dimethyl formamide (DMF).

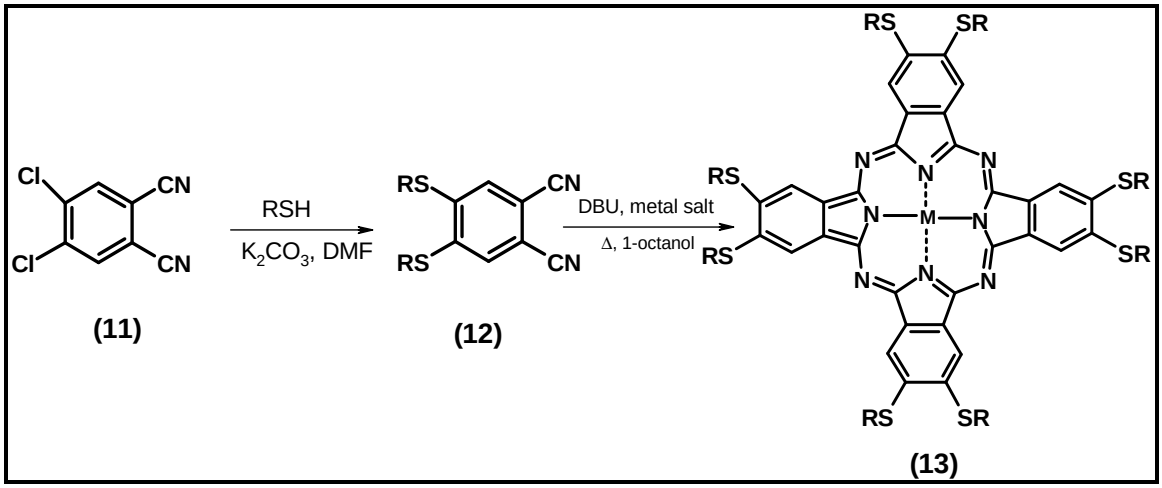

Scheme 1.3: Synthesis of peripheral substituted thiol derivatised phthalocyanine

The synthesis of octasubstituted alkylthio derivatised metallophthalocyanine substituted at the non- peripheral position is carried out using a method that has been reported by Cook's group, [20] that makes use of dicyanohydroquinone (**14**).

Formation of a triflate (**15**) is done by reacting 2, 6-dicyanohydroquinone (**14**) with $(CF_3SO_2)_2O$ in the presence of 2, 6-lutidine (a base) and dichloromethane (DCM) as a solvent as depicted in Scheme 1.4. Nucleophilic aromatic substitution of the alkylthio group occurs in the presence of a base (K_2CO_3) to form alkylthio substituted phthalonitrile, (**16**). The phthalonitrile (**16**) is refluxed in 1-pentanol in the presence of a metal salt and DBU, which is important in the cyclisation to form the MPc (**17**).

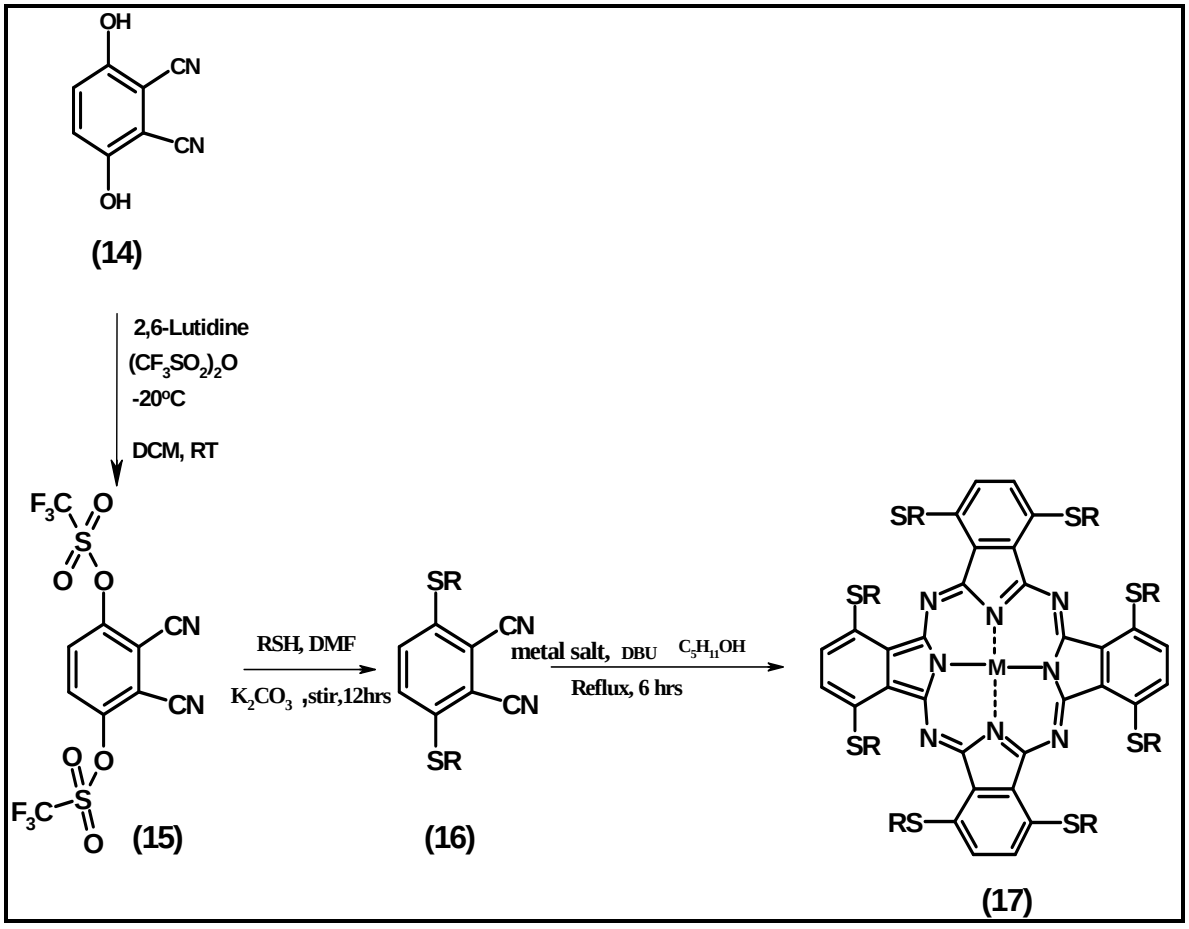

Scheme 1.4: Synthesis of non-peripherally substituted alkylthio MPc

Table 1.1 gives a representation of known alkylthio MPcs (M = Mn, V, Ti). For MnPc complexes, studies have concentrated mostly on β tetrasubstituted alkylthio derivatives [21, 22]. For TiPcs a number of tetrasubsituted alkylthio derivatives have been reported but only β derivatives are known for octasubstituted alkylthio derivatives [23-25]. The data for the VPc derivatives show that only the synthesis of β tetrasubstituted VPc has been reported [26]. Overall there is not much data on α octasubstituted MnPc, TiPc, VPc derivatives; hence this thesis will concentrate on these complexes. These complexes are expected to be highly red shifted in terms of Q band with potential applications as NIR absorbers as stated above. The complexes to be synthesised in this work are complexes **17** with M = Mn^{III}, $V^{IV}$and Ti^{IV} and R = C_5H_{11}. These complexes are octapentylthio phthalocyaninato manganese (III) acetate, octapentylthio phthalocyaninato titanium (IV) oxide and octapentylthio phthalocyaninato vanadium (IV) oxide abbreviated as AcMnOPTPc, OTiOPTPc and OVOPTPc, respectively.

Table 1.1 List of known Mn, Ti and V phthalocyanines containing alkylthio substituents at the peripheral and non-peripheral position

Complexes[a]	**Q band absorption(nm)**	**Solvent**	**Ref**
MnTBMPc	745	DCM	[21]
MnTDMPc	749	DCM	[21]
α-MnTMPyPc	758	DMSO	[22]
α-Q-MnTMPyPc[b]	741	DMSO	[22]
MnTMPyPc	730	DMSO	[22]
Q-MnTMPyPc[b]	719	DMSO	[22]
$OTiPc(SPh)_4$	714	DCM	[23]
α-$OTiPc(SPh)_4$	747	DCM	[23]
$OTiPc(SCH_2Ph)_4$	714	DCM	[23]
α-$OTiPc(SCH_2Ph)_4$	746	DCM	[23]
$OTi(SC_6H_{13})_4$	720	$CHCl_3$	[24]
$OTiPc(SC_6H_{13})_8$	739	$CHCl_3$	[24]
$OTiPc(SC_2H_4N(CH_3)_2)_4$	723	$CHCl_3$	[25]
$OTiPc(SC_2H_4N(CH_3)_2)_8$	739	$CHCl_3$	[25]
Vanadyl tetra-ortho-[(4-*t-butyl*) thiophenoxy)]Pc	748	DCM	[26]
Vanadyl tetra-ortho-(noctadecylthio)Pc	745	DCM	[26]

[a] TDMPc = tetra dodecylmercapto phthalocyanine, TBMPc = tetra benzylmercapto phthalocyanine, Ph = phenyl, TMPyPc = tetra mercaptopyridine phthalocyanine, [b]quaternized derivative

1.3 UV/Visible absorption spectra of MPcs

A UV/Visible absorption spectrum of MPcs, Fig. 1.2, is characterised by a Q band in the red area of the visible region, which has been explained, using the Gouterman's model [27,28], Fig. 1.3. The Q band is a transition from the highest occupied molecular orbital (HOMO), a_{1u}, to the lowest unoccupied molecular orbital, e_g. There is also the B band which is observed at the blue end of the spectrum, and consists of an overlap of B_1 and B_2 bands, Fig. 1.3. B_1 is due to a transition from the a_{2u} to the e_g and B_2 is due to a transition from the lower lying b_{2u} to the e_g orbital. The B_1 and B_2 bands are usually observed as a single broad band around the 340 nm region [29]. There are also the N, L and C band that are associated with MPcs. These are observed at wavelengths that are shorter than 300 nm and are due to transitions from the deeper HOMO orbitals. They are observed when UV transparent solvents are used.

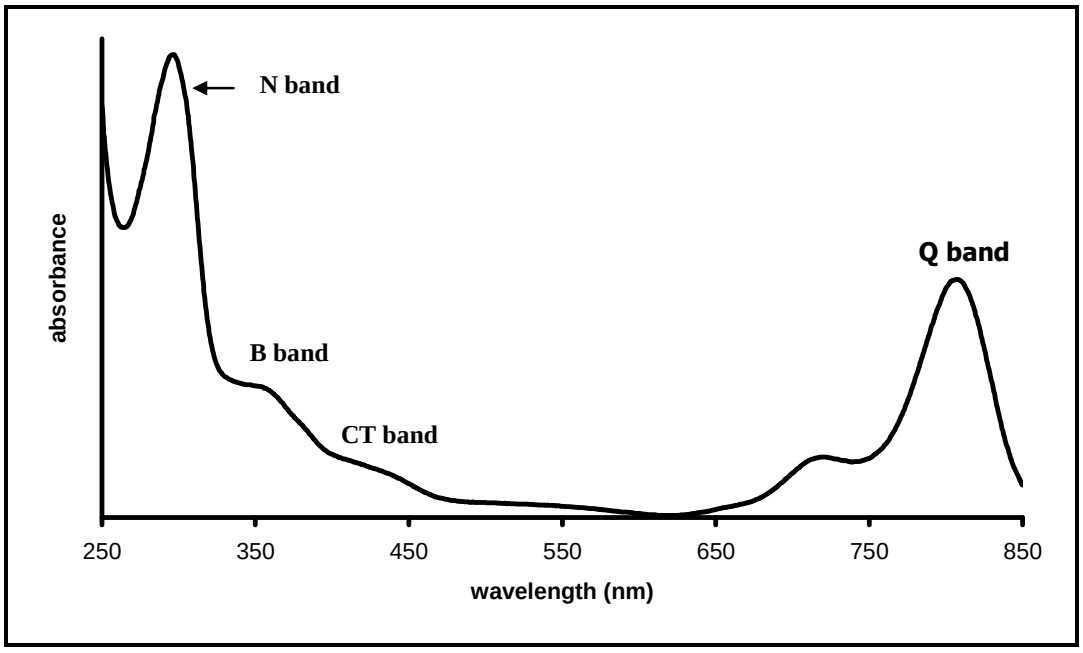

Figure 1.2: UV/Visible spectrum of a metallophthalocyanine

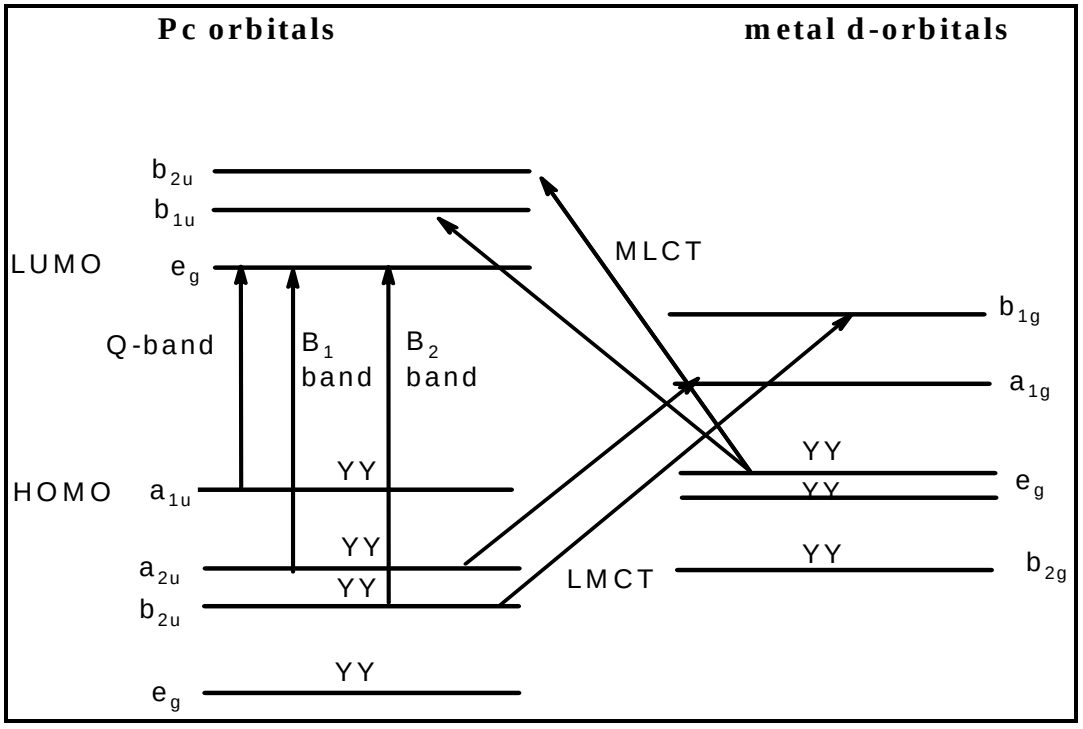

Figure 1.3: Gouterman's representation of the 4- orbital linear combination of atomic model

The position of the Q band is influenced by the point of substitution, which is whether the substituents are on the α or β positions. It has been observed that substitution at the α position results in greater shifts of the Q band to the infrared region [30, 31]. This can be attributed to a greater destabilisation of the HOMO when the substituent is at the α position in comparism with the β position, Table 1.1 (compare α-TiOPc$(SPh)_4$ and TiOPc$(SPh)_4$).

The position of the Q band is also influenced by the nature of the substituent with electron donating groups such as alkylthio and alkoxy groups leading to a more red shifted Q band [32, 33]. This is due to the destabilisation of the HOMO in a way that the distance between the HOMO and LUMO is shortened and hence lower energies are experienced [34].

Even though the sulphur and the oxygen atom are both electron donating, it has been found that the alkylthio substituted phthalocyanines lead to a more red shifted spectrum compared to the alkoxy [35]. This has been attributed to the fact that the 3p orbital of the sulphur group interacts more with the π bond cloud compared to the alkoxy group [36]. Electron withdrawing groups, tend to shift the Q band to the blue region [37]. The nature of the substituent together with the number of substituents affects the position of the Q band with an increase in the number from tetra to octa alkylthio substituents resulting in a shift to the near infrared region, this shift is clearly observed for MPcs that are substituted at the α position. The nature of the central metal has been observed to influence the position of the Q band, with a bathochromic shift being observed with an increase in the size of the central metal [38]. The oxidation state of the central metal also influences the Q band position, with a bathochromic shift being observed with increase in the oxidation state of the metal [22, 39]. Normally an unmetallated MPc has a Q band that is split; this is due to the

fact that the e_g orbital of the LUMO is non-degenerate. It has been found that as the position of the Q band of the unmetallated MPc moves more to the infra red region; it becomes observed as single band. This is due to the fact that there is generation of degeneracy as the Q band shifts to the red region [35].

There are other bands that can be observed in an MPcs electronic spectrum, such as the charge transfer (CT) bands [40], Fig. 1.2. There can be metal to ligand charge transfer (MLCT) or a ligand to metal charge transfer (LMCT) bands [41], Fig. 1.3. These weak bands are normally observed in the visible region between the Q band and B band or after the Q band in the near infra red or infra red region.

Charge transfer bands are observed for phthalocyanines with electroactive metal centres. This has been accounted by the fact that the d-orbitals of the electroactive metal [41] are found within the HOMO and LUMO of the phthalocyanine. The observed CT bands are due to the movement of electrons between the d-orbitals of the metal centre and the HOMO/LUMO state of the phthalocyanine.

1.4 Electrochemistry

The electrochemistry of metallophthalocyanines can be investigated by using voltammetric methods such as cyclic and square wave voltammetry and by spectroelectrochemistry.

1.4.1 Voltammetry

Cyclic voltammetry involves the reduction and oxidation of the species. Oxidation occurs on application of a positive going potential, an increase in the peak current with an increase in the potential is observed until the potential where the analyte is oxidised is reached, Fig 1.4. Thereafter a decrease in current occurs. The reduction of the species occurs with application of a negative going potential. The movement of the species to the electrode can be facilitated by migration, convection and diffusion. Diffusion is the movement of analyte due to concentration gradient. The latter is the one that is of interest when dealing with electroanalytical reactions. When working with voltammetry, specifically cyclic voltammetry, a system can be characterised as a reversible, quasi-reversible and irreversible. This is dependent on the ease of the redox reaction of the species and whether both the oxidised and reduced species are redox active. A reversible system shows the redox reaction of the species in the forward scan followed by the redox reaction upon application of a reverse scan, the Nernst equation applies to this system. The ratio of the reverse to forward peak currents is equal to unity for this system. ΔE (anodic to cathodic peak potential separation) is ~ 59 mV/n for a reversible system. Where n is the number of electrons.

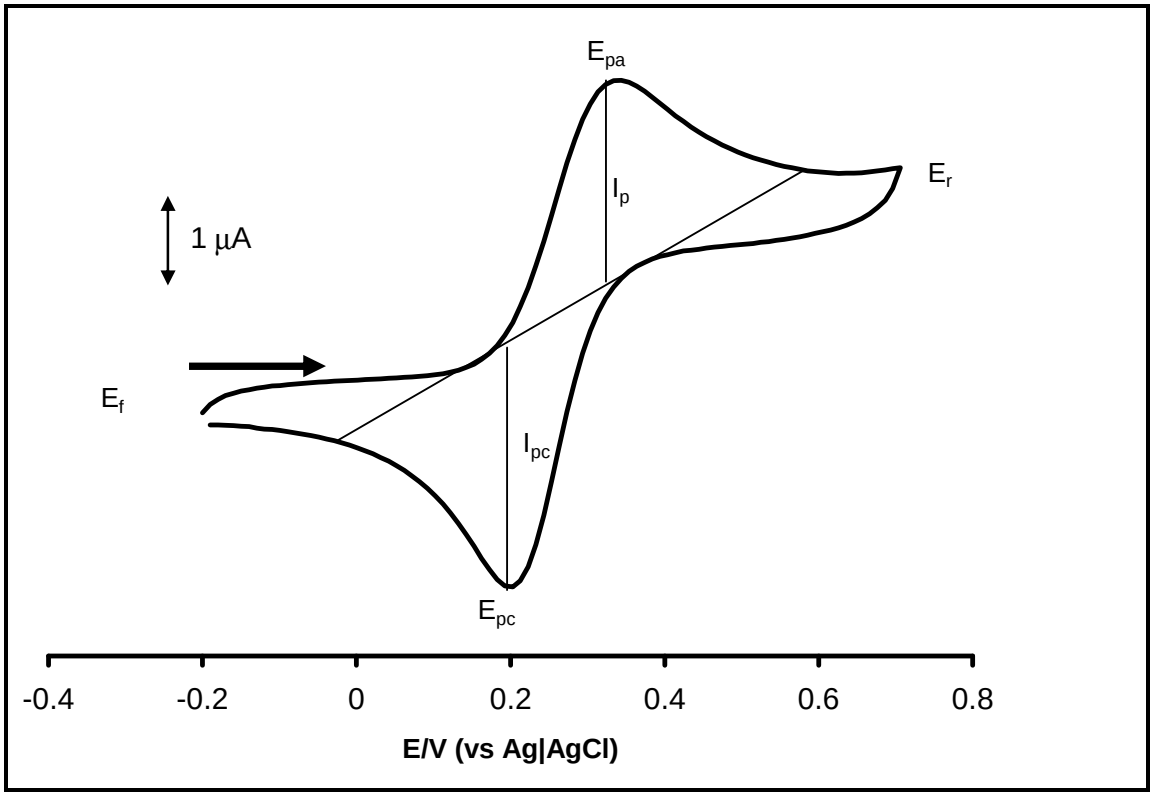

Figure 1.4: A typical cyclic voltammogram for a reversible system

The number of electrons transferred in this system is determined using Eq 1.1

$$\Delta E = RT/nF = 0.059V/n \qquad 1.1$$

where R is the universal gas constant, T is the temperature in Kelvin and F is the Faraday's constant (96485 C mol^{-1}). The half wave potential is determined using Eq 1.2.

$$E_{1/2} = (E_{pa} + E_{pc})/2 \qquad 1.2$$

The system is said to be quasi-reversible when the equilibrium concentration is not maintained between the redox species. This results in ΔE values that are greater than 59 mV for a one electron system with I_{pa}/I_{pc} deviating from unity.

An irreversible system is observed by the occurence of a forward peak with a peak in the reverse direction being very weak or not observed at all due to failure to regenerate the starting electroactive species. A shift in the potential with change in scan rates is observed for an irreversible system because of the slow electron transfer. The problem with cyclic voltammetry is that it has high background currents due to the charging current, this limits sensitivity. Hence another voltammetric method such as square wave voltammetry has to be used concurrently with cyclic voltammetry to increase the sensitivity. Square wave voltammetry is more sensitive because it eliminates the background charging current. In square wave voltammetry the current is read at each half cycle of the staircase waveform and thus the difference in current between successive half cycles is plotted against the potential. Hence in the study there will be utilisation of cyclic voltammetry and square wave voltammetry.

1.4.2 Spectroelectrochemistry

This is a method that makes use of spectroscopy with electrochemistry. The simplest spectroelectrochemical method is the one that makes use of UV/Visible spectroscopy. There is passage of charge while a change in the species is monitored by the change in absorption. There are two modes that can be utilised when using UV/visible spectroscopy. There is use of optically transparent electrodes (OTEs); these can be made of thin film semiconductors [42- 45] such as tin oxide and indium oxide or a fine wire mesh that is made of metals such as platinum, gold. There is also the use of an optically transparent thin layer electrode (OTTLE), which is an enclosed chamber with the electrodes within the chamber together with the solution [46]. Spectroscopic changes can be observed within a shorter time-frame, in seconds when making use of the OTTLE cell because of the low volumes used, 30-50 μl.

Use of spectroelectrochemistry makes it possible to observe changes that occur on the electroactive species with the application of certain overpotential and also calculation of the number of electrons that are involved in the reaction can be done using Eq 1.3,

$$Q = n.F.V.c \qquad 1.3$$

where n is the number of electrons, Q the charge, F the Faraday's constant, V is the volume of solution in the OTTLE cell and c is the concentration of the analyte.

1.4.3 General electrochemistry of metallophthalocyanines

The phthalocyanine ligand in its neutral state exists as Pc^{2-}. The Pc ligand can undergo up to two oxidation processes, that is Pc^{1-}/Pc^{2-} and Pc^{0}/Pc^{1-}. This occurs from the removal of electrons from the a_{1u} orbital (HOMO). The Pc can undergo up to six reduction processes, Pc^{2-}/Pc^{3-}, Pc^{3-}/Pc^{4-}, Pc^{4-}/Pc^{5-} and Pc^{5-}/Pc^{6-} [47]. A filling up of the e_g orbital (LUMO) is observed when the Pc ring is reduced as depicted in Fig. 1.5. Metal based processes are observed between the first ring reduction and oxidation for phthalocyanines that are substituted with redox active metals [48]. Otherwise for redox inactive metals, only processes due to the Pc ligand are observed [48]. The electrochemistry of metallophthalocyanines is influenced by the nature of the substituents on the phthalocyanine ring, which is whether they are electron donating or electron withdrawing. Electron donating substituents lead to an ease in oxidation of the species and difficulty in reduction [49]. Electron withdrawing groups lead to a greater ease in reduction with less ease in oxidation. The nature of the central metal (that is its oxidation state or whether its electroactive or not) also plays a role in the electrochemical behaviour of the MPc.

In MPc complexes metal based redox processes during spectroelectrochemistry are characterised by the shifting of the Q band either to the red or blue region of the

spectrum [50]. Ring or ligand based processes are characterised by the disappearance of the Q band and formation of weak bands between 500-600 nm region for the MPcs [50].

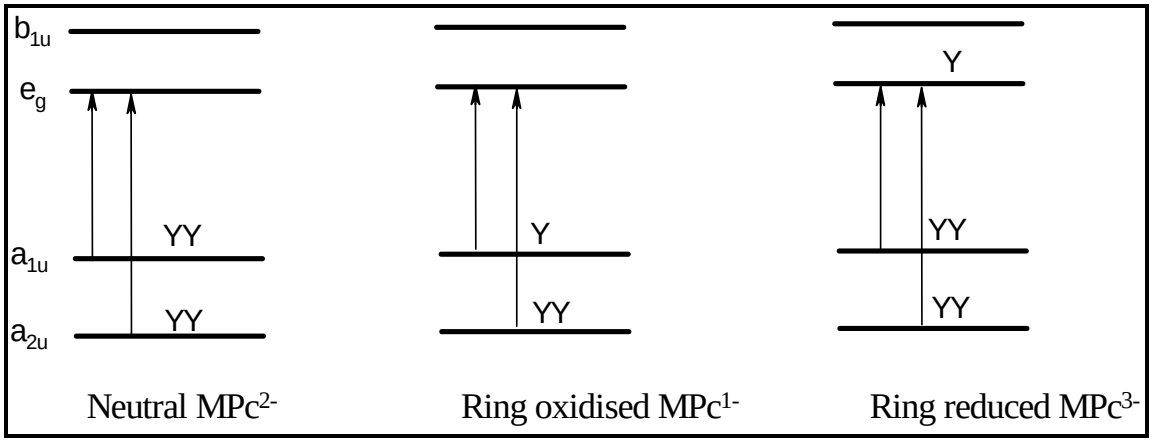

Figure 1.5: Electronic transitions upon oxidation and reduction of the Pc ring. where 'Y' represents an electron.

1.4.3.1 Electrochemistry of VPc

The electrochemistry of vanadium phthalocyanine is very limited [37, 51]. The electrochemistry of vanadium alkylthio phthalocyanine is unknown but Table 1.2 shows redox assignments of VPc with other substituents.

The study carried out by Kadish's group [51] using aryloxy and alkoxy phthalocyanines tetrasubstituted on the α position, showed three reduction couples and two oxidation couples which were all due to ring based processes.

Handa and co-workers used electron withdrawing fluoro substituents [37] for their study and three reduction couples were still observed but with one oxidation couple.

This is not surprising considering that electron withdrawing groups lead to less ease in oxidation of the electroactive species. The reduction processes were observed at less

negative potentials for the electron withdrawing fluoro substituents in comparism with the electron donating substituents. Thus all processes were ring based.

Table 1.2: Electrochemical data of VPc complexes. Half-wave potential (V vs SCE) in dimethyl formamide using tetrabutyl ammonium perchlorate (TBAP)

Complex	$V^{IV}Pc^{4-}/V^{IV}Pc^{5-}$	$V^{IV}Pc^{3-}/V^{IV}Pc^{4-}$	$V^{IV}Pc^{2-}/V^{IV}Pc^{3-}$	Ring oxidation	ref
$OV[(OC_6H_3(t\text{-}Bu)_2)_4Pc]$	-1.94	-0.97	-0.51	0.94, 1.34	[51]
$OV[(OC_8H_{17})_4Pc]$	-2.07	-1.12	-0.62	0.76, 1.21	[51]
$OV[(Bu)_4Pc]$		-1.08	-0.58	0.94	[51]
$OV(F_{16}Pc)$	-1.41	-0.62	-0.29	1.34	[37]

1.4.3.2 Electrochemistry of TiPc

The electrochemistry of titanium phthalocyanines is also not that extensive but it is very intriguing, with instances were two electrons have been reported to be involved in one electrochemical step [52]. The oxidation of titanium phthalocyanines is on the phthalocyanine ligand and has reportedly led to the decomposition of the species [53]. Reports on the electrochemistry of titanium phthalocyanine with alkylthio substituents are very limited as shown in Table 1.3. The study on the alkylthio substituted TiPc showed reduction processes that involved one electron with two processes being due to the metal centre and one being due to a Pc ring based process.

Table 1.3: Electrochemical data of TiPc complexes with alkylthio substituents in dimethyl formamide (DMF) using tetrabutyl ammonium fluoroborate ($TBABF_4$). Half-wave potential (V vs Ag|AgCl) [23].

Complex	$Ti^{II}Pc^{2-}$/ $Ti^{II}Pc^{3-}$	$Ti^{III}Pc^{2-}$/ $Ti^{II}Pc^{2-}$	$Ti^{IV}Pc^{2-}$/ $Ti^{III}Pc^{2-}$
α-OTi[$(SCH_2C_6H_6)_4$Pc]	-1.33	-0.46	-0.07
OTi[$(SCH_2C_6H_5)_4$Pc]	-1.30	-0.40	-0.09
α-OTi[$(SC_6H_5)_4$Pc]	-1.20	-0.37	-0.07
OTi[$(SC_6H_5)_4$Pc]	-1.28	-0.42	-0.09

1.4.3.3 Electrochemistry of MnPc

MnPc is the one that has been most widely investigated compared to the other mentioned metallophthalocyanines. Manganese can exist in various oxidation states, I-IV. It has been confirmed that the first reduction process that takes place is a metal based process; Mn^{III}/Mn^{II} for Mn^{III}Pc, Table 1.4. There has been some dispute on the first reduction of Mn^{II}Pc, with proposals that it is due to a metal based process that is $Mn^{II}Pc/Mn^{I}Pc$ and others proposing that it is a ring based process with $Mn^{II}Pc^{2-}/Mn^{II}Pc^{3-}$ [54]. It has been recently proven that the latter depends upon the nature of the substituent, where the substitution of a quaternized substituent leads to reduction of Mn^{II}Pc to Mn^{I}Pc [22], Table 1.4. The UV/Vis absorption spectrum for a well defined Mn^{IV}Pc is rare.

Table 1.4: Electrochemical data of MnPc complexes with alkylthio substituents. Half-wave potential (V vs Ag|AgCl)

Complex	$Mn^{II}Pc^{2-}/Mn^{II}Pc^{2-}$	$Mn^{II}Pc^{2-}/Mn^{I}Pc^{2-}$	$Mn^{III}Pc^{2-}/Mn^{II}Pc^{2-}$	$Mn^{III}Pc^{2-}/Mn^{IV}Pc^{2-}$	Ring oxidation	Solvent/ Electrolyte	ref
MnTBMPc	-0.84		-0.08	~0.3	0.87	DCM/$TBABF_4$	[21]
MnTDMPc	-0.98		-0.26	~0.3	0.83	DCM/$TBABF_4$	[21]
α-MnTMPyPc	-0.76		-0.051		1.18	DMF/$TBABF_4$	[22]
α-Q-MnTMPyPc[a]	-0.71	-0.59	-0.056		1.10	DMF/$TBABF_4$	[22]
MnTMPyPc			-0.057		1.34	DMF/$TBABF_4$	[22]
Q-MnTMPyPc[a]		-0.56	-0.063		1.13	DMF/$TBABF_4$	[22]

where TDMPc = tetra dodecylmercapto phthalocyanine, TBMPc = tetra benzylmercapto phthalocyanine, TMPyPc = tetra mercaptopyridine phthalocyanine,

[a] = quaternized derivative

As observed from the electrochemical data shown in Tables 1.2-1.4, the electrochemistry of thioPcs of vanadium derivatives is not known and for titanium as a central metal is still very limited. In addition data on α substituted thioPcs of both titanium and manganese is rare. Hence in this work, alkylthioPcs which have titanium, vanadium and manganese as a central metal will be synthesised and characterised by cyclic voltammetry (CV), square wave voltammetry (SWV) and spectroelectrochemistry.

1.5 Electrocatalysis

Eletrocatalysis involves the use of electrochemical methods to catalyse reactions. Use of electrochemistry is advantageous because it allows for simpler, cheaper and safer forms of reactions. Bare electrodes have been used in electrochemical reactions [55, 56] but the result has been that the reaction occurs at high potentials or not at all. Thus chemically modified electrodes are employed for electrochemical reactions, since they lead to lower overpotentials and increased current, hence sensitivity. MPcs have been confirmed as good electrocatalysts for various analytes [57-60]. This is partly due to their good thermal and chemical stability. Another factor is that the MPc can be tuned, by changing the nature of the central metal or the substituents, allowing them to act as catalysts for different analytes [61, 62]. During electrocatalysis the central metal or the Pc ring can undergo redox process before it acts as a mediator between the analyte and the electrode. After the reaction, it is expected that the MPc will go back to its original oxidation state as illustrated in equations 1.4 to 1.7.

$M^{II}Pc^{2-} + e^{-} \rightarrow M^{I}Pc^{2-}$ 1.4

$M^{I}Pc^{2-} + A \rightarrow M^{II}Pc^{2-} + P$ 1.5

OR

$M^{II}Pc^{2-} + e^{-} \rightarrow M^{II}Pc^{3-}$ 1.6

$M^{II}Pc^{3-} + A \rightarrow M^{II}Pc^{2-} + P$ 1.7

where A = analyte, P = product

MPcs are employed as electrocatalysts either when immobilised on electrodes (heterogenous catalysts) or in solution (homogenous catalysts).

The former is more common because it allows for an easier regeneration of the catalyst. There are various methods that are utilised in the modification of electrodes. These include spin coating, electropolymerisation [63], drop dry method, dip-dry method [64, 65] and formation of self assembled monolayers (SAMs). Formation of SAMs was employed in this work; hence it will be discussed in more detail.

1.5.1 Electropolymerisation

This involves the formation of a polymer on the electrode surface. This is done by repetitive scanning of the electrode in an electroactive [63] monomer. This method forms a stable polymer on the electrode surface. The other aspect of using this method is there are more electroactive sites that are found on the surface of the electrode since there is formation of a polymer. It is an easy reproducible method since it is dependent upon the number of scans.

1.5.2 Drop-dry method

As the name suggests, the species that is used to modify the electrode is dropped on the electrode surface and left to dry to form a film on the electrode surface [64, 65]. The problem with this method is that the film that is formed on the surface of the electrode is not stable. But it is commonly used because it is a fast method of modifying an electrode.

1.5.3 Self Assembled Monolayers (SAMs)

SAMs are highly ordered molecular assemblies that are formed by the adsorption of the compound onto the electrode surface [66]. SAMs form without any external factors which control the organisation of the molecules on the surface of the electrode.

SAMs may form as a result of the chemical bond that forms between the substrate which is the electrode surface, and the compound. An example of this is the self assembly of alkanethiols on gold [67, 68]; a strong chemical bond is formed between the gold surface and the sulphur group of the alkanethiol. Highly stable and ordered alkanethiol SAMs are formed on the gold surface. The alkyl chain allows the spontaneous ordering of the alkanethiol on the gold surface. Other surfaces such as mercury have also been explored for formation of SAMs [69]. The surface that has been used in this study (for the formation of SAMs using MPcs) is the gold surface. Since the method of SAM formation is simple, it allows for an easy way to modify an electrode for electrocatalytic purposes. The method involves the immersing of the clean electrode in a millimolar or micromolar solution of a particular modifier (that has been purged with N_2 or Ar) for a period of 24 hrs or more.

Alkylthio substituted MPcs are used in the study of the self assembling capabilities of MPcs on gold. Making use of MPcs that are not substituted with thiol or alkylthio groups has been explored in literature [70, 71]. These can be done by making use of mercaptopyridine species, these form a SAM on the surface and the central metal of the MPc is able to co-ordinate to the nitrogen moiety [70] of the mercaptopyridine. Thiols, such as 2-mercaptoethanol can also be used to modify the surface and co-ordination of the MPc to the thiol occurs via the Pc substituents [71]. The MPcs can be ordered in a flat orientation on the gold electrode (that is all the sulfur groups are attached to the substrate, electrode) or a vertical manner as shown in Fig. 1.6 [72, 73]. The vertical orientation is observed when one part of the molecule gets attached to the substrate.

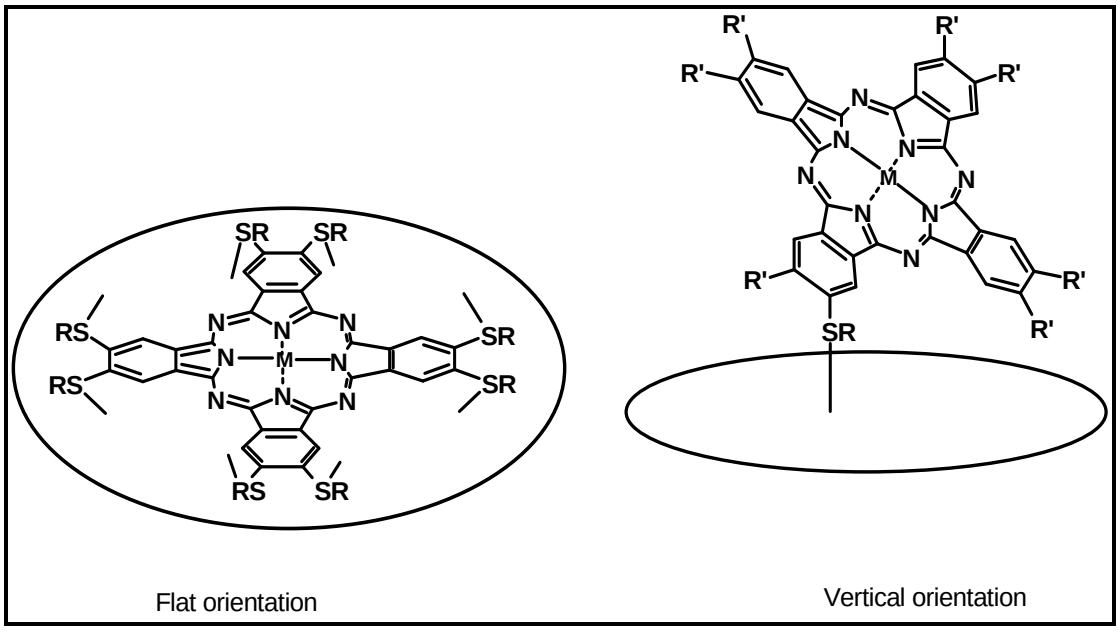

Figure 1.6: Orientation of SAMs on gold electrode

1.5.3.1 Characterisation of SAMs

SAMs are characterised using different methods such as scanning tunnelling microscopy, X-ray diffraction, impedance and voltammetrical methods [73-76].

Characteristaion of SAMs is important to determine whether the SAM formed is free from defects or pinholes. The degree at which the monolayer is defect free is determined by the surface roughness of the electrode [77]. In this study, cyclic voltammetry is used to characterise the SAMs formed. The points of interest that can be determined using voltammetry are the surface coverage or surface concentration, Γ_{MPc}, and ion barrier factor, Γ_{ibf}. The surface coverage can be determined using various methods, including:

(i) Determination of the surface coverage using equation 1.8

$\Gamma_{MPc} = Q/nFA$ 1.8

where Q is the background corrected charge of the anodic peak of the surface confined species, n the number of electrons, F is the faraday's constant and A is the surface area of the electrode.

(ii) Another method makes use of the charge difference that exists between the bare electrode and the SAM modified electrode in basic media as shown in Fig. 1.7. The charge difference between the bare gold (Q_{Bare}) and the MPc-SAMs (Q_{SAM}) is proportional to the fraction of the gold sites covered by the MPc-SAMs. This fraction is divided by three to get the charge proportion of gold sites covered with MPc-SAM, according to Eq. 1.9 [78, 79].

$$Au.H_2O + 2H_2O \rightleftharpoons Au(OH)_3 + 3H^+ + 3e^- \qquad 1.9$$

The value found for the charge proportion of gold sites covered with MPc-SAM is divided by the number of thiol or alkylthio arms to get the amount of gold sites covered by the MPc-SAM of thiol or alkylthio derivatised substituents. This value is then divided by the real surface area of the gold electrode surface to get the charge density proportional to each MPc molecule. These values can then be converted to the corresponding surface concentration (Γ_{MPc}, mol/cm^2) by dividing them with the Faraday constant (96485 C mol^{-1}). When dealing with MPc-SAMs a surface coverage that is approximately 1x10^{-10} mol cm^{-2} confirms monolayer formation on the electrode [80].

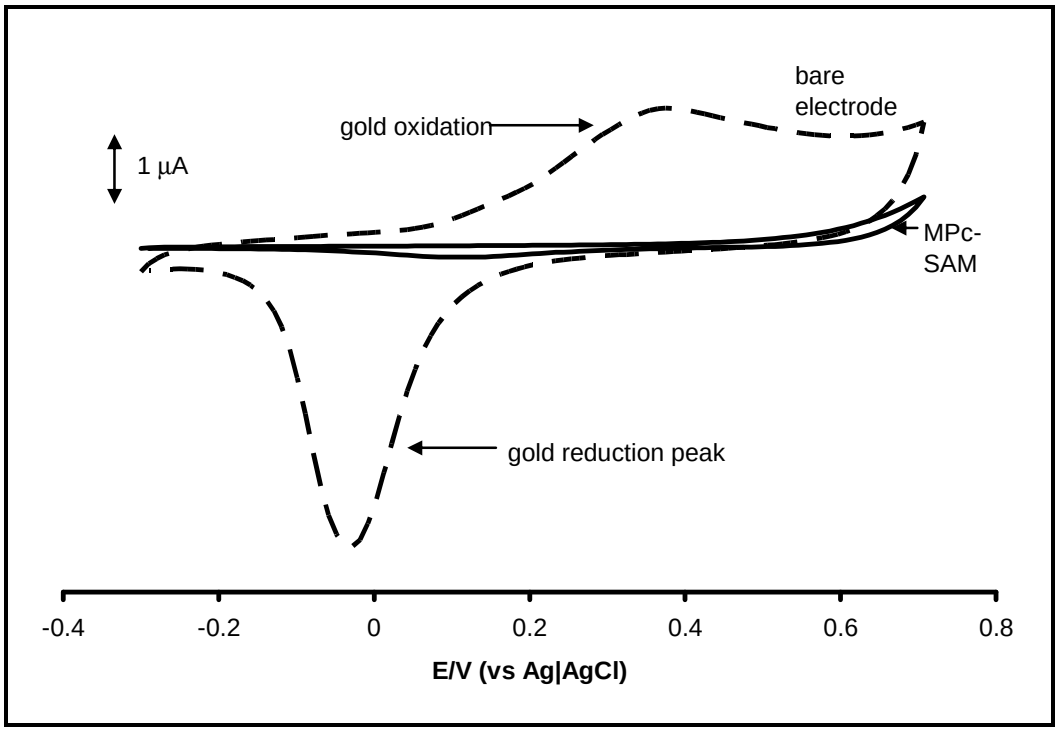

Figure 1.7: Cyclic voltammogram of the bare and modified electrode in basic media

Another important aspect of the characterisation of SAMs is the determination of the ion barrier factor (Γ_{ibf}), which is the measure of the MPc-SAMs effectiveness in preventing the interaction of the surface with the electrolyte.

The Γ_{ibf} is determined using Eq. 1.10:

$$\Gamma_{ibf} = 1 - (Q_{SAM}/Q_{BARE}) \qquad 1.10$$

where Q_{SAM} is the charge of the MPc-SAM and Q_{BARE} is the charge for the bare electrode in basic media as shown in Fig. 1.7. The voltammogram of MPc-SAM is supposed to show the blockage of the gold redox process, in comparism to the bare gold electrode in basic media. Other methods used to determine the integrity of the SAMs on gold electrodes include, the blockage of the underpotential deposition of copper using $CuSO_4$ and the blockage of the $[Fe(H_2O)_6]^{2+}/Fe(H_2O)_6]^{3+}$ redox couple of $Fe(NH_4)(SO_4)_2$.

1.5.3.2 MPc-SAMs based on VPc, MnPc and TiPc

There has not been much study in the formation of MPc-SAMs that are based on VPc and TiPc. The attachment of VPc on preformed SAM on gold has been reported [81], but no report on thioPc VPc for SAM formation. There are no reports on formation of SAMs using TiPc. Some studies have been done on the formation of MPc-SAMs that are based on MnPc [82, 83]. SAMs that are formed as a result of substitution on the periphery of the MnPc has been explored and successfully used for the catalysis of sulfite [83]. MnPc-SAM formed by co-ordination of MPc to preformed SAM of mercaptopyridine on gold provides SAMs that are well packed on the electrode surface [82, 84], which display good catalytic activity with decrease in overpotential up to 0.2 V being observed in the detection of L-cysteine. This work reports for the first time on SAMs of VPc, MnPc, TiPc substituted on the non-peripheral positions with pentylthio groups.

1.6 MPcs as Electron Mediators for Determination of L-cysteine

1.6.1 Background on L-cysteine

L-Cysteine is one of the few amino acids that contain sulfur. This feature makes it possible for the amino acid to bond in such a way that the structure of the proteins is maintained [85]. Oxidation of L-cysteine to L-cystine has been investigated using various electrochemical means, including the use of MPc-SAM modified electrodes [86-91]. Lowered overpotentials have been observed when using MPc-SAMs as shown in Table 1.5, when compared to unmodified electrodes. Another point is that the use of MnPc SAMs for the investigation of the oxidation of L-cysteine is limited

as depicted in Table 1.5 which shows the list of some complexes that have been used for the oxidation of L-cysteine on a gold surface, CoPc based SAMs are the most widely reported. TiPc or VPc derivatives have not been explored for SAM formation.

Table 1.5: Complexes used for the oxidation of L-cysteine on SAM of MPcs

Complex	L-cysteine oxidation potential(V)	Ref
CoTCAClPc	0.45	[91]
CoPc	0.20	[82]
FePc	0.18	[82]
MnPc	0.20	[83]
CoOBTPc	~0.40	[90]
CoTEThPc	0.53	[88]

where TCAClPc = Tetracarboxy acid chloride phthalocyanine, OBTPc = Octabutylthio phthalocyanine, TEThPc = Tetraethoxy thiophene phthalocyanine

1.7 Summary of Aims of Thesis

(i) The purpose of this work is to synthesise MnPc, VPc, TiPc that absorb in the near infra red region, this is achieved by substitution of pentylthio substituents at the non-peripheral position of the Pc ring, Fig. 1.8. The names of the complexes are octapentylthio phthalocyaninato manganese (III) acetate (**AcMnOPTPc**), octapentylthio phthalocyaninato vanadium (IV) oxide (**OVOPTPc**) and octapentylthio phthalocyaninato titanium (IV) oxide (**OTiOPTPc**).

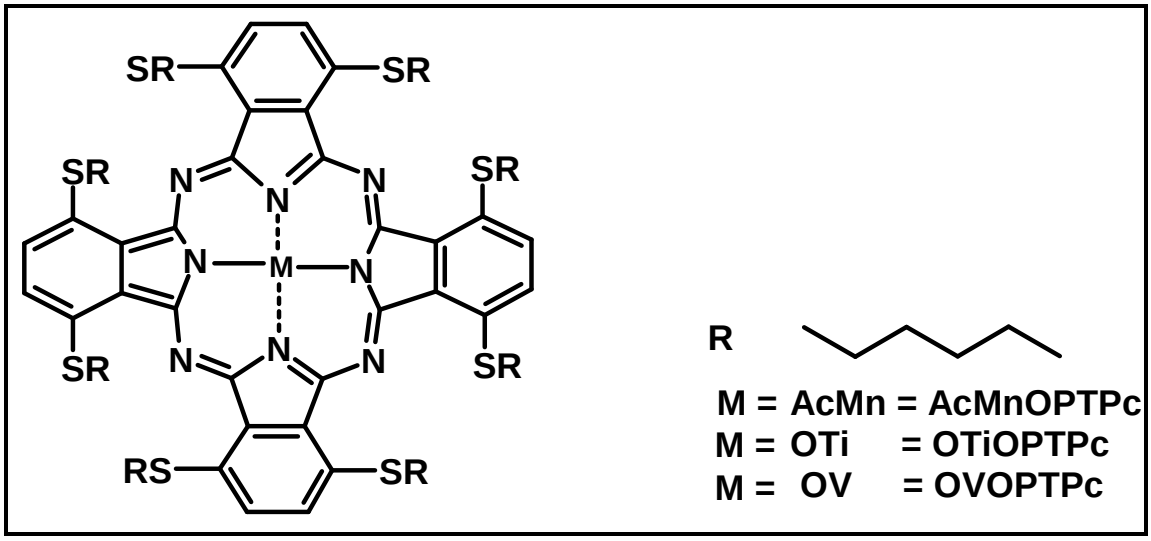

Figure 1.8: Structure of the synthesised MPcs

(ii) The electrochemical characterisation of the alkylthio derivatised MPc complexes will also be carried out since there is limited data on the electrochemistry of alkylthio or thiol derivatised MnPc and TiPc. There is no reported data on the electrochemistry of thiol or alkylthio derivatised for VPc.

(iii) Studies on the self assembled monolayer of the MPc complexes on gold electrode is carried out so as to determine the behaviour of the complexes on an electrode surface

(iv) Lastly, the electrocatalytic behaviour of the MPcs towards the oxidation of L-cysteine is investigated.

CHAPTER 2

EXPERIMENTAL

2.1 Materials

Acetone, manganese acetate, dimethylsulphoxide (DMSO), 1-pentanethiol, titanium butoxide, 1,8-diazabicyclo{5.4.0}-undec-7-ene (DBU), tetrabutylammonium tetrafluoroborate ($TBABF_4$), 1-pentanol and L-cysteine were purchased from Sigma Aldrich. Potassium carbonate, ammonium ferrous sulphate, sodium carbonate, deuterated chloroform ($CDCl_3$), 2,3-dicyanohydroquinone, *p*-toluenesulfonylchloride, chloroform and dichloromethane (DCM) were procured from Merck. Ethanol, KOH, ammonium ferrous sulfate, pH 4 buffer tablets, was purchased from Saarchem. Ferricyanide ($K_3[Fe(CN)_6]$ was purchased from ACE chemicals. Millipore water is from Milli-Q-water Water System (Millipore corp., Bedford, MA, USA). Solvents were dried and distilled before use. Column chromatography was performed on silica gel 60 (0.04 – 0.063 mm).

2.2 Apparatus

UV/Vis spectra were recorded on a Cary 500 and Cary 50 UV/Vis/NIR spectrophotometer. IR (KBr discs) was recorded on a Perkin-Elmer spectrum 2000 FTIR spectrometer. ^1H NMR spectra were recorded using a Bruker AVANCE II+ 600 MHz spectrometer. Elemental analyses were performed at the University of Cape Town using a Thermo Electron iCAP 6000 ICP.

Cyclic voltammogram experiments were done using Autolab potentiostat PGSTAT 30 (Eco Chemie, Utretch, The Netherlands) driven by the General Purpose Electrochemical Systems data processing software (GPES and FRA, version 4.9, Eco Chemie). A three electrode system consisting of a platinum wire as a counter electrode, Ag|AgCl as a pseudo reference electrode and a working electrode which is either a glassy carbon electrode or a gold electrode was used. Spectroelectrochemical

data were obtained using a home made optically transparent thin-layer electrochemical (OTTLE) cell which was connected to a Bioanalytic Systems (BAS) CV 27 voltammograph.

2.3. Synthesis

For the synthesis of phthalonitriles (**18** and **19**), a procedure similar to that reported in literature [20] was employed with slight modification as follows:

2.3.1. 3,6-Bis(4'-methylphenylsulfonyloxy) phthalonitrile (18), Scheme 3.1

p-Toluenesulfonyl chloride (5.16 g, 27 mmol) was added to a mixture of 2,3-dicyanohydroquinone (**14**) (2 g, 12.5 mmol) and potassium carbonate (6.9 g, 50 mmol) in acetone (15 ml). The mixture was heated to reflux for 2 hours. Thin layer chromatography (TLC) was performed to determine the consumption of compound **14**. The mixture was cooled to room temperature and poured to water (40 ml). The mixture was stirred for 1 hour in water. The light brown product was filtered and oven dried to give **18**. Yield: 4.51g (79 %) IR [(KBr) ν_{max}/cm^{-1}]: 3432, 3239, 3085, 2243, 2226 (CN), 1504, 1449, 1315, 1279, 1204, 1174, 1142, 1021, 1004, 979, 934, 847, 749, 694, 638, 614.

2.3.2. 3,6-di(pentathio)-4,5-dicyanobenzene (19), Scheme 3.1

The 1-pentanethiol (2.39 g, 22.9 mmol) was dissolved in DMSO under a nitrogen atmosphere and 3,6-bis(4'-methylphenylsulfonyloxy) phthalonitrile (**18**) (4.30 g, 9.18 mmol) was added. The mixture was stirred for 15 minutes and finely ground anhydrous potassium carbonate (5.07 g, 36.7 mmol) was added portionwise for two

hours while stirring. The mixture was stirred under a nitrogen atmosphere for 12 hours. Water was added and the aqueous phase extracted using chloroform (3 x 50 ml). The extracts were further treated with 5% sodium carbonate solution (2 x 250 ml). The solution was further treated with water (2 x 250 ml) and the solvent was evaporated off using a rotavapor. The product (**19**) was recrystallised from ethanol. Yield: 2.19g (71.7 %). IR [(KBr)ν_{max}/cm^{-1}]: 3084, 2951, 2930, 2864, 2378(S-C), 2225(C≡N), 1444, 1283, 1202, 1181, 1173, 1145, 877, 847, 827, 725, 547, 447.

^{1}H-NMR($CDCl_3$):δ, ppm 7.49 (2-H,s,Ar-H), 2.99-3.02 (4-H,t, -CH_2), 1.63-1.71 (4-H,m, -CH_2), 1.37-1.46 (4-H,m, -CH_2), 1.28-1.36 (4-H, m,-CH_2), 0.88-0.91 (6-H, t,-CH_3).

2.*3.3. 1,4,8,11,15,18,22,25-Octapentylthiophthalocyaninato manganese(III) acetate (AcMnOPTPc), Scheme 3.2*

3,6-Dipentylthiophthalonitrile (**19**) (0.4 g, 1.20 mmol) in 1-pentanol (3.5 ml) was refluxed under a nitrogen atmosphere and manganese(III) acetate (0.069 g, 0.40 mmol) was added. After the addition of DBU (0.13 ml, 0.86 mmol), the reaction was continued for 6 hours. The mixture was cooled and column chromatography over silica was done with $CHCl_3$ as eluent. Yield: 0.23g (42%). UV/Vis (DCM): λ_{max} (nm) (log ε) 363(4.52) 553(3.96) 794(4.22) 893 (4.82). IR [(KBr) ν_{max}/cm^{-1}]: 2959, 2925, 2855, 2369 (S-C), 1557, 1461, 1361, 1310, 1283, 1263, 1225, 1210, 1190, 1149, 1102, 1072, 1024, 932, 802 (Mn-O), 750, 584, 560. ^{1}H NMR (600MHz, $CDCl_3$): δ, ppm 7.41 (8H, s, Ar-H), 3.01 (16H, t, S-*CH_2*), 1.74 (16H, quintuplet, *CH_2*), 1.46 (16H, quintuplet, *CH_2*), 1.36 (16H, sextuplet, *CH_2*), 1.24 (3H, s, OAc), 0.91 (24H, t, *CH_3*). $C_{74}H_{99}N_8S_8O_2Mn$: Calc %. C 61.55, H 6.91, N 7.76. Found: C 61.72, H 7.33, N 7.03 %.

2.3.4. 1,4,8,11,15,18,22,25-Octapentylthiophthalocyaninato vanadium(IV) oxide (OVOPTPc)

OVOPTPc was prepared as described above for **AcMnOPTPc**, using compound **19 (**0.4 g, 1.20 mmol), 1-pentanol (3.5 ml), vanadium (IV) tetrachloride (0.069 g, 0.40 mmol) and DBU (0.13 ml, 0.857 mmol). Purification was done using column chromatography over silica (eluent: $CHCl_3$). Yield: 0.24g (42%). UV-Vis (DCM): λ_{max} (nm) (log ε) 344(3.96) 754(3.46) 850 (4.24). IR [(KBr) ν_{max}/cm^{-1}]: 2955, 2916, 2853, 2363(S-C), 1555, 1456, 1357, 1306, 1281, 1221, 1208, 1186, 1147, 1112, 1075, 992, 925(V=O), 810, 794, 775, 759, 741, 584, 533. ^{1}H NMR (600 MHz, $CDCl_3$): ppm 7.42 (8H, s, Ar-H), 2.93 (16H, t, S-*CH_2*), 1.75 (16H, quintuplet, *CH_2*), 1.47 (16H, quintuplet, *CH_2*), 1.35 (16H, sextuplet, *CH_2*), 0.90 (24H, t, *CH_3*). Calc %: C 61.90, H 6.92, N 8.02. Found: C, 61.53; H, 7.04; N, 7.56 %.

2.3.5. 1,4,8,11,15,18,22,25- Octapentylthiophthalocyaninato titanium(IV) oxide (OTiOPTPc)

OTiOPTPc was prepared as described above for **AcMnOPTPc**, using compound **19** (0.45 g, 1.203 mmol), titanium butoxide (0.136 ml, 0.40 mmol), DBU (0.25 ml, 1.68 mmol) and 1-pentanol (3.4 ml). The purification was done using column chromatography over silica with $CHCl_3$ as eluent. Yield: 0.12 g (22%). UV/Vis (DCM): λ_{max} (nm) (log ε) 352(3.84) 718 (3.52) 808(3.91). IR [(KBr) ν_{max}/cm^{-1}]: 2955, 2930, 2961, 2354 (S-C), 1713, 1649, 1560, 1459, 1371, 1274, 1178, 1145, 1108, 1060, 824 (Ti-O), 759, 643, 596, 534. ^{1}H NMR (600 MHz, $CDCl_3$): δ, ppm 7.47 (8H, s, Ar-*H*), 3.00 (16H, t, S-*CH_2*), 1.67 (16H, quintuplet, *CH_2*), 1.42 (16H, m, *CH_2*), 1.34

(16H, sextuplet,CH_2), 0.90 (24H, t, CH_3). $C_{73}H_{99}N_8S_8OTi$: Calc %.C 62.04, H 6.94, N 8.05. Found: C 61.74, H 7.26, N 7.83%.

2.4. Electrochemical characterisation

Electrochemical experiments were performed in dry DCM containing tetrabutylammonium tetrafluoroborate ($TBABF_4$) as a supporting electrolyte. Prior to scans, the working electrode was polished with alumina paste on a Buehler felt pad, followed by washing with deionised water and rinsing with DCM. Square wave voltammetry parameters were: step potential 5 mV; amplitude 20 mV at a frequency of 25 Hz.

2.5 Formation of SAMs

The formation of SAMs was achieved by firstly, polishing the gold electrode on slurries of alumina (<10 μm) on a Si-C emery paper, then on a Buehler felt pad to a mirror-like finish. The electrode was immersed in ethanol and sonication was done to remove the alumina residue particles. The electrode was further treated by immersing it in piranha solution (1:3, v/v, 30% H_2O_2 and concentrated H_2SO_4), to remove any organic materials that could be still on the electrode. The electrode was rinsed with ultrapure Millipore water. Multiple scans were run in pH 4 buffer in order to obtain a stable voltammogram. The pretreated electrode was immersed in 1 mM solution of OVOPTPc, OTiOPTPc or AcMnOPTPc, under an atmosphere of Ar for 48 hours. The electrode was rinsed with DCM and Millipore water prior to electrochemical experiments. The SAMs formed are represented as OVOPTPc-SAM, OTiOPTPc – SAM and AcMnOPTPc-SAM.

Cyclic voltammograms of the MPc-SAM were characterized using 0.01 M KOH solution (using a potential window of - 0.3 to 0.7 V was used), 1 mM ammonium

ferrous sulfate in 0.5 M $HClO_4$ (using a potential window of - 0.2 to 0.7 V) in order to check the blockage of the anodic gold oxide formation and the passivation Fe^{2+} /Fe^{3+} couple and 1 mM solution of ferricyanide was also used for characterization purposes.

CHAPTER 3

RESULTS AND DISCUSSION

Firstly synthesis of three alkythio MPcs is described. The metallophthalocyanines synthesised have different metal centres with the same subsituents. The metals used are manganese, titanium and vanadium. These were characterised using spectroscopic methods such as UV/Visible absorption, ^{1}H NMR and IR spectroscopy. The second section involves the electrochemical characterisation of the MPcs using cyclic, square wave voltammetry and spectroelectrochemistry. Interesting redox properties are observed for the MPcs synthesised. The last section describes the use of the MPcs in the formation of SAMs. Electrochemical characterisation (specifically cyclic voltammetry) of the MPc-SAMs is depicted together with the use of the MPc-SAMs in the oxidation of L-cysteine.

3.1 Synthesis and spectroscopic characterisation

3.1.1 Phthalonitriles

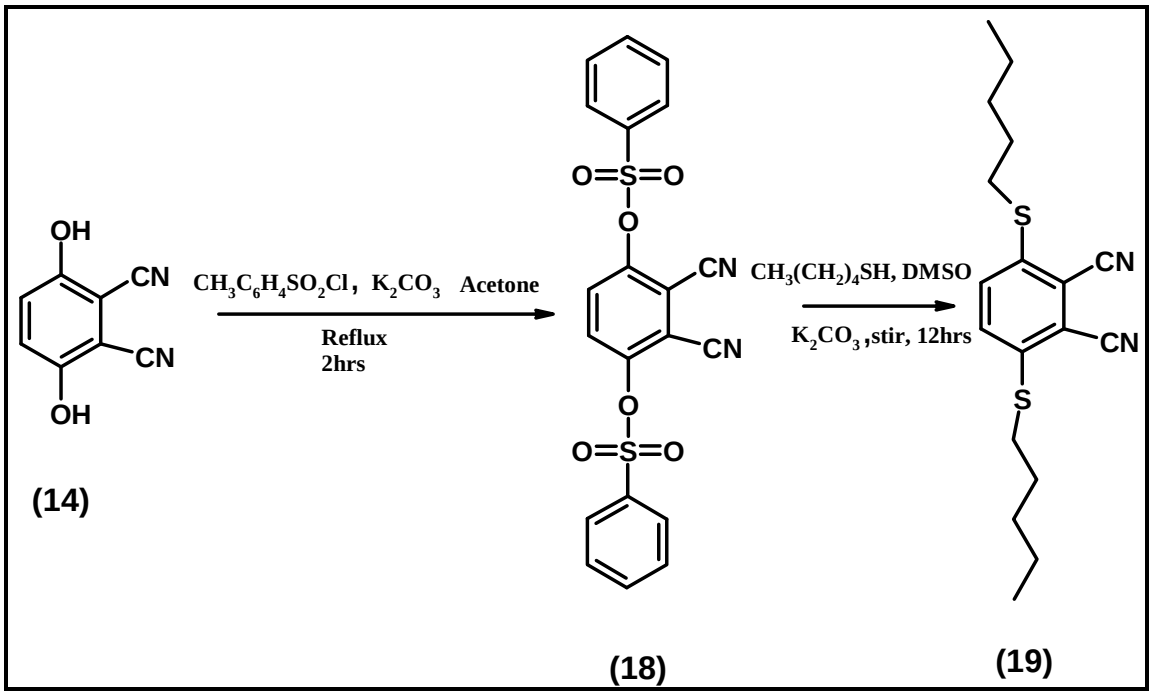

Scheme 3.1: Synthetic route for pentylthio phthalonitrile

Dicyanohydroquinone (**14**) was tosylated using toluene sulfonyl chloride in the presence of a base (K_2CO_3) with acetone as a solvent. Formation of a tosylate (**18**) instead of the triflate (**15**), reported by Cook's group, was undertaken because tosylation occurs in a shorter period of time using cheaper reactants. Also tosylation is done because the tosyl moiety is a better leaving group than the hydroxyl group due to its electron withdrawing abilities, hence better yields for **19** are expected. The completion of the reaction to form compound **18** from **14** was confirmed by making use of thin layer chromatography (TLC), which showed the complete consumption of **14** to form compound **18**. The pentylthio phthalonitrile (**19)** was obtained from **18** in high yields (~72%) with the S-C stretching vibration at 2378 cm^{-1} and C≡N stretch

observed at 2225 cm^{-1}. Further characterisation of **19** was done using ^1H NMR in $CDCl_3$, with peaks due to the aromatic ring observed at 7.49 ppm and integrating for 2 protons, a triplet that integrated for 4 protons was observed at 2.99-3.02 ppm due to -S-*CH_2*-, a multiplet at 1.63-1.71 ppm due to -S-CH_2-*CH_2*- integrated for 4 protons, another multiplet was found at 1.37-1.46 ppm due to S-CH_2-CH_2-*CH_2*- and it integrated for 4 protons, a multiplet peak at 1.28-1.36 ppm due to S-CH_2-CH_2-CH_2-*CH_2*- integrated for 4 protons and a triplet peak at 0.88- 0.91 ppm due to S-CH_2-CH_2-CH_2-CH_2-*CH_3* integrated for 6 protons.

3.1.2 Phthalocyanines

Table 3.1: Q band and charge transfer bands of metallophthalocyanines studied in this thesis in DCM

Complex	**λ_{max}(nm) CT band**	**λ_{max}(nm) Q band**
$AcMn(SC_5H_{11})_8$	553	893
$OTi(SC_5H_{11})_8$	551	808
$OV(SC_5H_{11})_8$	565	842

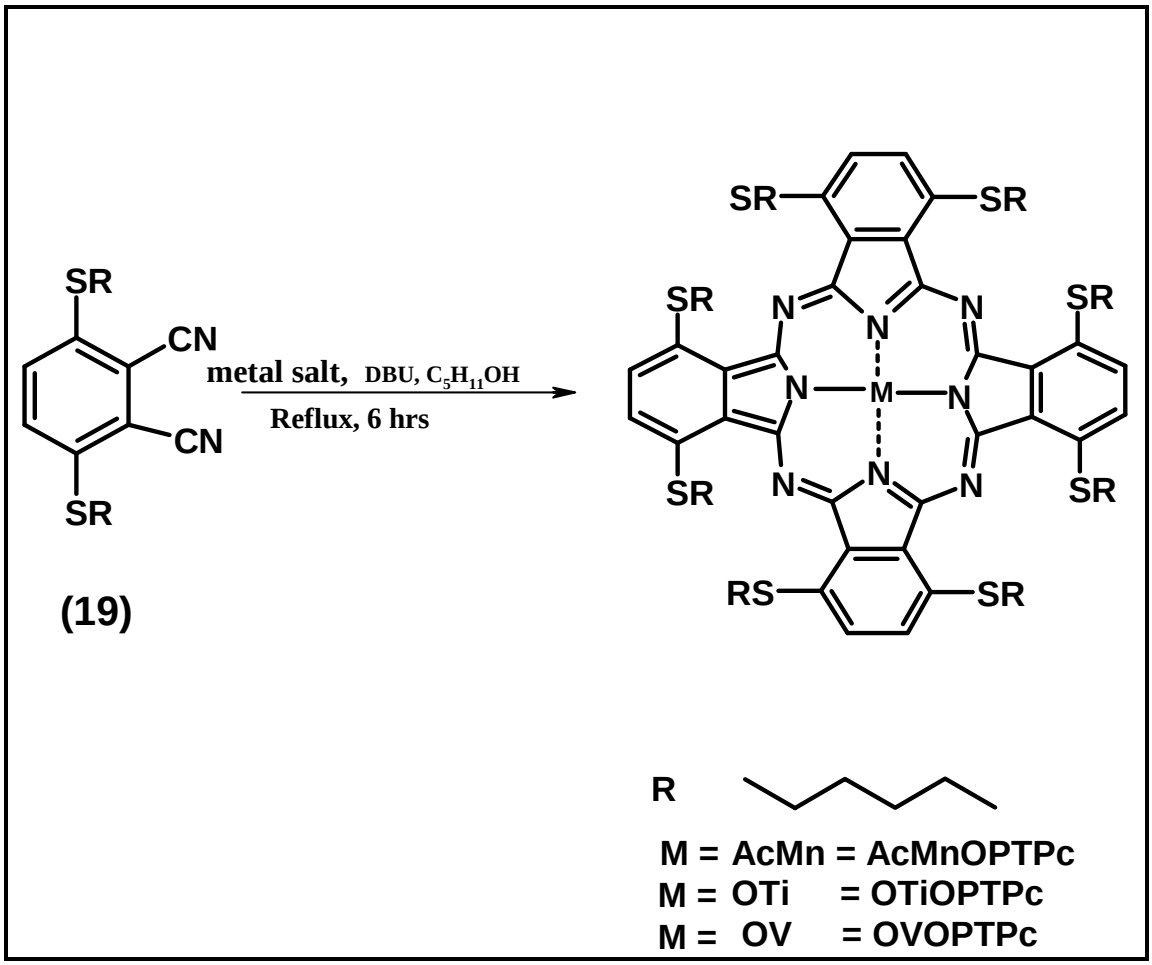

Scheme 3.2: Synthesis of Phthalocyanine complex **AcMnOPTPc**, **OVOPTPc** and **OTiOPTPc**

The MPc complexes **AcMnOPTPc**, **OTiOPTPc** and **OVOPTPc**, shown in Scheme 3.2, were synthesized by refluxing complex **19** in 1-pentanol in the presence of a catalyst (DBU) and a suitable metal salt. The synthesised MPcs are soluble in DCM, $CHCl_3$, THF and toluene. Infrared spectroscopy was also used to confirm the cyclisation of **19** with the disappearance of the C≡N stretching vibration that was observed at 2225 cm^{-1}. The V-O and Ti-O stretching vibrations were observed at 925 $cm^{-1}$and 824 cm^{-1} for complexes, **OVOPTPc** and **OTiOPTPc** respectively.

The Mn-O stretching vibration from the acetate axial ligand was observed at 802 cm^{-1}. The elemental analysis for all the complexes agreed with the expected results. Further confirmation of the acetate moiety being an axial ligand to **AcMnOPTPc** was done using ^1H NMR in $CDCl_3$ with singlet peak due to the protons of the acetate being observed at 1.24 ppm with the expected integration value of three protons. The ^1H NMR resonance due to the Pc ring is observed within the 7.41-7.47 ppm range for all the complexes. The signal integrated for eight protons. The peaks for the pentylthio substituents were observed in the ^1H NMR of each complex at around the same region (within ~ 1 ppm to 3 ppm range).

The formation of the MPc was confirmed using UV/Visible spectroscopy, which shows the typical Q band as depicted in Figure 3.1. The UV/Vis absorption spectra of all the complexes show the rarely seen N band. This band is due to transitions from deeper HOMO levels to the LUMO. The Q band for **AcMnOPTPc**, **OVOPTPc** and **OTiOPTPc** complexes is not in the visible region of the spectrum due to the point of substitution (α position), the central metal and also the nature of the substituent (electron donating). As a result, the colour of the complexes is not the typical blue or green. **OTiOPTPc** complex showed a red colour when in solution and **AcMnOPTPc** and **OVOPTPc** are purple in solution. Since the Q band is not in the visible region, the colour of the complexes is attributed to the bands between 500-600 nm (charge transfer bands), Table 3.1. When looking at Table 3.1, it can be concluded that the central metal plays a role in the position of the Q band as observed by its shift, with **AcMnOPTPc** absorbing at 893 nm, **OVOPTPc** at 842 nm and **OTiOPTPc** at 808 nm. Charge transfer bands between the 500-600 nm range were observed for all the synthesised complexes because of the electroactive nature of the central metals.

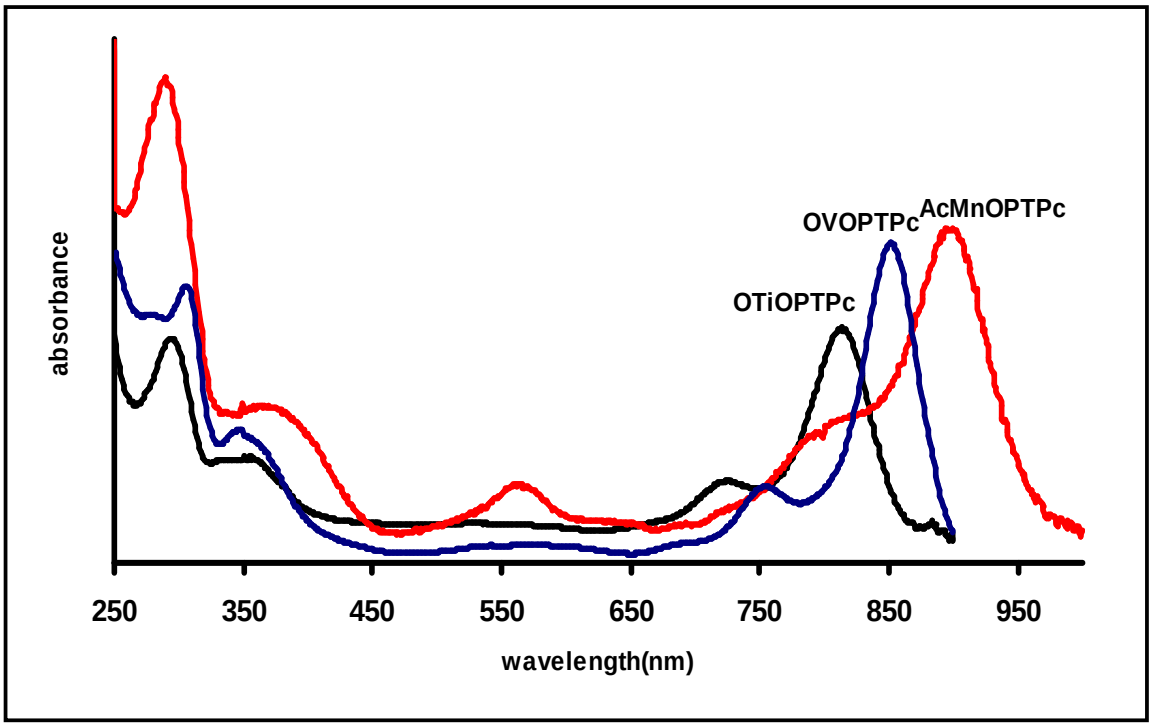

Figure 3.1: UV/Visible absorption spectrum for **AcMnOPTPc**, **OVOPTPc** and **OTiOPTPc** in DCM. Concentration = ~1 x10^{-5} M

3.2 Electrochemical characterisation of the Alkylthio Pcs

The redox properties of the complexes were studied in solution using cyclic and square wave voltammetry in DCM with $TBABF_4$ as an electrolyte.

3.2.1 Electrochemistry of AcMnOPTPc

3.2.1.1 Voltammetry

The cyclic (CV) and square wave (SWV) voltammetry of **AcMnOPTPc** were performed in de-aerated DCM containing $TBABF_4$ as electrolyte, Fig. 3.2. The half-wave potentials ($E_{1/2}$) for the complex are summarised in Table 3.2 together with reported data of other alkylthio derivatised MnPc. **AcMnOPTPc** complex exhibits four main reduction processes labelled **I** ($E_{1/2}$ = +0.47 V), **II** ($E_{1/2}$ = +0.75 V), **III** ($E_{1/2}$ = -0.46 V), and **IV** ($E_{1/2}$ = -1.24 V) vs. Ag|AgCl, Table 3.2. All the redox processes showed both the cathodic and anodic components; however peak separations were larger than the expected 59 mV, suggesting slow electron transfer. The cathodic to anodic peak separation (ΔE) ranged from 70 to 120 mV. A ΔE value of 90 mV was obtained for ferrocene. The cathodic to anodic peak current ratio (I_{pc}/I_{pa}) were near unity, except for **IV** which showed a weak anodic component. For all redox couples, plots of peak current (I_p) vs. the square root of scan rate ($v^{1/2}$) were linear, thus suggesting diffusion control at the electrode surface.

The first reduction for a $Mn^{III}Pc$ gives $Mn^{II}Pc$; process **III** may be assigned to $Mn^{III}Pc^{-2}/Mn^{II}Pc^{-2}$, even though in comparism with other MnPcs in Table 3.2 process **III** (-0.46 V) is shifted to much more negative potentials with the closest being for MnTDMPc (-0.26 V). This emphasises the fact that the nature of substituent, length of chain and point of substitution (α or β) affects the potentials. Process **IV** may either be due to $Mn^{II}Pc^{-2}/Mn^{II}Pc^{-3}$ or $Mn^{II}Pc^{-2}/Mn^{I}Pc^{-2}$. As stated in the introduction, both $Mn^{I}Pc^{-2}$ and $Mn^{II}Pc^{-3}$ species have been proposed. However, the latter species has been reported by several authors [21, 54, 92]. The former has been observed for

positively charged quaternized MnPc derivatives (Q-MnTMPyPc and α-Q-MnTMPyPc) [22] as shown in Table 3.2. The first oxidation in Fig. 3.2b (process **I**) showed an overlap of two peaks, which were not clearly resolved even when using the more sensitive SWV, Fig 3.2a. Such closely spaced redox couples may be associated with the presence of aggregates [48]. On dilution of the solution, the splitting is not evident. The last oxidation process **II** is in the range of ring-based processes in comparison to other MnPc complexes. The nature of the couples as well as the number of electrons transferred was confirmed by spectroelectrochemistry.

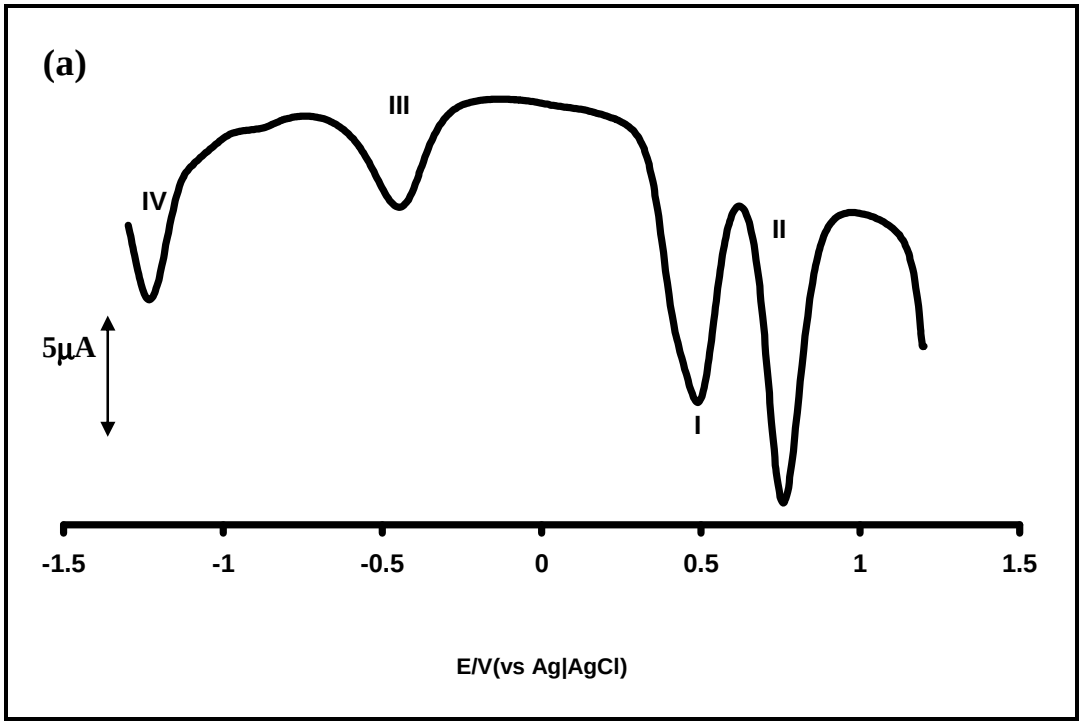

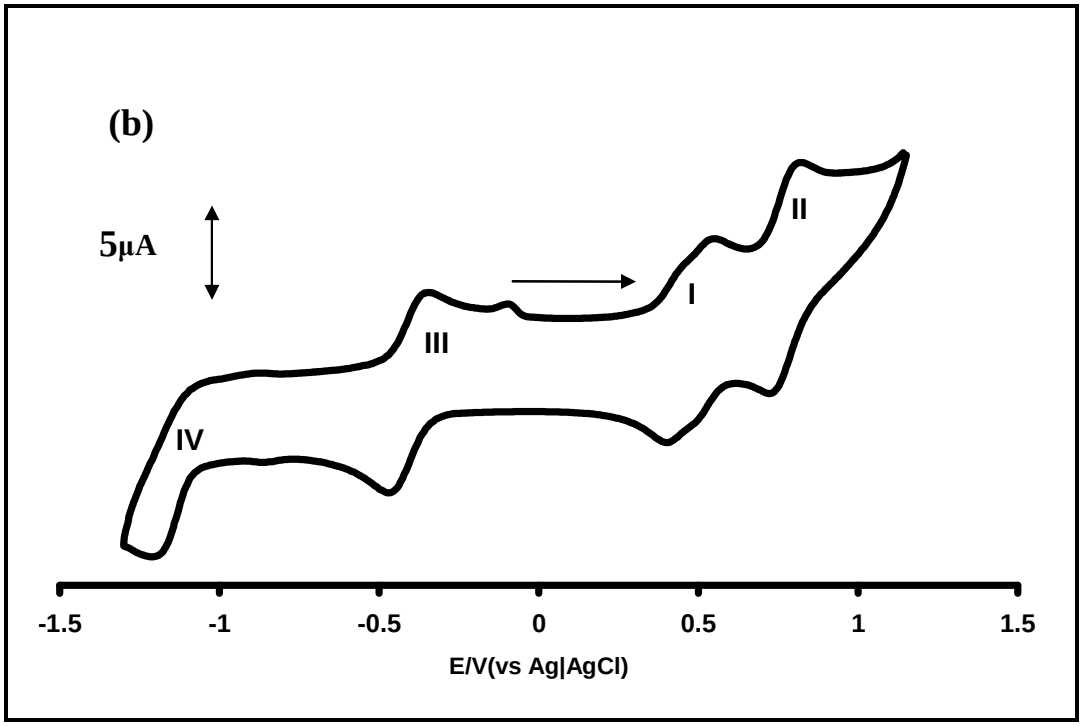

Figure 3.2: Square wave (a) and cyclic (b) voltammograms for **AcMnOPTPc** in DCM containing 0.1 M $TBABF_4$. Scan rate = 100 mV s^{-1}.

Table 3.2: Electrochemical data of alkylthio derivatised MnPc complexes. Unless otherwise stated, the data collected in DMF containing $TBABF_4$. Half-wave potential ($E_{½}$) as V vs Ag|AgCl

Complexa[a]	$Mn^{II}Pc^{-2}$/ $Mn^{II}Pc^{-3}$ (**IV**)	$Mn^{II}Pc^{-2}$/ $Mn^{I}Pc^{-2}$ (**IV**)	$Mn^{III}Pc^{-2}$/ $Mn^{II}Pc^{-2}$ (**III**)	$Mn^{IV}Pc^{-2}$/ $Mn^{III}Pc^{-2}$ (**I**)	$Mn^{IV}Pc^{-1}$/ $Mn^{IV}Pc^{-2}$ (**II**)	ref
AcMnOPTPc[b]	-1.24		-0.46	0.47	0.75	This work
MnTBMPc	-0.84		-0.08	~0.3	0.87	[21]
MnTDMPc	-0.98		-0.26	~0.3	0.83	[21]
α-MnMPyPc	-0.76		-0.051		1.18	[22]
α-Q-MnMPyPc[c]	-0.71	-0.59	-0.056		1.10	[22]
MnMPyPc			-0.057		1.34	[22]
Q-MnMPyPc[c]		-0.56	-0.063		1.13	[22]

[a] TDMPc = tetra dodecylmercapto phthalocyanine, TBMPc = tetra benzylmercapto phthalocyanine, TMPyPc = tetra mercaptopyridine phthalocyanine,

[b] values recorded in DCM containing $TBABF_4$, [c] quaternized derivative

3.2.1.2 Spectroelectrochemistry

Fig. 3.3a shows the spectral changes observed during the reduction of **AcMnOPTPc** at potentials of process **III**. The starting spectrum in Fig. 3.3a is slightly shifted to longer wavelengths compared to Fig. 3.1, due to the presence of an electrolyte in DCM for the former. Upon reduction, there was a blue shift in the Q band from 908 to 795 nm, Table 3.3, with a concurrent decrease of the charge transfer bands at 571 nm, and the colour of the complex changed from purple to blue. These spectral changes occurred with clear isosbestic points at 831 nm, 634 nm and 536 nm indicating that the redox process involves only two species. A shift in the position of the Q band without a decrease in its intensity is indicative of a metal-based process and the blue shift in the Q band upon reduction is typical of $Mn^{III}Pc^{-2}$ to $Mn^{II}Pc^{-2}$ reduction [54]. Thus spectral changes in Fig. 3.3a confirmed that process **III** is due to the redox couple $Mn^{III}Pc^{-2}/Mn^{II}Pc^{-2}$ (n was calculated, from Q = n.F.c.V, to be approximately 1, n = 0.8).

Fig. 3.3b shows spectral changes observed on application of potentials of process **IV**. A drastic decrease in the intensity of the Q-band and the formation of new features between 500 and 700 nm is typical [50] of ring-based processes in MPc complexes. Hence the spectral changes are assigned to $Mn^{II}Pc^{-2}/Mn^{II}Pc^{-3}$. As mentioned in the introduction, the first reduction in $Mn^{II}Pc^{-2}$ complexes has been reported to occur either at the metal to form $Mn^{I}Pc^{-2}$ species or at the ring to form $Mn^{II}Pc^{-3}$ species. The latter is observed in this work and has been reported by our group [21] and others [92]. To confirm the origin of the oxidation processes (**I** and **II**), controlled potential electrolysis was also conducted, Fig. 3.4. Spectral changes showed a shift in the Q

band from 908 nm to 920 nm, Fig. 3.4b. The shift in the Q-band is typical [54] of metal-based oxidation, hence the formation of a $Mn^{IV}Pc^{-2}$ species. The spectrum of $Mn^{IV}Pc$ species is not well known apart from a recent report [92]. This work provides another example of a relatively well-defined spectrum of the rare $Mn^{IV}Pc^{-2}$ species. The application of potential of process **II** resulted in the collapse of the Q band and the formation of new peaks at 809 and 720 nm with an increase in intensity at ~ 520 nm, Fig. 3.4c. The collapse of the Q band and the formation of new less intense bands is typical [50] of ring oxidation in MPc complexes. Thus couple **II** is assigned to a $Mn^{IV}Pc^{-1}/Mn^{IV}Pc^{-2}$ process.

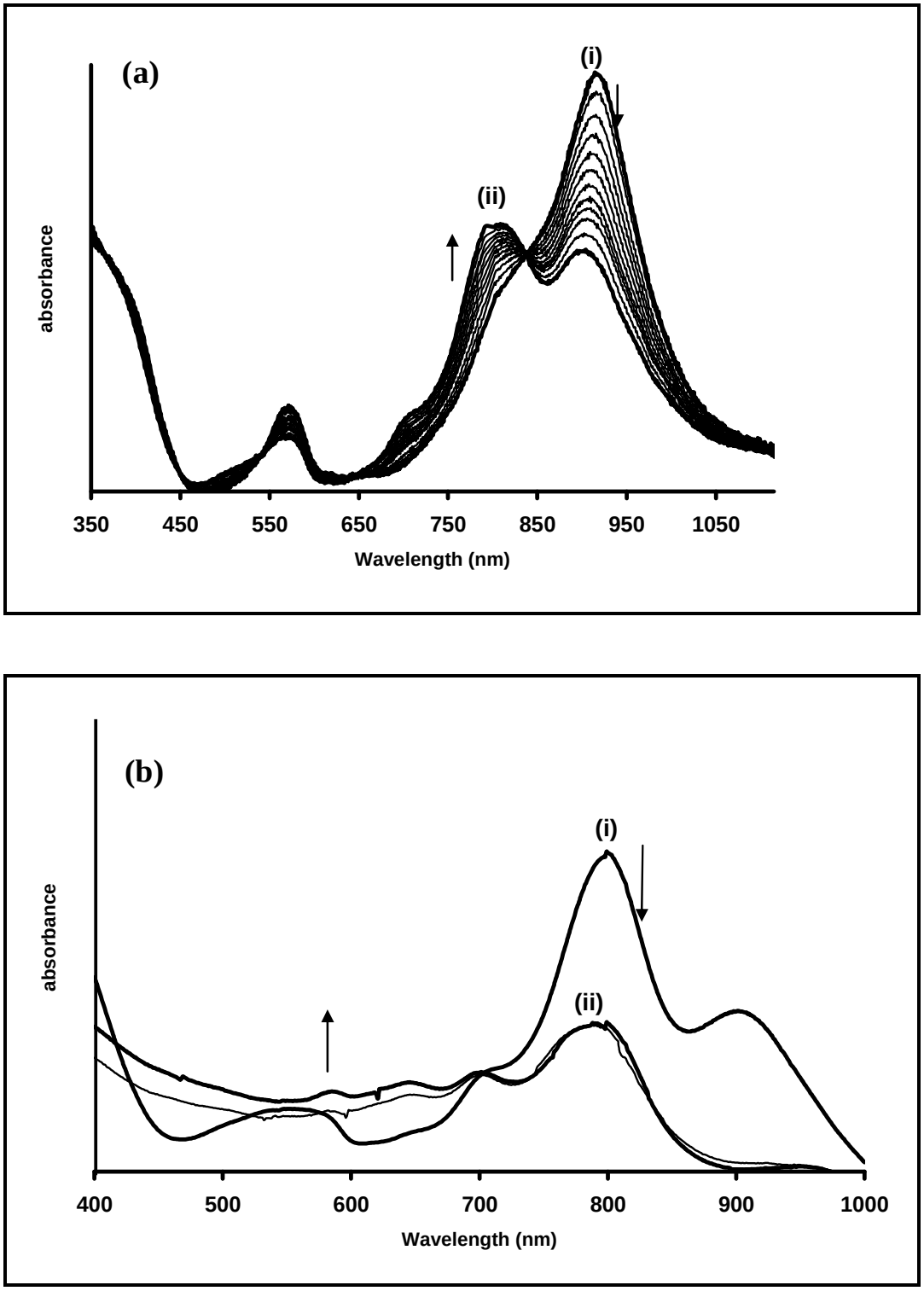

Figure 3.3: UV-Vis spectral changes for **AcMnOPTPc** observed using controlled potential electrolysis at (a) -0.5V (Process **III**) and (b) -1.3V (Process **IV**). (i) before electrolysis and (ii) at the end of electrolysis. Electrolyte = DCM containing 0.1 M $TBABF_4$. First scan in (b) same as last scan in (a).

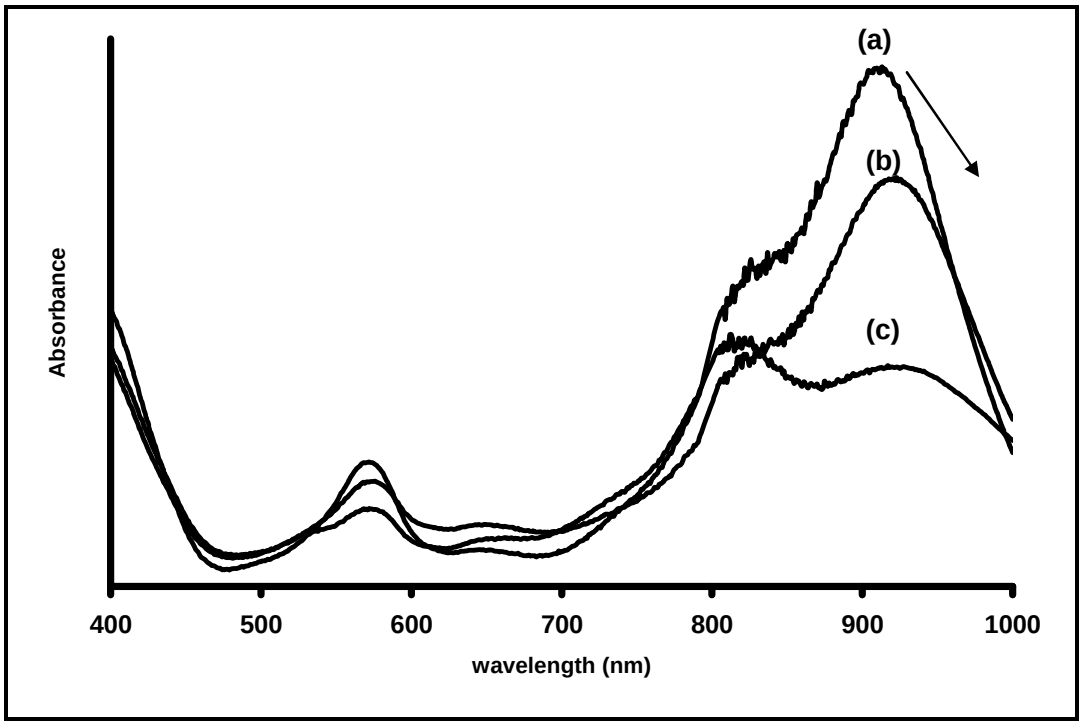

Figure 3.4: UV-Vis spectral changes for **AcMnOPTPc** observed before (a) and after controlled potential electrolysis at +0.9 V (Process **I**) (b) and at + 1.2 (c) (Process **II**). Electrolyte = DCM containing 0.1 M $TBABF_4$.

Table 3.3: Q band assignments in DCM containing $TBABF_4$ unless otherwise stated[a].

Complex	**λ (nm)**		
	$M^{IV}Pc$	$M^{III}Pc$	$M^{II}Pc$
AcMnOPTPc	920	908 (893)	795
OVOPTPc	853 (842)		
OTiOPTPc	814 (808)	774	769

[a]Values in brackets are in DCM only with no electrolyte.

3.2.2 Electrochemistry of OVOPTPc

3.2.2.1 Voltammetry

The cyclic (CV) and square wave (SWV) voltammetries of complex **OVOPTPc** were performed in de-aerated DCM containing $TBABF_4$ as electrolyte, Fig. 3.5. Two oxidation and three reduction couples are observed. This is one of the few VPc complexes which show two oxidation peaks [51]. The half-wave potentials ($E_{1/2}$) for complex **OVOPTPc** are summarised in Table 3.4 together with reported data for some VPc derivatives. The redox processes for complex **OVOPTPc** are labelled **I** ($E_{1/2}$ = 0.59 V), **II** ($E_{1/2}$ = 0.97 V), **III** ($E_{1/2}$ = -0.58 V), and **IV** ($E_{1/2}$ = -0.93 V), **V** ($E_{1/2}$ = -1.18 V), versus Ag|AgCl in Fig. 3.5. All the redox processes showed both the cathodic and anodic components. The cathodic to anodic peak separation (ΔE) ranged from 90 to 120 mV, suggesting slow electron transfer. A ΔE value of 90 mV was obtained for ferrocene. The cathodic to anodic peak current ratio (I_{pc}/I_{pa}) were near unity. For all redox couples, plots of peak current (I_p) versus the square root of scan rate ($v^{1/2}$) were linear, thus suggesting diffusion control at the electrode surface. Table 3.4 also shows that the **OVOPTPc** complex reported in this work and containing sulfur groups (due to the greater electron donating effect of the sulfur group) is more easily oxidised than the complexes containing oxo groups though different substituents are attached. It would therefore be expected that the **OVOPTPc** complex would be more difficult to reduce; this is the case in Table 3.4 when comparing with fluorinated $OVPcF_{16}$. Also comparing **OVOPTPc** with other complexes in Table 3.4, which exhibited only ring based oxidation and reduction processes, we would expect the former also to show only ring based processes since the peak potentials are comparable except for slight differences due to the different

substituents. Also the redox processes are in the range for ring-based processes in MPc complexes [48].

The first oxidation process showed an overlap of two peaks labelled **I'** and **I**. The overlap is probably due to aggregation at concentrations used for cyclic voltammetry. Such closely spaced cyclic voltammograms are associated with aggregation [48]. On dilution of the solution, there was disappearance of process **I'**, only one process remained as **I**.

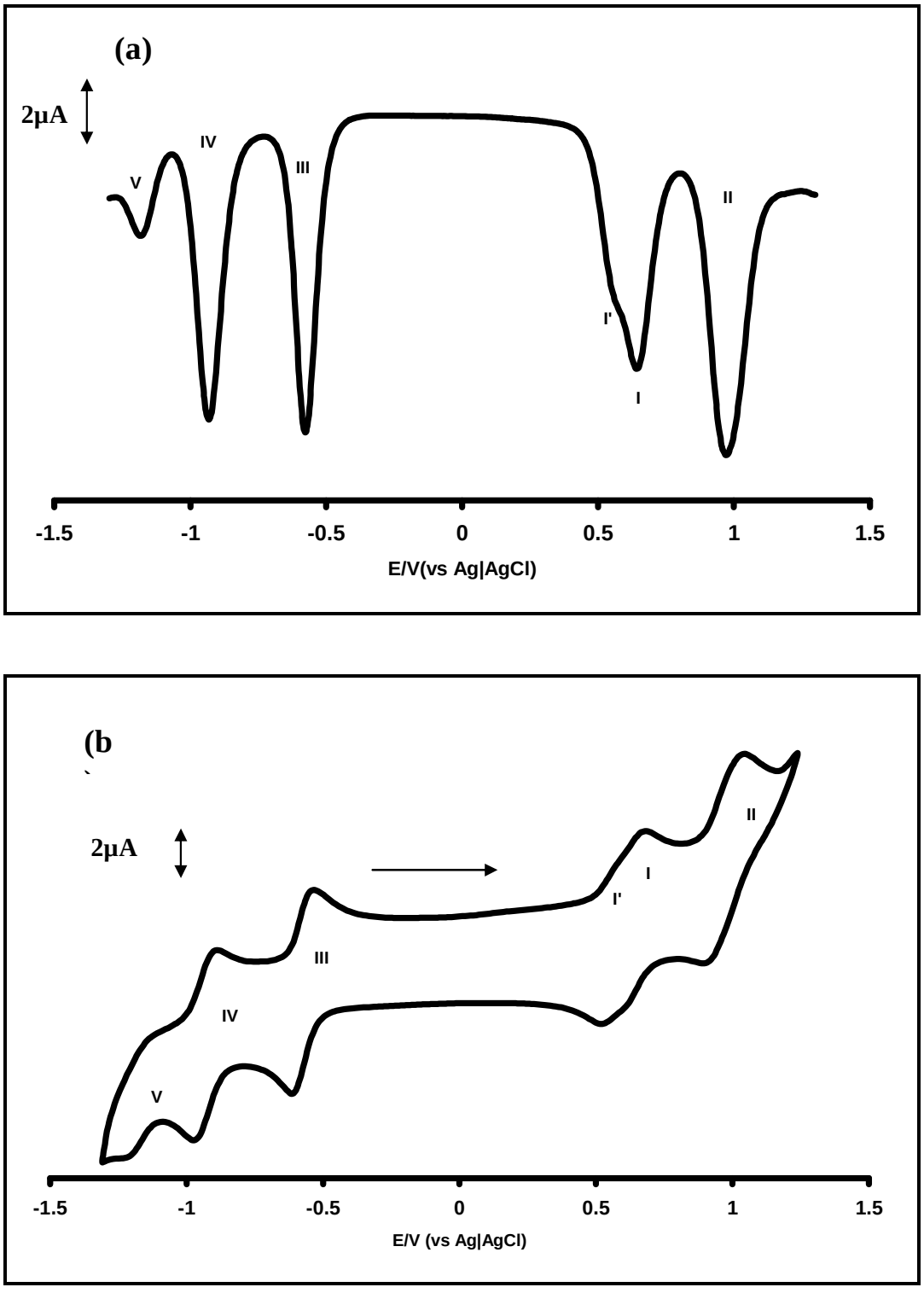

Figure 3.5: Square wave (a) and cyclic (b) voltammograms of **OVOPTPc** in DCM containing $TBABF_4$. Scan rate = 100 mV s^{-1}.

Table 3.4: Electrochemical data of OVPc complexes. Unless otherwise stated, the data collected in DMF containing tetrabutylammonium perchlorate (TBAP). Half-wave potential ($E_{½}$) as V vs SCE unless otherwise stated.

Complex	$V^{IV}Pc^{4-}$/ $V^{IV}Pc^{5-}$ (**V**)	$V^{IV}Pc^{3-}$/ $V^{IV}Pc^{4-}$ (**IV**)	$V^{IV}Pc^{2-}$/ $V^{IV}Pc^{3-}$ (**III**)	$V^{IV}Pc^{1-}$/ $V^{IV}Pc^{2-}$ (**I**)	$V^{IV}Pc^{0}$/ $V^{IV}Pc^{1-}$ (**II**)	ref
OVOPTPc[a]	(-1.18) -1.14	(-0.93) -0.89	(-0.58) -0.54	(0.59) 0.68	(0.97) 1.02	This work
$OV[(OC_6H_3(t\text{-}Bu)_2)_4Pc]$	-1.94	-0.97	-0.51	0.94	1.34	[51]
$OV[(OC_8H_{17})_4Pc]$	-2.07	-1.12	-0.62	0.76	1.21	[51]
$OV[(Bu)_4Pc]$		-1.08	-0.58	0.94		[51]
$OV(F_{16}Pc)$	-1.41	-0.62	-0.29	1.34		[37]

[a] values recorded in DCM containing $TBABF_4$. Values in brackets are vs. Ag|AgCl. A conversion factor of E½ (SCE) = E½ (Ag|AgCl) + 0.045 V has been applied [48]

3.2.2.2 Spectroelectrochemistry

Fig. 3.6a shows the spectral changes observed during the reduction of **OVOPTPc** at potentials of process **III**. At the high concentrations used for the OTTLE cell, the original spectrum before reduction is broad due to aggregation. Aggregation in MPc complexes is usually depicted as a coplanar association of rings progressing from monomer to dimer and higher order complexes. Aggregation is dependent on the concentration, nature of the solvent, nature of substituents, complexed metal ions and temperature [93]. In the aggregated state the electronic structure of the complexed

phthalocyanine rings are perturbed resulting in alternation of the ground and excited state electronic structures [94], thus broadening of the spectra.

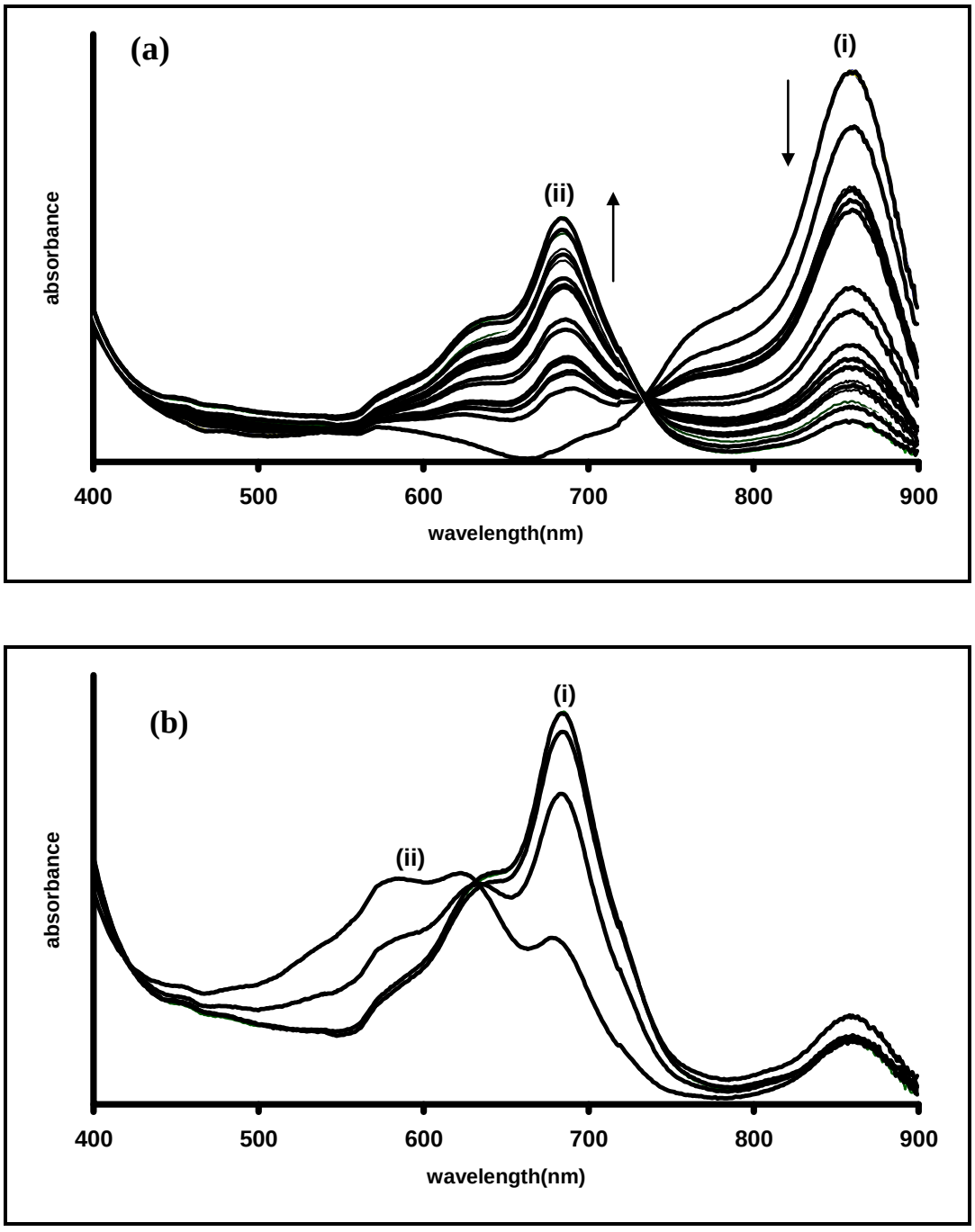

Figure 3.6: UV–Vis spectral changes for **OVOPTPc** observed using controlled potential electrolysis at (a) -0.7 V, (b) -1.2. First spectrum in (b) is the same as the last spectrum in (a). Electrolyte = DCM containing 0.1 M $TBABF_4$. Electrolysis time was 30 min for each redox process.

Upon reduction of **OVOPTPc**, there is a blue shift in the Q band from 853 to 680 nm and at the same time the colour of the complex changed from purple to green, Fig. 3.6a. A shift of peaks in the presence of electrolyte (from 842 nm (DCM only) to 853 nm (DCM with electrolyte)) is observed; Table 3.3. These spectral changes occurred with a clear isosbestic point at 731 nm. The number of electrons transferred (n) was calculated to be approximately 1. Metal-based redox processes can be identified using UV–Vis spectra since a definite shift in the Q band (without significant lowering in intensity) is generally observed [54]. Spectral changes in Fig. 3.6a are not similar to those observed for ring reduction in OVPc derivatives (OV[Pc(OC_6H_3(t-Bu)$_2$)$_4$] and OV[Pc(C_8H_{17})$_4$]) [51], in that new weak bands were observed at 571, 618 and 646 nm upon reduction of the latter complexes. For **OVOPTPc** complex, the peak at 680 nm is quite intense, but since only ring based processes have been reported [37, 47, 51] for VPc complexes, the spectral changes observed in Fig. 3.6a may be associated with ring based reduction (to Pc(-3) species), with differences in absorption band intensity and positions being due to differences in substituents. The green colour of ring reduced VPc derivative **(OVOPTPc)** observed in this work, is uncommon in phthalocyanine chemistry, where reduction leads to purplish colour. The green colour is due to the fact that the shift of the main absorption band is to 680 nm, while in general for Pcs, the main (weak) absorption bands occur between 500 and 600 nm [50, 95] for ring reduction. The peak at 680 nm is intense relative to the original species with a reduction in log ε of only 20% (assuming complete transformation) compared to the more common ring reduction in Pcs with large reduction in intensity upon reduction. Fig. 3.6b shows spectral changes observed on further reduction at potentials of couple **IV**. There was emergence of new peaks at 578 and 620 nm. The spectral changes shown in Fig. 3.6b are similar to those

observed for other OVPc derivatives, (OV[Pc(OC_6H_3(t-Bu)$_2$)$_4$] and OV[Pc(C_8H_{17})$_4$]) which were assigned to ring based processes [51]. Thus spectral changes shown in Fig. 3.6b are assigned to the formation of Pc^{-4} species, hence the couple $V^{IV}Pc^{-3}/V^{IV}Pc^{-4}$. Process **V** may be assigned to further ring reduction and the formation of $V^{IV}Pc^{-5}$.

Spectroelectrochemical characterisation was also done to determine the origin of the oxidation couples. Fig. 3.7 shows the spectroelectrochemical changes observed upon oxidation at the potential of process **I**. Oxidation at the potential of peak **I** showed the decrease in intensity of the Q band and formation of a weak new peak in the 500–700 nm region, this is indicative of a ring based process and assigned to the oxidation of $V^{IV}Pc^{-2}$ to $V^{IV}Pc^{-1}$, Fig. 3.7.

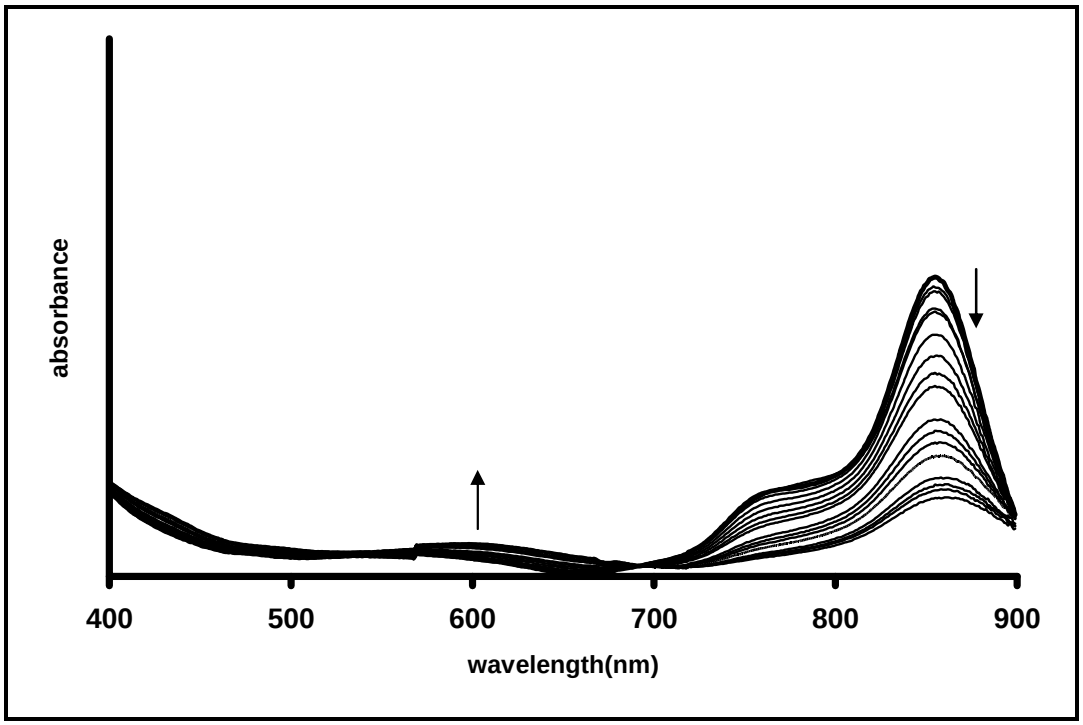

Figure 3.7: UV–Vis spectral changes for **OVOPTPc** observed using controlled potential electrolysis at 0.8 V electrolyte = DCM containing 0.1 M $TBABF_4$. Electrolysis time was 30 min

3.2.3 Electrochemistry of OTiOPTPc

3.2.3.1 Voltammetry

Detailed electrochemical characterisation of substituted OTiPcs is still under-developed. The cyclic (CV) and square wave voltammograms (SWV) of the complex was performed in de-aerated DCM containing $TBABF_4$ as electrolyte, Fig. 3.8. The half-wave potentials ($E_{1/2}$) of the couples are listed in Table 3.5. Four main redox processes (**I** to **IV**) are observed in Fig. 3.8. Couples **III** (-0.73 V) and **IV** (-1.09 V) are well defined and reversible with cathodic to anodic peak separation (ΔE) of ~ 100 mV. The cathodic to anodic peak current ratio (I_{pc}/I_{pa}) were near unity and linear

plots of I_p versus square root of the scan rate ($\upsilon^{1/2}$) were obtained for couples **III** and **IV**.

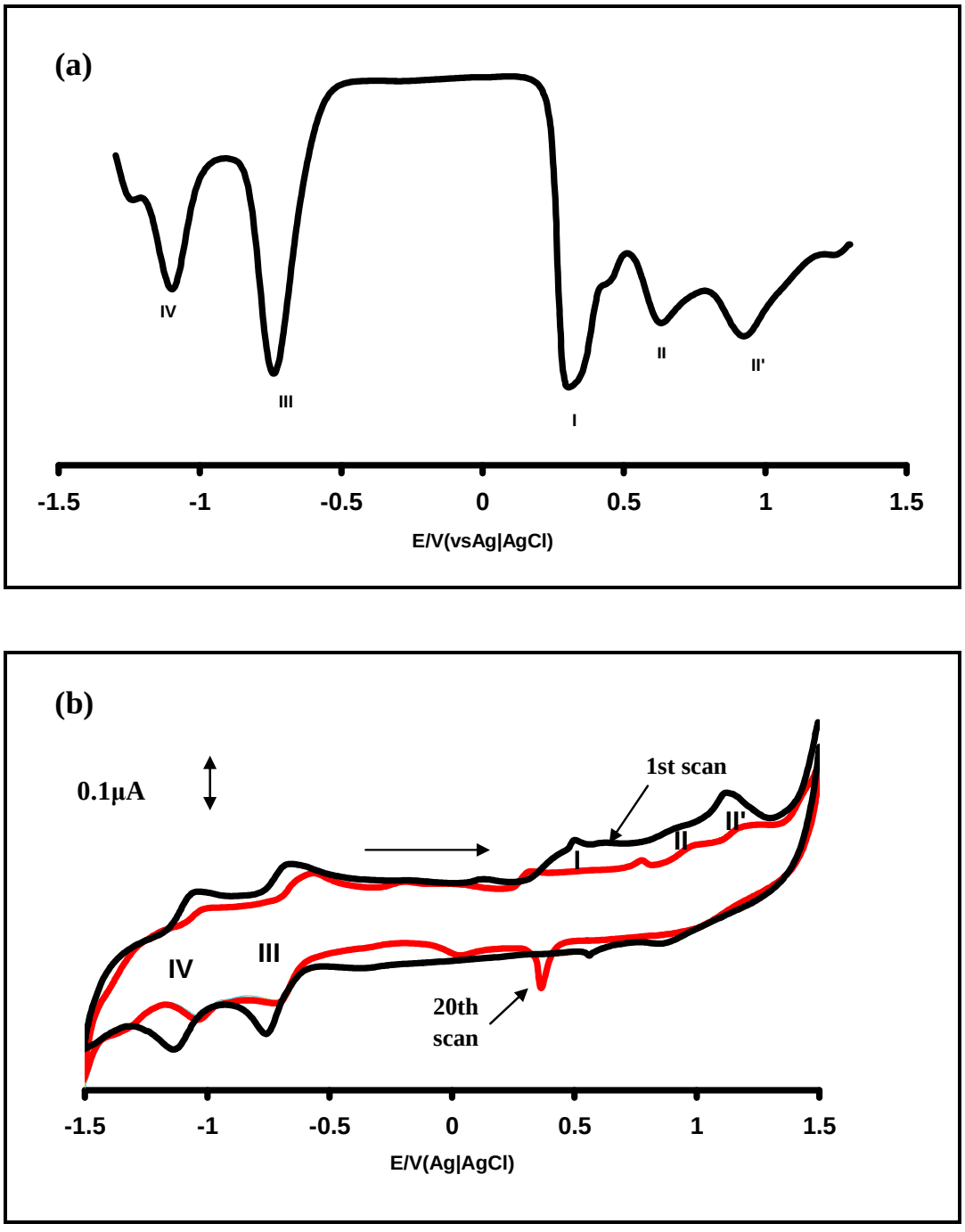

Figure 3.8: Square wave (a) and cyclic (b) voltammograms of **OTiOPTPc** in DCM containing 0.1 M $TBABF_4$. The SW voltammogram is for the 10th scan. Scan rate = 100 mV s^{-1}.

Couples **III** and **IV** shifted to more positive potentials with scan number (Fig. 3.8b) probably due to polymerization effects discussed below. The oxidation process showed a peculiar behaviour in that the anodic process **I** had a broad pre-peak followed by a sharp peak typical of adsorption [96, 97]. It is known [96] that the adsorption of a product of the electrode reaction results in the formation of a sharp peak preceded by a more regular peak, the latter being due to the diffusion of the electroactive species from solution to the electrode. During the first scan in Fig. 3.8b, a broad peak preceding a sharp peak around 0.5 V was observed. The cathodic (return) scan of process **I (**Fig. 3.8b) showed a sharp peak corresponding to the peak observed in the forward direction. The peak separation for couple **I** was zero confirming that the process is due to adsorption species. On subsequent scans (20^{th} scan in Fig.3.8b) a sharp peak was observed at 0.36 V due to desorption of the adsorbed species. Process **I** moved to less positive potentials after several scans, again with a peak separation of 0 V due to adsorbed species. The cyclic voltammograms obtained for second and subsequent scans show more weak peaks (between 0.5 and 1 V) that are most likely due to the polymer formed on cycling the monomer in solution. Electropolymerisation of the complex onto the electrode is probably facilitated through radical polymerisation from sulphur groups, as is the case with amino groups in MPc complexes [98]. Adsorption and sharp peaks have been observed before for thiol substituted ZnPc complexes [99], and the complexes showed decomposition on oxidation. For process **I**, plots of scan rate versus current were linear (figure not shown) confirming adsorption of the complex. Process **II** in Fig. 3.8b showed regular (not sharp) anodic and cathodic currents during the first scan, probably due to diffusion of the complex from the solution. An irreversible peak (**II'**) is observed in Fig. 3.8b near 1 V. It has been reported [100] that depending on the

ring substituents, oxidation of the TiPc complexes may or may not be observed, depending on whether the substituents result in the shift of potentials to values where oxidation can no longer be observed since it is outside the usable range of the solvent-electrolyte-electrode system employed. The thiol ligands employed in this work are expected to make oxidation easier, hence allowing the observation of the oxidation peaks.

Table 3.5: Electrochemical data of alkylthio derivatised TiPc complexes. Unless otherwise stated, the data collected in DMF containing $TBABF_4$. Half-wave potential ($E_{½}$) as V vs Ag|AgCl.

Complex	$Ti^{II}Pc^{2-}$/ $Ti^{II}Pc^{3-}$ (**V**)	$Ti^{III}Pc^{2-}$/ $Ti^{II}Pc^{2-}$ (**IV**)	$Ti^{IV}Pc^{2-}$/ $Ti^{III}Pc^{2-}$ (**III**)	Oxidation processes	ref
OTiOPTPc[a]		-1.09	-0.73	0.54 (**I**), 0.36 (**II**), 0.95 (**II'**)	This work
α[$(SCH_2C_6H_6)_4$Pc]TiO	-1.33	-0.46	-0.07	No oxidation processes	[23]
[$(SCH_2C_6H_5)_4$Pc]TiO	-1.30	-0.40	-0.09	No oxidation processes	[23]
α-[$(SC_6H_5)_4$Pc]TiO	-1.20	-0.37	-0.07	No oxidation processes	[23]
[$(SC_6H_5)_4$Pc]TiO[a]	-1.28	-0.42	-0.09	No oxidation processes	[23]

[a] Values recorded in DCM containing $TBABF_4$.

3.2.3.2 Spectroelectrochemistry

Spectroelectrochemistry was employed to confirm the redox processes. Fig. 3.9a shows the UV/Vis spectral changes observed on reduction of **OTiOPTPc** at potentials of process **III**. The Q band of **OTiOPTPc** is shifted to longer wavelengths in the presence of an electrolyte, from 808 nm to 814 nm, as shown in Table 3.3. The Q band shifts from 814 nm to 774 nm with isosbestic points at 797, 719, 629 and 534 nm. The spectral changes are typical [54] of metal based reduction in MPc complexes and are similar to those observed for thiol substituted TiPc complexes [23]. Further reduction at potentials of process **I**, resulted in spectral changes shown in Fig. 3.9b and consisted of the shift in the Q-band from 774 nm to 769 nm which shows the formation of $Ti^{II}Pc^{-2}$ species similar to literature reports [100]. In both cases n was found to be unity confirming one electron transfer. Attempts to oxidize complex **OTiOPTPc** resulted in decomposition, Fig. 3.10. Such decomposition on oxidation of thiol MPc complexes has been reported, and is as discussed above [99].

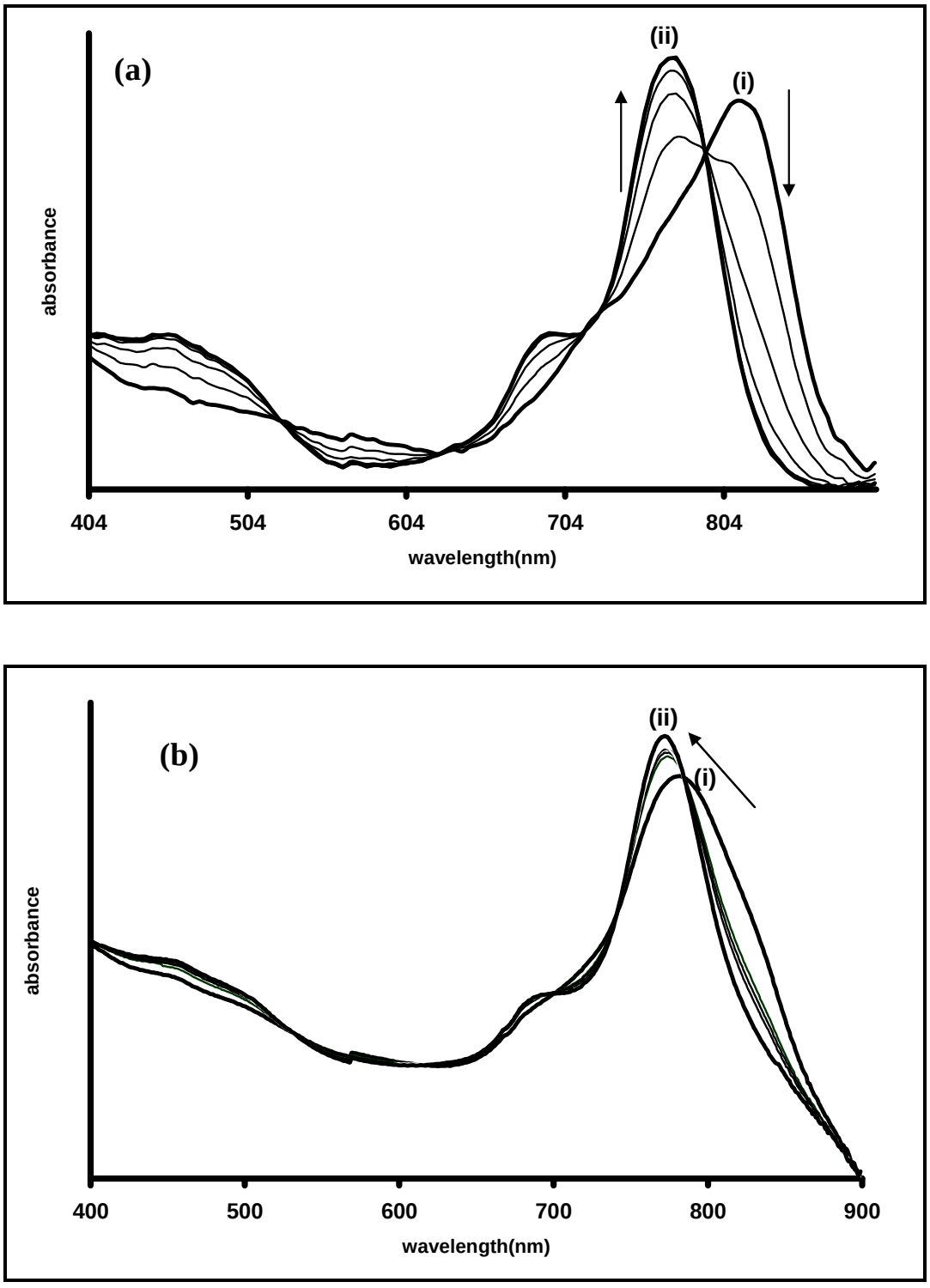

Figure 3.9: UV-Vis spectral changes for **OTiOPTPc** observed using controlled potential electrolysis at (a) -0.9V (Process **III**) and (b) -1.3V (process **IV**). (i) before electrolysis and (ii) at the end of electrolysis. Electrolyte = DCM containing 0.1 M $TBABF_4$.

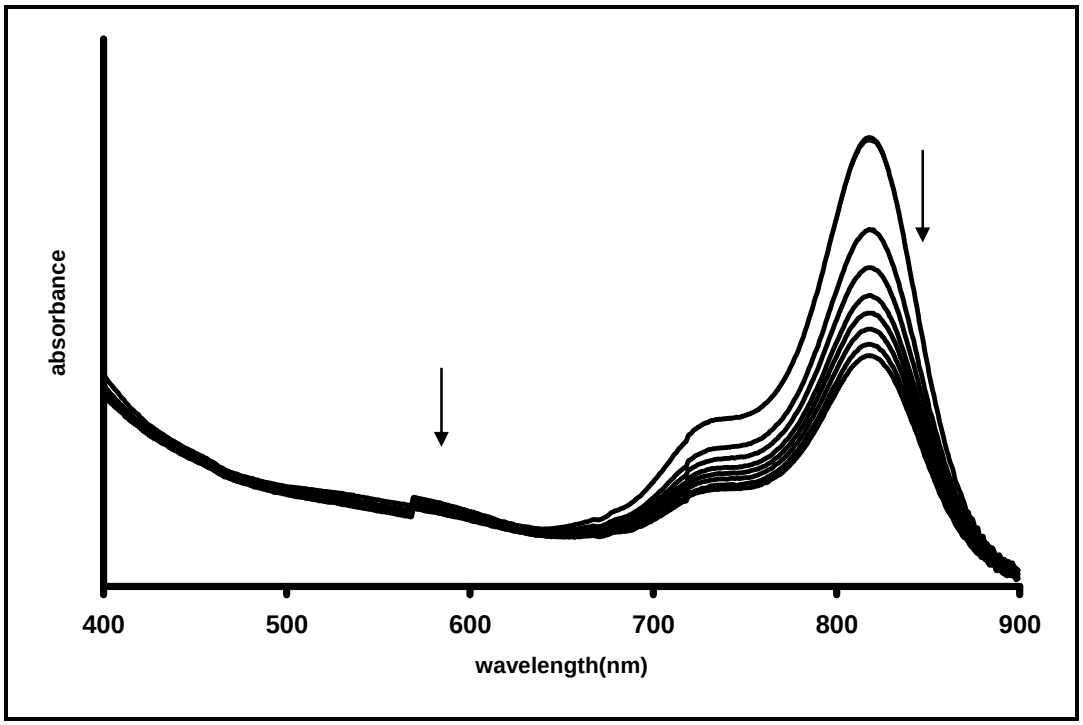

Figure 3.10: UV-Vis spectral changes for **OTiOPTPc** observed during controlled potential electrolysis at +1.0 V (Process **I**), Electrolyte = DCM containing 0.1 M $TBABF_4$.

3.3 Self assembled monolayer of MPc on Au

MPc-SAMs were successfully formed using **AcMnOPTPc**, **OVOPTPc** and **OTiOPTPc**. The formed SAMs were characterized using cyclic voltammetry. The integrity of the SAMs formed was determined by looking at the blockage of the Au oxidation peak in basic media (0.01M KOH), $[Fe(H_2O)_6]^{3+}/[Fe(H_2O)_6]^{2+}$ redox couple of $Fe(NH_4)(SO_4)_2$ and by also looking at the effect of MPc-SAM on the $[Fe(CN)_6]^{4+}/[Fe(CN)_6]^{3+}$ redox couple.

Table 3.6: A synopsis of the characterization parameters of AcMnOPTPc, OVOPTPc and OTiOPTPc self assembled on Au electrode surface

MPc-SAM	Γ_{MPc}[a] ($x10^{-10}$ mol cm^{-2})	Γ_{MPc}[b] ($x10^{-10}$ mol cm^{-2})	Γ_{ibf}
AcMOPTPc-SAM	1.41	1.31	0.89
OVOPTPc-SAM	0.93	1.15	0.90
OTiOPTPc-SAM	1.45	1.49	0.92

[a] values determined using equation 3.2, [b] values determined using equation 3.3

3.3.1 Characterisation of OVOPTPc-SAM, OTiOPTPc-SAM and AcMnOPTPc-SAM

In order to estimate the surface concentration of the complexes on gold electrodes, the real surface areas of the gold electrodes were first determined using the conventional method, using Randles-Sevcik equation [78], Eq 3.1:

$$I_{pa} = (2.69 \times 10^5)\, n^{3/2}\, D^{1/2}\, \nu^{1/2}\, AC \qquad 3.1$$

where n is the number of electron transferred (n = 1), D is the diffusion coefficient of $[Fe(CN)_6]^{3-}$ (7.6 x10^{-6} cm^2/s [78]), *v* is the scan rate, A is the effective surface area, C is the bulk concentration of $[Fe(CN)_6]^{3-}$ (1mM). A plot of I_{pa} vs $v^{1/2}$ was generated and the slope was used to determine the effective real surface area, A. The values of the real surface area were 0.0224 cm^2, 0.0253 cm^2 and 0.030 cm^2 for **OTiOPTPc**-SAM, **AcMnOPTPc**-SAM and **OVOPTPc**-SAM, respectively.

Using cyclic voltammogram the real gold surface area is expected to be larger than the geometric area (0.0201 cm^2) due to surface roughness, as the values show. The trend in the real surface area among the MPc-SAMs was **OVOPTPc**-SAM > **AcMnOPTPc**-SAM > **OTiOPTPc**-SAM.

The surface roughness is equal to I_{pa} (experimental)/I_{pa} (theoretical), where I_{pa} (theoretical) is the current determined from equation 3.1, using the geometric surface area (0.0201 cm^2) of the electrode and I_{pa} (experimental), which is the current from the experiment. The values determined for the surface roughness are 1.11, 1.26, and 1.49 for **OTiOPTPc**-SAM**, AcMnOPTPc**-SAM and **OVOPTPc**-SAM respectively.

The surface coverage or concentration of the SAM (Γ_{MPc}) was determined using the peaks in Fig. 3.11 and equation 3.2 which was introduced in Chapter 1 as equation 1.8.

$$\Gamma_{MPc} = Q/nFA \qquad 3.2$$

where Q is the background corrected charge of the cathodic peaks in Fig. 3.11, n the number of electrons, F is the faraday's constant and A is the real surface area of the electrode. The calculated surface coverages for **OVOPTPc**-SAM, **OTiOPTPc**-SAM and **AcMnOPTPc**-SAM are 0.93 x 10^{-10}, 1.45 x 10^{-10} and

1.41 x 10^{-10} mol cm^{-2}, respectively. The determined values for the **OVOPTPc**-SAM, **OTiOPTPc**-SAM and **AcMnOPTPc**-SAM are close to 1 x 10^{-10} mol cm^{-2}, confirming monolayer formation [80].

The surface concentration was estimated using a second method. The charge difference between the bare gold (Q_{Bare}) and the MPc-SAM's (Q_{SAM}) (Fig. 3.11) is proportional to the fraction of the gold sites covered by the MPc-SAMs.

This fraction is divided by three to get the charge proportion of gold sites covered with MPc-SAM, according to equation 3.3 which was introduced in Chapter 1 as Eq 1.9 [79].

$$Au.H_2O + 2H_2O \rightleftharpoons Au(OH)_3 + 3H^+ + 3e^- \qquad 3.3$$

The amount of gold sites covered by the MPc-SAM is then divided by eight (each MPc molecule is assumed to consume eight gold sites since the complexes are octa substituted with alkyl thio groups) and then divided by the real surface area of the gold electrode surface to get the charge density proportional to each MPc molecule. These values can then be converted to the corresponding surface concentration (Γ_{MPc}, mol/cm^2) by dividing them with the Faraday constant (96485 C mol^{-1}). The surface concentrations found were 1.15 x10^{-10}, 1.31 x10^{-10} and 1.49 x10^{-10} mol cm^{-2} for **OVOPTPc**, **AcMnOPTPc** and **OTiOPTPc** respectively, values which are similar to those determined using equation 3.2, indicating monolayer formation.

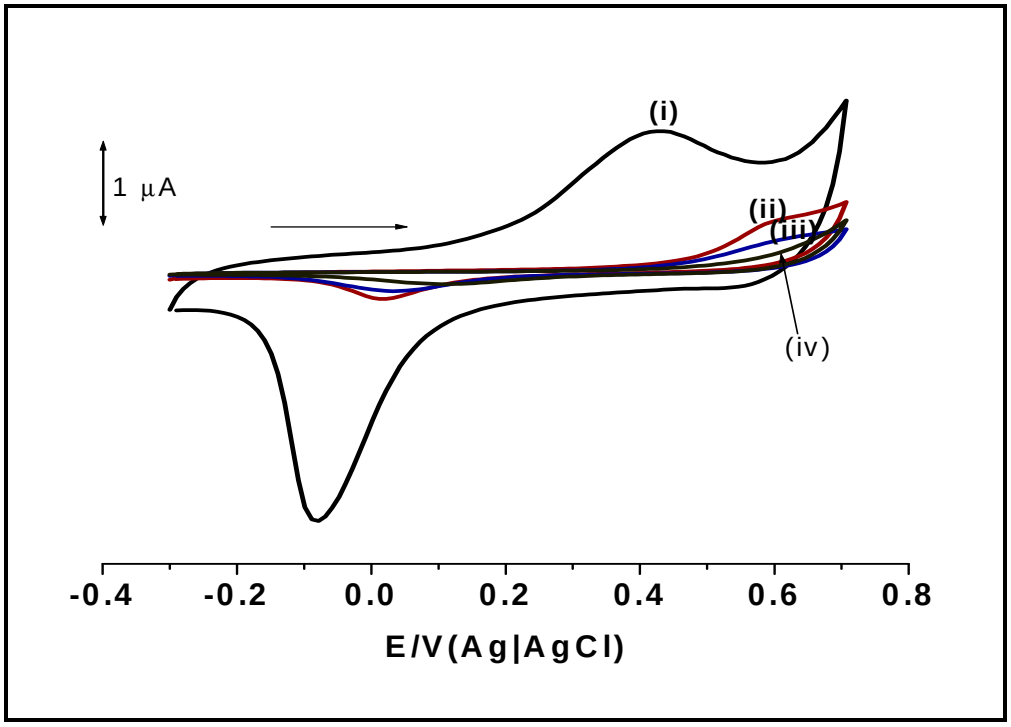

Figure 3.11: Cyclic voltammograms of (i) bare Au electrode (ii) **AcMnOPTPc**-SAM (iii) **OTiOPTPc**-SAM, (iv) **OVOPTPc**-SAM in 0.01 m KOH. Scan rate = 100 mVs^{-1}

As previously mentioned; methods that are used to determine the integrity of the SAMs on gold electrodes include, the blockage of the gold oxide peak [101, 102] and the blockage of the Fe^{3+}/Fe^{2+} redox couple. Fig. 3.11 shows that all MPc-SAMs exhibit blockage of the gold oxidation/reduction process in 0.01 M KOH as judged by the decrease in the peaks on modification of the electrode. The **OVOPTPc**-SAM (Fig. 3.11 (iv)) showed virtually no peak at -0.1 V due to gold oxide reduction, while AcOMnOPThPc-SAM (Fig. 3.11 (ii)), and **OTiOPTPc**-SAM (Fig. 3.11 (iii)) showed some peaks, but very small, thus the increasing order of blockage is **OVOPTPc**-SAM > **OTiOPTPc**-SAM > **AcMnOPTPc**-SAM. The peaks near 0.6 V for the modified electrode could be due to the MPc ring processes.

Using Fig. 3.11, the formed SAMs were further characterized by determining the ion barrier factor ($\Gamma_{ibf.}$). This is done by monitoring the disappearance of the gold oxide

reduction peak in Fig. 3.11. The Γ_{ibf} is the measure of the MPc-SAMs effectiveness in preventing the interaction of the gold electrode surface with the electrolyte.

The Γ_{ibf} was determined using Eq. 3.4 which was introduced in Chapter 1 as Eq 1.10

$$\Gamma_{ibf} = 1 - (Q_{SAM}/Q_{BARE}) \qquad 3.4$$

where Q_{SAM} is the charge when **OVOPTPc**-SAM, **OTiOPTPc**-SAM or **AcMnOPTPc**-SAM is used and Q_{BARE} is the charge for the bare electrode at - 0.1 v in Fig. 3.11. The Γ_{ibf} values were determined for **OVOPTPc**-SAM, **OTiOPTPc**-SAM and **AcMnOPTPc**-SAM to be 0.90, 0.92 and 0.89 respectively. This means that the modified surfaces are able to act as efficient barriers for the electrolyte with ion barrier factor values that are approximately 0.9 for all the complexes.

Fig 3.12a shows the inhibition of the $[Fe(H_2O)_6]^{3+}/[Fe(H_2O)_6]^{2+}$ redox process in the presence of SAMs. The $[Fe(H_2O)_6]^{3+}/[Fe(H_2O)_6]^{2+}$ redox process is a known reversible process of $Fe(NH_4)(SO_4)$ solution at bare gold electrodes, SAM modification of gold electrodes results in this process being inhibited. Comparing the three electrodes, **AcMnOPTPc**-SAM (Fig. 3.12a(ii)) shows larger currents and **OVOPTPc**-SAM (Fig. 3.12a(iv)) the lowest currents, showing again that the latter gives a better blockage of the electrode with the trend being the same as was observed for blockage of the gold oxide peak in Fig. 3.11, which is **OVOPTPc**-SAM > **OTiOPTPc**-SAM > **AcMnOPTPc**-SAM in terms of blocking the $[Fe(H_2O)_6]^{3+}/[Fe(H_2O)_6]^{2+}$ process.

The fast electron transfer of the $[Fe(CN)_6^{3-}]$ /$[Fe(CN)_6^{4-}]$ redox couple is not inhibited by the SAMs as shown in Fig. 3.12b as compared to the $[Fe(H_2O)_6]^{3+}$/$[Fe(H_2O)_6]^{2+}$ redox process (Fig. 3.12a), but there was a decrease in the current intensity coupled with an increase in cathodic to anodic peak potential separation (ΔE) on going from unmodified Au (ΔE = 91 mV) to **OTiOPTPc**-SAM (ΔE = 180 mV), **OVOPTPc**-SAM (ΔE = 113 mV) and **AcMnOPTPc**-SAM (ΔE = 107 mV). A slight shift of the half-wave potential for the $[Fe(CN)_6^{3-}]$ /$[Fe(CN)_6^{4-}]$ from $E_{½}$ = 0.14 V (Au) to **OTiOPTPc**-SAM ($E_{½}$ = 0.13 V), followed by **OVOPTPc**-SAM ($E_{½}$ = 0.12 V) and **AcMnOPTPc**-SAM ($E_{½}$ = 0.12 V) was observed. The lack of inhibition of $[Fe(CN)_6^{3-}]$ /$[Fe(CN)_6^{4-}]$ redox couple has been observed before using adsorbed cobalt tetra-aminophthalocyanine films on vitreous carbon electrodes [64]. It was reported [64] that both modified and unmodified electrodes showed the same redox potential and almost equal peak currents intensities for the $[Fe(CN)_6^{3-}]$ /$[Fe(CN)_6^{4-}]$ redox reaction, and that the modified electrodes act as electronic conductors which allow rapid electron transfer to the solution species [64]. The lack of inhibition for this couple was also observed for MnPc-SAMs [103].

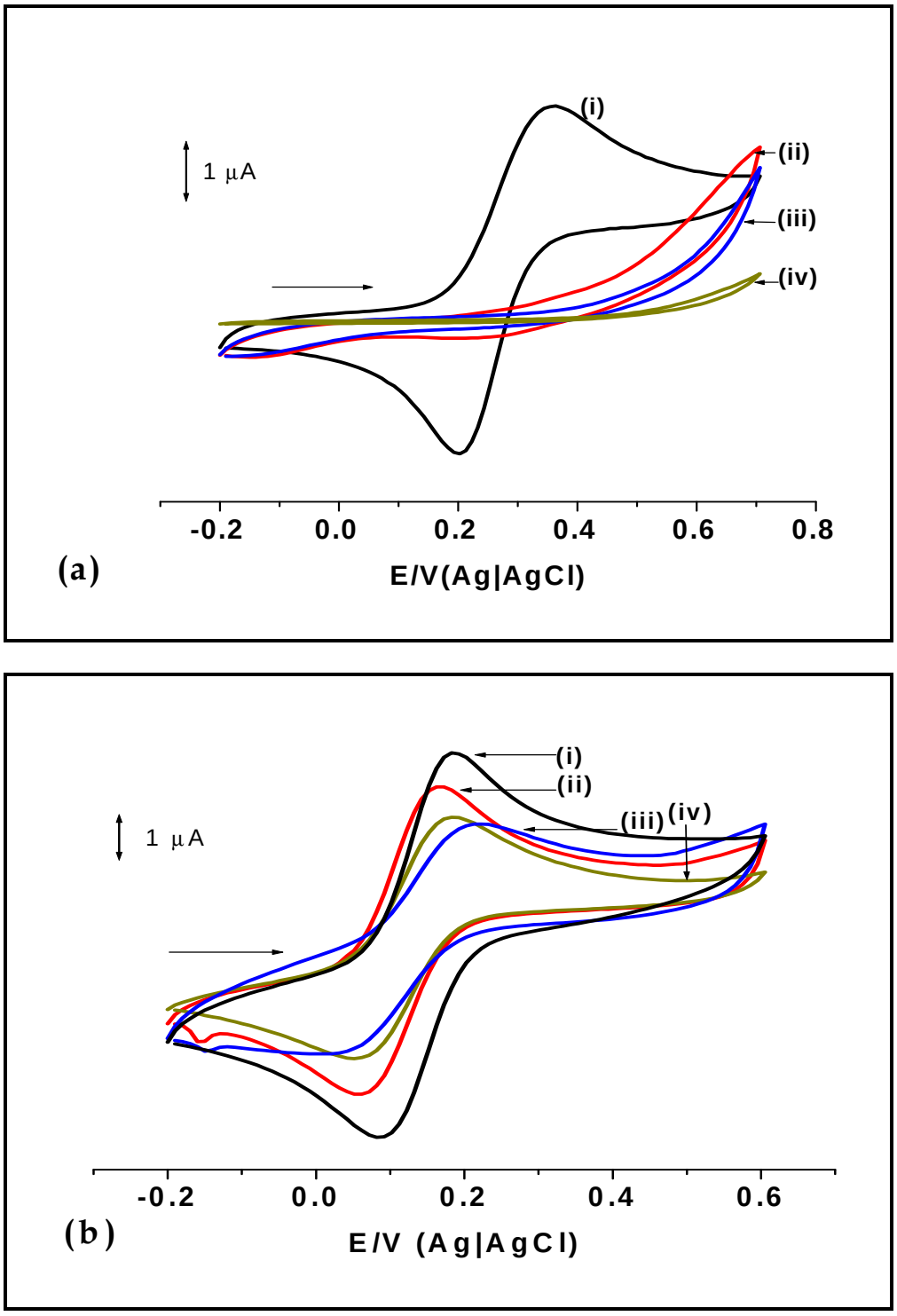

Figure 3.12: Cyclic voltammograms in (a) 1 mol cm^{-3} $Fe(NH_4)(SO_4)_2$ in 0.5 M $HClO_4$ and (b) 1mM $K_3Fe(CN)_6$ in 0.1 M KCl solution of (i) bare Au electrode (ii) **AcMnOPTPc**-SAM (iii) **OTiOPTPc**-SAM and (iv) **OVOPTPc**-SAM.
Scan rate = 100 mVs^{-1}.

3.3.2 MPc-SAM redox couples in pH 4 buffer

The MPc-SAM modified electrode was cyclised in pH 4 buffer in order to determine the peak potentials of the SAMs, Fig. 3.13. This pH was employed since it is used for L-cysteine analyses. Peaks due to the Mn^{IV}/Mn^{III} couple, Fig 3.13a, were observed for **AcMnOPTPc**-SAM at potentials that are between ~0V and 0.2 V which is comparable with the potential values which have been previously [83] reported. The **OTiOPTPc**-SAM (Fig. 3.13b) showed a weak feature near 0V assigned to a ring oxidation process in comparison with literature for adsorbed TiPc derivatives [104] Repetitive scanning in pH 4 buffer of the **OVOPTPc**-SAM, Fig 3.13c showed two redox couples which may be attributed to $V^{IV}Pc^{1-}/V^{IV}Pc^{2-}$ for couple **I** and $V^{IV}Pc^{0}/V^{IV}Pc^{1-}$ for couple **II** in comparison with the study of the electrochemistry of the complex in solution. The plots of peak currents, I_p for the redox processes for the SAMs versus the scan rates (Figs. 3.13 insets) were linear showing that the complexes are surface confined onto the gold electrodes.

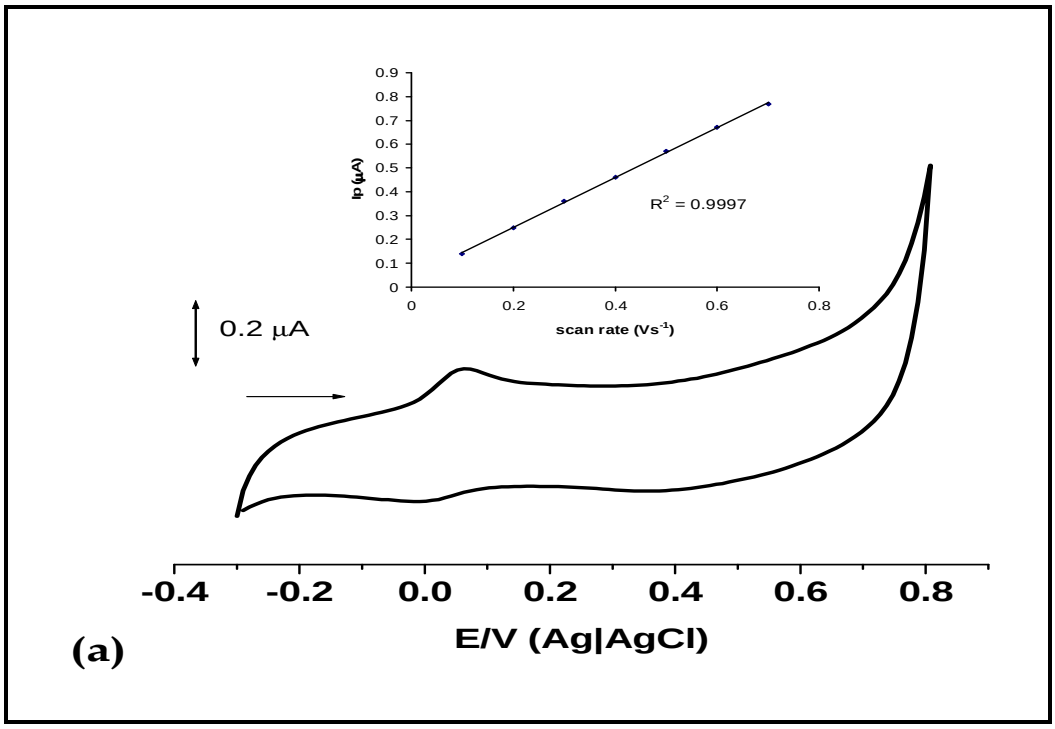
Ip (μA)
scan rate (Vs-1)
R2 = 0.9997
0.2 μA
-0.4 -0.2 0.0 0.2 0.4 0.6 0.8
E/V (Ag|AgCl)
(a)

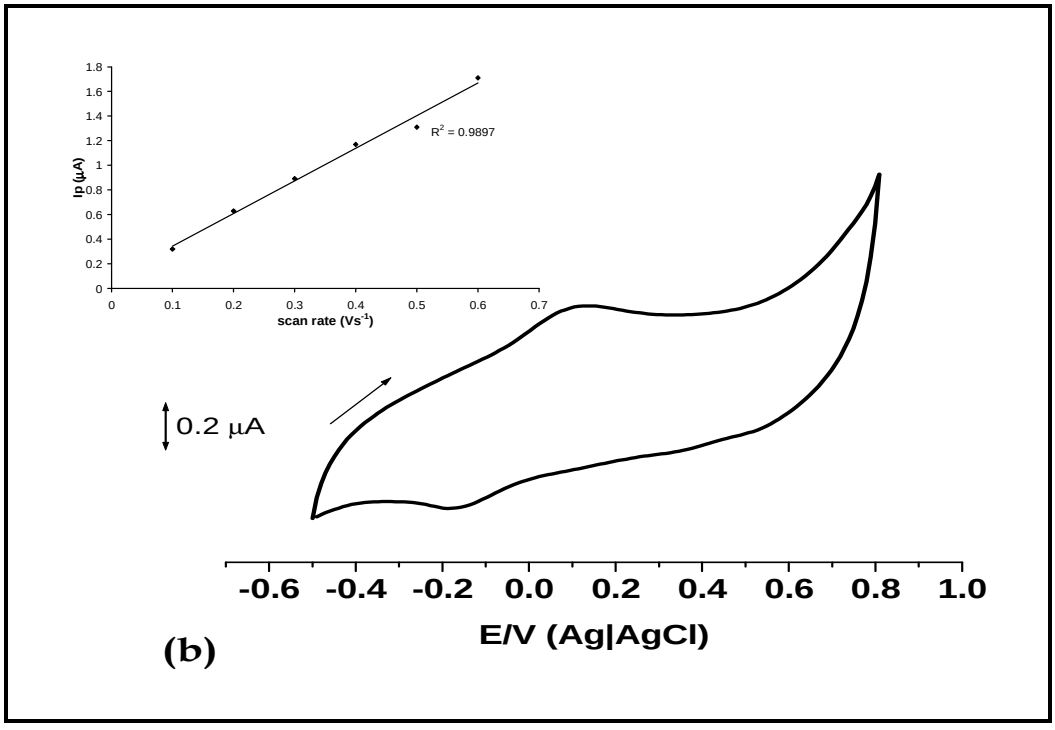
Ip (μA)
scan rate (Vs-1)
R2 = 0.9897
0.2 μA
-0.6 -0.4 -0.2 0.0 0.2 0.4 0.6 0.8 1.0
E/V (Ag|AgCl)
(b)

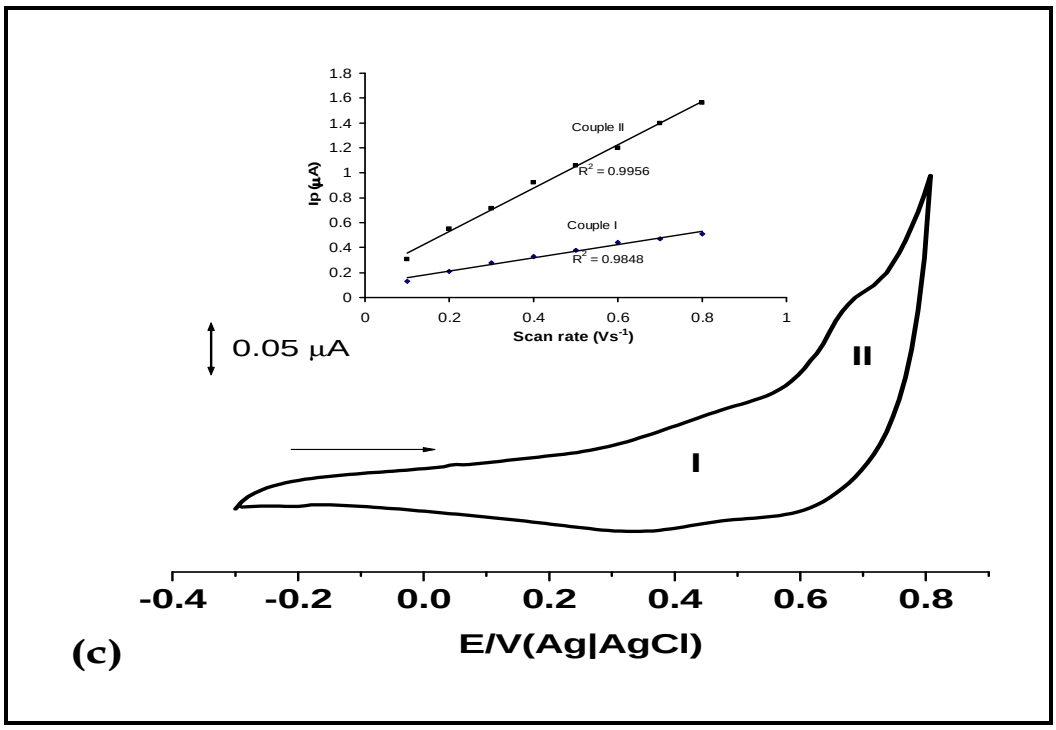

Figure 3.13: Cyclic voltammograms of (a) **AcMnOPTPc**-SAM (b) **OTiOPTPc**-SAM (c) **OVOPTPc**-SAM, all with their current vs scan rate graphs, in pH 4 buffer. Scan rate = 50 mVs^{-1}. Insets: plot of scan rate versus current.

3.4 Electrocatalytic studies using L-cysteine

As expected no oxidation of L-cysteine was observed on bare gold electrode, Fig. 3.14 (iv). Upon modification of the electrode with SAM, Fig 3.14(i) (ii) (iii), the oxidation of L-cysteine was observed at E_p values of 0.52 V, 0.62 V and 0.64 V, Table 3.7, for **AcMnOPTPc**-SAM, **OVOPTPc**-SAM and **OTiOPTPc**-SAM respectively. The low potential for the oxidation of cysteine on **AcMnOPTPc**-SAM may be related to the fact that a metal centered redox process is involved in this complex as opposed to the ring with the other two. In terms of catalytic currents, the following order is obtained: **AcMnOPTPc**-SAM > **OVOPTPc**-SAM > **OTiOPTPc**-SAM.

The oxidation of L-cysteine is observed within the range of the Mn^{IV}/Mn^{III} couple for **AcMnOPTPc**-SAM, $V^{IV}Pc^{1-}/V^{IV}Pc^{2-}$ couple (couple **I**) for **OVOPTPc**-SAM and $Ti^{IV}Pc^{1-}/Ti^{IV}Pc^{2-}$ couple for **OTiOPTPc**, hence the oxidation of cysteine is catalysed by these processes in the respective SAMs.

The total number of electrons for L-cysteine oxidation on the MPc-SAMs was determined using Eq 3.5:

$$I_p = 2.99x10^5 n[(1-\alpha)n_a]^{1/2} AC_o D^{1/2} \upsilon^{1/2} \qquad 3.5$$

where A is the effective area of the electrode, C_o is the concentration of the L-cysteine (1 mM), D the diffusion coefficient of L-cysteine (4.8 X 10^{-5} cm^2s^{-1} [90]), n_α is the number electrons involved in the rate determining step (determined below using Tafel slopes), α is the electron transfer coefficient, n = total number of electrons. The number of electrons was found to be unity.

Table 3.7: Electrochemical parameters of L-cysteine during oxidation at modified electrode with different metal complexes in pH 4 phosphate buffer

Complex	Ep V (vs Ag|AgCl)	Tafel slope mv/decade	α	% decrease in current after 10 scans	LoD ($x10^{-4}$)
AcMnOPTPc	0.52	125	0.47	7	0.75
OVOPTPc	0.62	110	0.53	29	1.01
OTiOPTPc	0.64	154	0.38	29	0.91

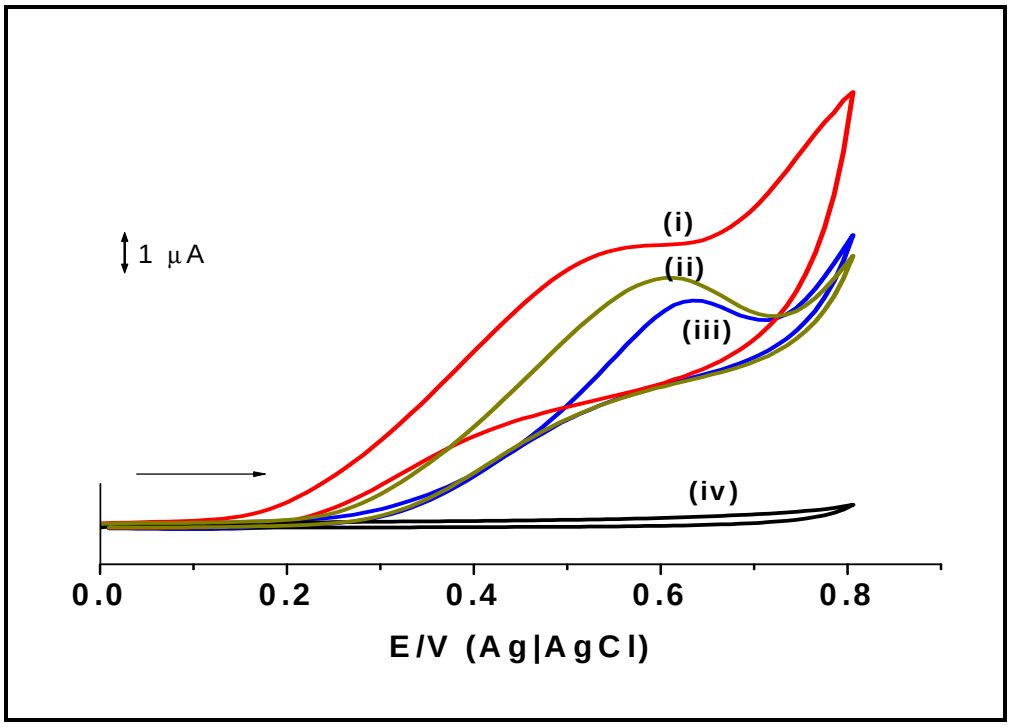

Figure 3.14: Cyclic voltammograms of 1 mM L-Cysteine (in ph 4 buffer) on (i) **AcMnOPTPc**-SAM (ii) **OVOPTPc**-SAM (iii) **OTiOPTPc**-SAM (iv) bare Au electrode. Scan rate = 50 mVs^{-1}

Further details of the mechanism that is involved in oxidation of L-cysteine could be determined by calculating the Tafel slopes of each MPc-SAM, using Eq 3.6.

$$E_p = \frac{b}{2}\log\nu + K \qquad 3.6$$

where ν is the scan rate and b = 0.059/αn is the Tafel slope, n number of electrons involved in the rate determining step. From the plot of Ep vs log v, Fig 3.15a, Tafel slope values of 125 mV/decade, 154 mV/decade and 110 mV/decade were determined for **AcMnOPTPc**-SAM, **OTiOPTPc**-SAM and **OVOPTPc**-SAM respectively. Tafel slope values that are close to 120 mV/decade mean that the first electron transfer is the rate determining step, as it is observed for all the MPc-SAMs. The Tafel slope is significantly larger for the **OTiOPTPc**, this can be accounted for by possible

interaction between the analyte, L-cysteine and **OTiOPTPc** in the reaction intermediate or to chemical reactions coupled to electrochemical step [103].

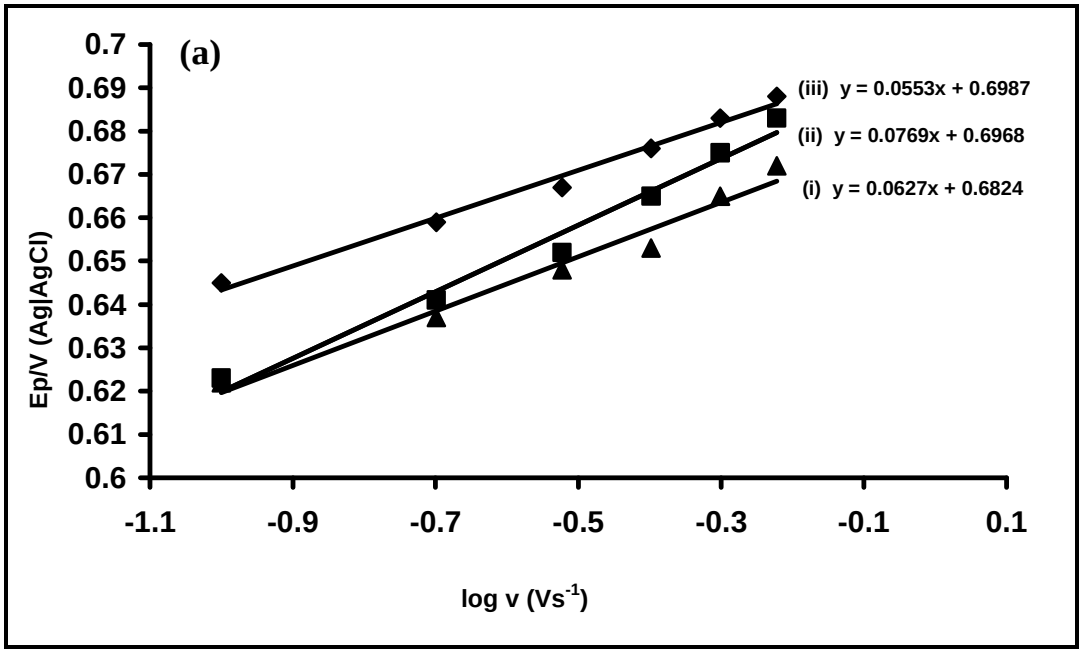

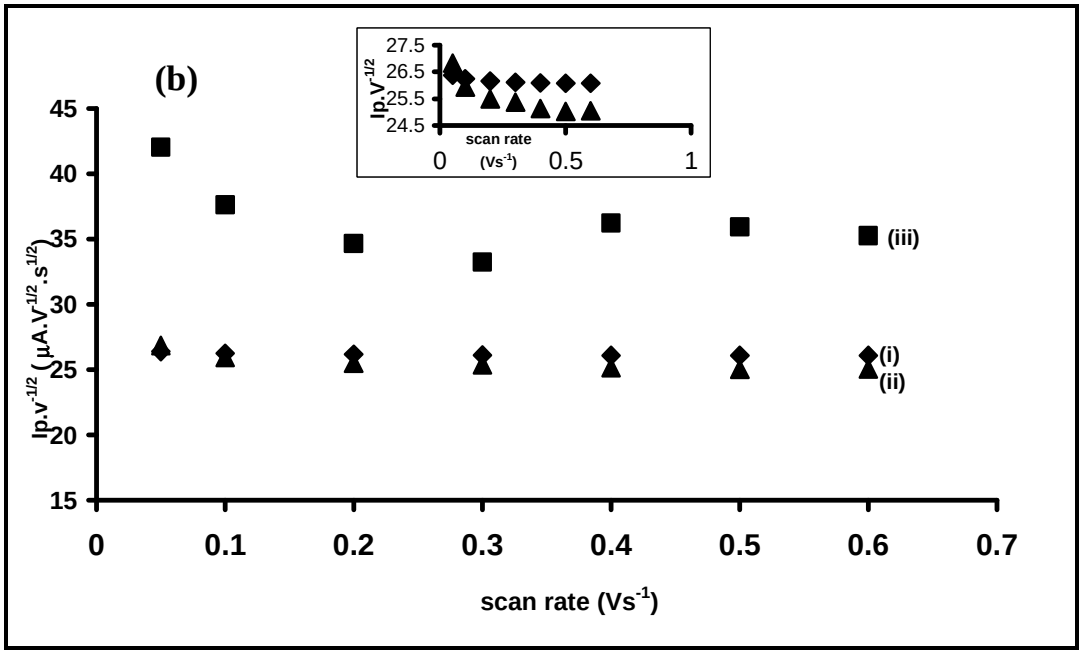

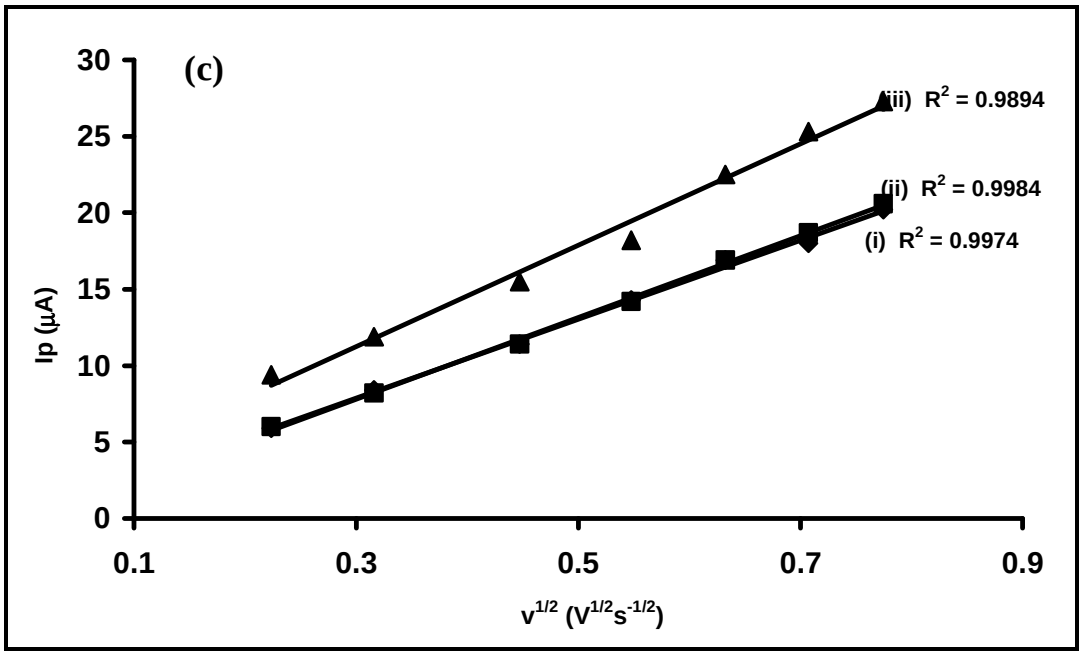

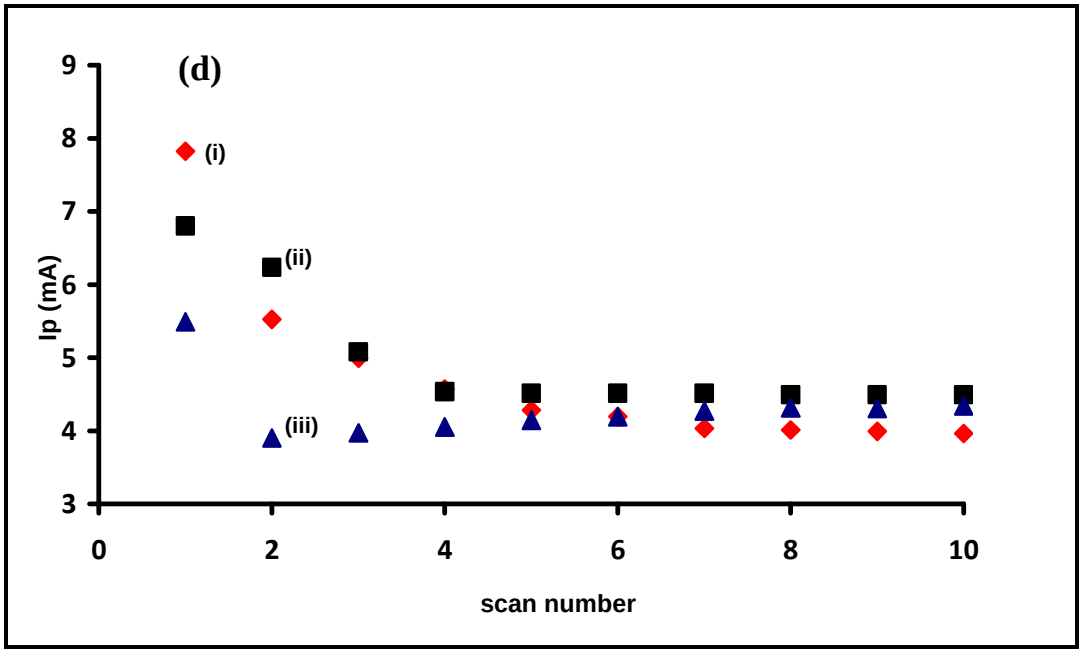

Figure 3.15 : Plot of (a) Ep vs log *v*, (b) sweep-rate normalised current density ($I_p v^{-1/2}$) versus the sweep rate (inset = expansion of (ii) and (iii)), (c) peak current and square root of the scan rate and (d) current vs cyclic voltammogram scan number for analysis of L-cysteine by (i) **AcMnOPTPc**-SAM (ii) **OTiOPTPc**-SAM and (iii) **OVOPTPc**-SAM.

Based on the above discussion the following mechanisms can be proposed for **AcMnOPTPc**:

$$AcMn^{III}OPTPc^{2-} \longrightarrow [AcMn^{IV}OPTPc^{2-}]^{+} + e^{-}$$

$$[AcMn^{IV}OPTPc^{2-}]^{+} + RSH \longrightarrow AcMn^{III}OPTPc^{2-} + RS^{\bullet} + H^{+}$$

$$RS^{\bullet} + RS^{\bullet} \longrightarrow RS\text{-}SR$$

For **OVOPTPc** and **OTiOPTPc** the mechanism is as follows:

$$OM^{IV}OPTPc^{2-} \longrightarrow [OM^{IV}OPTPc^{1-}]^{+} + e^{-}$$

$$[OM^{IV}OPTPc^{1-}]^{+} + RSH \longrightarrow OM^{IV}OPTPc^{2-} + RS^{\bullet} + H^{+}$$

$$RS^{\bullet} + RS^{\bullet} \longrightarrow RS\text{-}SR$$

where RSH is L-cysteine and RSSR is the oxidation product cystine.

The electron transfer coefficients (α) values were determined to be 0.47, 0.38 and 0.53 for **AcMnOPTPc**-SAM, **OTiOPTPc**-SAM and **OVOPTPc**-SAM respectively, Table 3.7. Electron transfer values that are close to 0.5 suggest that there is equal probability of the transition state favouring reactant or product formation.

The plots of sweep-rate normalised current density ($I_p v^{-1/2}$) versus the sweep rate show typical behaviour for a catalytic process [105], Fig. 3.15b. Fig, 3.15c shows a near linear relationship between the peak current and square root of the scan rate, indicating that the cysteine electrocatalytic oxidation is diffusion controlled.

The modified electrodes were investigated for stability and reproducibility by repetitively scanning (10 scans) 1 mM cysteine in pH 4 buffer, Fig. 3.15d. About 7 (for **AcMnOPTPc**-SAM) to 29 % (for **OVOPTPc** and **OTiOPTPc**) decrease in

catalytic peak current was observed after the 1st scan, an indication that there is some passivation on the electrode surface by the oxidation product cystine. Thereafter, the peak currents stabilized showing no significant differences between the subsequent scans and hence high resistance to passivation. The electrode could be regenerated by rinsing in buffer.

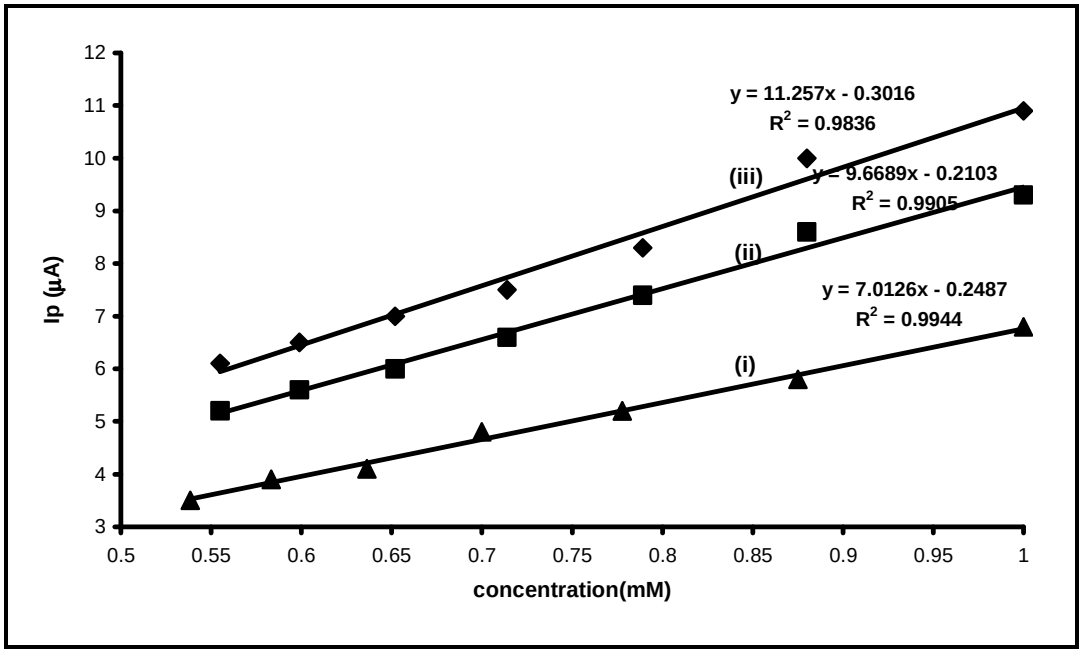

Figure 3.16: Dependence of cysteine concentration on currents for (i) **AcMnOPTPc**-SAM, (ii) **OVOPTPc**-SAM and **OTiOPTPc**-SAM

Fig. 3.16 shows a linear dependence of cysteine concentration on currents and the detection limits for cysteine analysis were determined using 3σ criterion, with the σ value being determined from six replicate measurements, and the values found were 0.75×10^{-4} M, 0.91×10^{-4} M and 1.01×10^{-4} M for **AcMnOPTPc**, **OTiOPTPc** and **OVOPTPc** respectively. Thus the limits of detection improve as follows: AcOMnOPThPc > **OTiOPTPc** > **OVOPTPc**. This trend does not conform to the

trend in surface coverage which is as follows: **OTiOPTPc** > **AcMnOPTPc** > **OVOPTPc**, suggesting that other factors are important for the electrocatalytic activity of the molecules. In terms of stability and the detection limits, MnPc derivative performs better than the other two complexes.

This could be related to the ease of formation of a reactive intermediate between L-cysteine and the MnPc derivative.

CHAPTER 4

CONCLUSIONS

4.1 General Conclusions

The synthesis of pentyllthio substituted Pcs with vanadium, manganese and titanium as a central metal was carried out. These MPc complexes showed Q bands in the near infrared region (898 nm for **AcMnOPTPc**, 842 nm for **OVOPTPc** and 808 nm for **OTiOPTPc**). The Q band is found in the infra red region because of the electron donating properties of the pentylthio and also because of α substitution. The synthesised MPcs have the potential to be used as infra red absorbers. They are red and purple in solution which is different from the norm of green or blue Pcs. Based on the above observations, the synthesis of MPcs was considered successful.

The electrochemical characterisation of the complexes showed that the electron donating ability of the alkylthio substituent led to an ease in the oxidation with oxidation redox peaks being observed for the **OTiOPTPc** even though for other reported thio substituted TiPcs oxidation peaks are difficult to observe. Also the electron donating ability of the substituents led to the rare observation of the Mn^{IV}/Mn^{III} redox couple. This was proven by spectroelectrochemistry which clearly showed the shifting of the Q band from 908 nm to 920 nm. The spectroelectrochemistry of the **AcMnOPTPc** revealed that the first reduction was metal based (Mn^{III}/Mn^{II}) and the second reduction was ring based. The spectrum for the various oxidation state of Mn in **AcMnOPTPc** shows that with increase in the oxidation state of the Mn from Mn^{II} to Mn^{IV}, there is a shift of the Q band towards the red end of the spectrum.

There electrochemistry of thiol or alkylthio substituted VPcs is not known. The CV of the **OVOPTPc** showed two redox couples on the oxidation side, as evidence of the electron donating ability of the substituents. This is one of the few VPc complexes that has shown two oxidation peaks. The spectroelectrochemical data of the first

reduction peak showed a shift of the Q band from 846 nm to 680 nm with a change in colour from purple to green. This change would normally be evidence of a metal based process but was assigned as a ring based process owing to the reported electrochemical data on VPcs.

The SAMs of **OTiOPTPc**, **AcMnOPTPc** and **OVOPTPc** have been formed with surface coverages ranging as follows: **OTiOPTPc** > **AcMnOPTPc** > **OVOPTPc**. The modified electrodes were able to oxidize L-cysteine, with the AcOMnOPThPc being the one that could oxidize L-cysteine at relatively lower potentials, 0.52 V. The rate determining step for the reaction involves one electron, this was determined from the Tafel slopes. The limits of detection improved as follows: **AcMnOPTPc** (0.75×10^{-4} M) > **OTiOPTPc** 0.91×10^{-4} M) > **OVOPTPc** (1.01×10^{-4} M) and the stability of the electrodes followed the trend: AcOMnOPThPc > **OTiOPTPc** = **OVOPTPc**, thus showing that AcOMnOPThPc is the best catalyst.

4.2 Recommendations for Further studies

These may include the analysis of the self assembly that forms on the gold electrode using techniques such as X-ray photoelectron spectroscopy and atomic force microscopy. Study of the MPc-SAMs of these molecules as sensors for molecules that have the potential to be harmful to the environment, these include pesticides.

REFERENCES

References

1. A. von Braun, J. Tschemiac, *J. Chem. Ber.*, **40** (1907) 2709
2. R.W Linstead, A.R Lowe, *J. Chem Soc.*, (1934) 1031
3. E. Ben-Hur, I. Rosenthal, C.C Leznoff, *J. Photochem. Photobiol.*, **2** (1988) 1243
4. P. Qian, J.F. Evensen, C. Rimington, J. Moan, *Cancer Lett.*, **3** (1987) 1
5. L. Polo, A. Segala, G. Jori, G. Bocchioti, G. Verna, R. Franceschini, R. Mosca, P.G De Filippi, *Cancer Lett.*, **109** (1996) 57
6. L. Valli, *Adv. in Colloid and Interface Sci.*, **116** (2005) 13
7. T.V Basova, E.K Kol'tsov, I.K Igumenov, *Sens. Actuators B*, **105** (2005) 259
8. J.W. Gadner, M.Z Iskandarani, B. Bott, *Sens. Actuators B*, **9** (1992) 133
9. P.R Somani, S. Radhakrishnan, *Mat. Chem.*, **77** (2002) 117
10. G. de la Torre, P. Vasquez and F. Agulló-López, *Adv. Mater. Chem.*, **9** (1997) 265
11. G. de la Torre, P. Vaquez, F. Agulló-López and T. Torres, *J. Mater. Chem.*, **8** (1998) 1671
12. Z.R Hong, Z.H Huang, X.T Zena, *Thin Solid Films*, **515** (2007) 3019
13. P. Kivits, R. Debouts, J. Van Der Veen, *J. Appl. Phys.*, **A26** (1981) 101
14. D. Gu, Q. Chen, J. Shu, X. Tang, F. Gan, S. Shen, K. Liu, H. Xu, *Thin Solid Films* **257** (1995) 88
15. A.W. Snow in: *The Porphyrin Handbook*, K.M Kadish, K.M Smith, R. Guilard (Eds.), Academic Press: New York, 2003, Vol.17, chapter 109, pp130-176
16. M. Durmuş, T. Nyokong, *Tetrahedron*, **63** (2007) 1385

17. W Chidawanyika, T. Nyokong, *J. Photochem. Photobiol. A: Chem.*, 2008 (in press)
18. G. Schmid, M. Sommerauer, M. Hanack, *Angew. Chem. Int. Ed. Engl.*, **32** (1993) 1422
19. S. Khene, D.A Geraldo, C.A Togo, J. Limson, T. Nyokong, *Electrochim. Acta*, **54** (2008) 183
20. P. M Burnham, M.J Cook, L.A Gerrard, M.J Heeney, D.L Hughes, *J. Chem Soc. : Chem. Commun.*,(2003) 2064
21. B. Agboola, T. Nyokong, *Electrochim. Acta*, **52** (2007) 2520
22. N. Sehlotho, M. Durmuş, T. Nyokong, *Inorg. Chem. Comm.*, **11** (2008) 479
23. P. Tau, T. Nyokong, *Dalton Trans.*, (2006) 4482
24. Y. Arsanoğlu, A.M Sevim, E. Hamuryudan, A. Gül, *Dyes Pigm.*, **68** (2006) 129
25. Y. Arsanoğlu, E. Hamuryudan, *Dyes Pigm.*, **72** (2007) 129
26. Buckingham; Mark R, Evans; Christopher M., Ellis; Richard J., Jackson; Andrew C., Assignee Minnesota mining company, US Patent 5168031, (1992)
27. M. Gouterman, *J. Mol. Spectrosc.*, **6** (1961) 138
28. C. Weiss, H. Kobayashi, M. Gouterman, *J. Mol. Spectrosc.*, **16** (1965) 415
29. L. Boucher, *Coordination Chemistry in Macrocyclic Compounds*, G. A Melson (Ed), Plenium Press, 1971, pp 461
30. M.J Cook, A.J Dunn, S.D Howe, A.J Thomson, *J. Chem. Soc.:Perkin Trans 1*, (1988) 2453
31. R. M Christie, *Dyes Pigm.*, **27** (1995) 35

32. V. Chauke, A. Ogunsipe, M. Durmuş, T. Nyokong, *Polyhedron*, **26** (2007) 2663

33. I. Yilmaz, A. Gürek, V. Ahsen, *Polyhedron*, **24** (2005)

34. T. Muto, T. Temmo, M. Kimura, K. Hanabusa, H. Shirai, *J. Org. Chem.*, **66** (2001) 6109

35. N. Kobayashi, H. Ogata, N. Nonaka, E. A Luk'yanets, *Chem. Eur. J.*, **9** (2003) 5123

36. L. Guo, D.E Ellis, B.M Hoffman, Y. Ishikawa, *Inorg. Chem*., **35** (1996) 5304

37. M. Handa, A. Suzuki, S. Shoji, K. Kasuga, K. Sogabe, *Inorg. Chim. Acta*, **230** (1995) 41

38. W. Chidawanyika, A. Ogunsipe, T. Nyokong, *New J. Chem*., **31** (2007) 377

39. J. Obirai, T. Nyokong, *Electrochim. Acta*, **50** (2005) 3296

40. M.J Stillman, A.J Thompson, *J. Chem. Soc.: Faraday Trans. 2*, (1974) 805

41. A.B.P Lever , S. Licoccia, P.C Minor, B.S Ramaswamy, S.R Pickens, K.J Magnell, *J. Am. Chem. Soc.*, **103** (1981) 6800

42. S. Donner, H-W Li, E.S Yeung, M.D Porter, *Anal.Chem.*, **78** (2006) 2816

43. J. López-Palacios, A. Colina, A. Heras, V. Ruiz, L. Fuente, *Anal Chem.*, **73** (2001) 2883

44. W. R. Heineman, *Anal. Chem.*, **50** (1978) 390A

45. 11. T. P. DeAngelis, R. W. Hurst, A. M. Yacynych, H. B. Mark, Jr., W. R. Heineman, J. S. Mattson, *Anal. Chem.*, **49** (1977) 1395

46. A.J Bard, L.R Faulkner, *Electrochemical Methods: Fundamentals and Application*, 2nd ed, John Wiley and Son, NewYork, (2001) Ch. 17

47. M. L'Her, A. Pondaven in: *The Porphyrin Handbook*, K.M Kadish, K.M Smith, R. Guilard (eds) , Academic Press, California, Vol 16 (2003) 117

48. A.B.P. Lever, E.R. Milaeva, G. Speier, in: *Phthalocyanines: Properties and Applications*,C.C. Leznoff, A.B.P. Lever (Eds.), VCH Publishers, New York, Vol. 3 (1993) Ch 1

49. Ö. Bekaroğlu, *Appl. Organomet. Chem.*, **10** (1996) 605

50. M.J. Stillman, in: *Phthalocyanines: Properties and Applications*, C.C. Leznoff, A.B.P.Lever (Eds), VCH Publishers, New York, Vol. 3 (1993) Ch. 5

51. Z. Jiang, Z Ou, N. Chen, J. Wang, J. Huang, J. Shao, K.M Kadish, *J. Porphyrins Phthalocyanines*, **9** (2005) 352

52. P. Tau, T. Nyokong, *Polyhedron*, **25** (2006) 1802

53. A Koca, Y. Arslanoğlu, E. Hamuryudan, *J. Electroanal. Chem*., **616** (2008) 107

54. M.J. Stillman, T. Nyokong, in: C.C. Leznoff, A.B.P. Lever (Eds.), *Phthalocyanines: Properties and Applications*, vol. 1, VCH, New York, 1989 (Chapter 3)

55. M.C Granger, J.S Xu, J.W Strojek, *Anal. Chim. Acta*, **397** (1997) 145

56. X. Xing, D. A Scherson, *Anal. Chem*., **60** (1988)1723

57. J. Zagal, *Coord. Chem. Rev*, **119** (1992) 89

58. J F.J. Rawson, W.M. Purcell, J. Xu, D.C. Cowell, P.R. Fielden, N. Biddle, J.P. Hart, *Electrochim. Acta*, **52** (2007) 7248

59. C. Song, L. Zhang, J. Zhang, *J. Electroanal. Chem.*, **587** (2006) 293

60. Ö.A. Osmanbaş, A. Koca, M. Kandaz, F. Karaca, *Int. J. Hydrogen Energy*, **33** (2008) 3281

61. S. Maree, T. Nyokong, *J. Electroanal. Chem.*, **492** (2000) 120

62. N. Nombona, P. Tau, N. Sehlotho, T. Nyokong, *Electrochim. Acta*, **53** (2008) 3139

63. J. Obirai, T. Nyokong, *Electrochim. Acta*, **49** (2004) 1417

64. S. Griveau, J. Pavez, J. H. Zagal and F. Bedioui, *J. Electroanal. Chem.*, **497** (2001) 75

65. J. Prekumar and R. Ramaraj, *J. Photochem. Photobiol. A*: Chem., **110** (1998) 53

66. S. L. Buell and J. N. Demas, *J. Phys. Chem*., **87** (1983) 4675

67. P. Janda, J. Weber, L. Dunsch and A. B. P. Lever, *Anal. chem.*, **68** (1996) 960

68. A. E. Kaifer and M. Gomez-Kaifer, *Supramol. Electrochem.*, Willey, VCH, New York, 1999

69. J. Wang, B. Zeng, C. Fang, *Anal. Sci*., **16** (2000) 457

70. G. Kalyuzhny, A. Vaskevich, G. Ashkenasky, A. Schanzer, I. Rubinstein, *J. Phys. Chem. B*, **104** (2000) 8283

71. P.N Mashazi, P. Westbroek, K.I Ozoemena, T. Nyokong, *Electrochim. Acta*, **53** (2007) 1858

72. L.Y He, B.J Xiang, Y.J Yang, *Russ. J. Electrochem*., **40** (2004) 849

73. N. Muskal, D. Mandler, *Electrochim. Acta*, **45** (1999) 537

74. H. Yamada, H. Imahori, S. Fukuzumi, *J. Mat. Chem*., **125** (2002) 9129

75. H. Imahori, H. Norieda, H. Yamada, Y. Nishimura, I. Yamazaki, Y. Sakata, S. fukuzumi, *J. Am. Chem. Soc*., **123** (2001) 100

76. C.D Bain, G.M Whitesides, *J. Am. Chem. Soc*., **110** (1988) 3665

77. G. Mani, D. M Johnson, D. Marton, M.D Feldman, D. Patel, A.A Ayon, C.M Agrawal, *Biomaterials*, **29** (2008) 4561

78. H.O Finklea, in: *Electroanalytical Chemistry*, Vol. 19, A.J Bard and I Rubinstein (Eds.), Marcel Decker, New York, 1996, pp 109

79. K. Juodkazis, J. Juodkazyte, *Electrochem. Comm.*, **1** (2001) 315

80. N. Kobayashi, P. Janda, A.B.P Lever, *Inorg. Chem.*, **31** (1992) 5172

81. C-Q Sun, G-I Liu, H-A Zhang, *Gaodeng Xuexia Huaxue Xuebao*, **19** (2005) 791

82. K.I Ozoemena, T. Nyokong, *Electrochim. Acta*, **51** (2006) 2669

83. B. Agboola, T. Nyokong, *Talanta*, **72** (2007) 691

84. T.R. Ralph, M.L Hitchman, J.P Millington, F.C Walsh, *J. Electroanal. Chem.*, **375** (1994) 17

85. N. Maleki, A. Safavi, F. Sedaghati, F. Tajabadi, *Anal. Biochem*., **367** (2007) 149

86. M.G Li, Y. J Shang, Y.C Gao, G.F Wang, B. Fang, *Anal. Biochem*., **341** (2005) 52

87. A. Abbaspour, A. Ghaffarined, *Electrochim. Acta*, **53** (2008) 6643

88. N. Sehlotho, T. Nyokong, *Electrochim. Acta*, **51** (2006) 4463

89. L-C. Chen, K-C. Ho, *Sensors and Actuators B: Chemical.*, **130** (2008) 418

90. K.I Ozoemena, P. Westbroek, T. Nyokong, *Electrochem. Comm.*, **3** (2001) 529

91. P.N Mashazi, K.I Ozoemena, D. Maree, T. Nyokong, *Electrochim. Acta*, **51** (2006) 3489

92. C.C Leznoff, L.S Black, A. Heibert, P.W Causey, D. Christendat, A.B.P Lever, *Inorg. Chim. Acta*, **359** (2006) 2690

93. H. Enkelkamp, R.J.M Nolte, *J. Porphyrins Phthalocyanines*, **4** (2000) 45

94. D.D Dominguez, A.W Snow, J.S Shirk, R.G.S Pong, *J. Porphyrins Phthalocyanines*, **5** (2001) 582

95. J Mark, M.J Stillman in: *The Porphyrin Handbook*, K.M Kadish, K.M Smith, R. Guilard (eds) , Academic Press, California, Vol 16 (2003) 117

96. P.T Kissinger, C.R Reddy, R.E Shoup, W.R Heinemann in *Laboratory techniques in Electroanal. Chem.*, P.T Kissinger and W.R Heinemann (Eds), 2nd ed (1996), Marcel Dekker, New York

97. I. Prieto, T. Martin, E. Munoz, T.L Camacho, *J. Phys. Chem.*, **99** (1995) 14083

98. J. Obirai, T. Nyokong, *Electrochim. Acta*, **49** (2004) 1417

99. K. Takahashi, M. Kawashima, Y. Tomita, M. Itoh, *Inorg. Chim. Acta*, **232** (1995) 69

100. P. Tau, T. Nyokong, *Electrochim. Acta*, **52** (2007) 3641

101. E. Sabatini, I. Rubinstein, *J. Phys Chem.*, **91** (1987) 666

102. D. Losic, J.G Shapter, J.J Gooding, *Langmuir*, **17** (2001)3307

103. B. Agboola, P. Westbroek, K.I. Ozoemena, T. Nyokong, *Electrochem. Comm.*, **9** (2007) 310

104. P. Tau, T. Nyokong, *J. Electroanal. Chem.*, **611** (2007) 10

105. C.A. Caro, F. Bedioui, J.H. Zagal, *Electrochim. Acta*, **47** (2002) 1489.